SYNTHESIS OF INORGANIC NANOWIRES BY USING PEPTIDE NANOTUBES AS THE TEMPLATES VIA BIOLOGIC RECOGNITION

by

LINGTAO YU

A dissertation submitted to the Graduate Faculty in Chemistry in partial fulfillment of the requirements for the degree of Doctor of Philosophy, The City University Of New York

2006

UMI Number: 3204990

UMI Microform 3204990

ProQuest Information and Learning Company
300 North Zeeb Road
P.O. Box 1346
Ann Arbor, MI 48106-1346

This manuscript has been read and accepted for the Graduate Faculty in Chemistry in satisfaction of the dissertation requirements for the degree of Doctor of Philosophy.

January 2006	Prof. Hiroshi Matsui
Date	Chair of Examining Committee
January 2006	Prof. Gerald Koeppl
Date	Executive Officer

Dr. Hiroshi Matsui

Dr. Zhonghua Yu

Dr. Charles Michael Drain
Supervisory Committee

THE CITY UNIVERSITY OF NEW YORK

Abstract

SYNTHESIS OF INORGANIC NANOWIRES BY USING PEPTIDE NANOTUBES AS THE TEMPLATES VIA BIOLOGIC RECOGNITION

by

Lingtao Yu

Adviser: Professor Hiroshi Matsui

Nanomaterials and nanoscale engineering will play a critical role in the future of materials science, electronic technology and biotechnology. Inspired by nature, biomineralization is becoming an important technique to synthesize inorganic nanomaterials. This is a recognization process which is based on molecular complementarity between protein and specific crystal phases of metals or semiconductors. This approach can produce nanomaterials with precisely controlled morphology and crystalline structure under mild conditions. In this dissertation, sequenced histidine–rich peptides are used to fabricate morphology-controlled nanocrystals on the surface. Various inorganic nanocrystals are produced accurately, efficiently and reproducibly by choosing different peptide sequences for different metals. Biomineralization of nanotubes is achieved by incorporating these sequenced histidine-rich peptides onto templated peptide nanotubes. The biological recognition of the specific peptide sequences toward particular metals and semiconductor leads to the efficient coatings of such inorganic nanocrystals as Ag, Pt, Cu, Ni and ZnS on the nanotubes. This method allows for the synthesis of

nanotubes uniformly coated by highly crystalline metal nanocrystals with a high-density surface coverage. It has been demonstrated that the size, shape and packing density of the nanocrystals can be regulated via changes in the pH of the solution, which leads to conformational changes in the peptide. By this means, different inorganic nanowires can be synthesized with tunable surface morphology which results in tunable physical properties that could be used as the building blocks for the fabrication of nanodevices.

ACKNOWLEDGMENTS

I wish to thank my advisor, Prof. Hiroshi Matsui, for his guidance and support during my PhD research. His patience, enthausiasm, encouragement and friendship made the past four and half years an enjoyable experience in my life. To me, he is not only a true scientist, but a great educator. I will always be grateful to him for the opportunities that he provided me with, to grow as a chemist.

I would like to thank all the colleagues in Matsui group for the good time we shared. I thank Dr. I. A Banerjee and Dr Xueyun Gao, for helping me solve a lot of problems during the research and for their valuable discussions. I thank Professor A. Tsiola and K. Fath at the Core Facilities for Imaging at Queens College-CUNY for TEM. I thank Professor Y. Xu at Hunter College for CD spectroscopy.

Professors C. M. Drain and Professor Z. Yu are gratefully acknowledged for taking time to serve on my Ph. D. committee. They are very appreciated for the encouragement, help and discussion on my researches. I would like to thank Professor K. Grohmann from Hunter College and Professor G. Koeppl from Graduate Center of CUNY, for their patience and dedication in helping graduate students.

The U.S. Department of Energy is acknowledged for financial support throughout my graduate years.

I am eternally grateful to my wife, Qiong Zhang, whose love and support means the world to me. I feel incredibly fortunate to have her in my life, and could not imagine how I could have been through these years in the U.S. without her.

Finally, I am truly grateful to my parents and my brother for their constant support and motivation during my academic pursuits.

Dedicated to my wife Qiong Zhang

and

my parents

INDEX

ABSTRACT II

ACKNOWLEDGMENTS IV

LIST OF TABLES IX

LIST OF FIGURES X

CHAPTER 1 INTRODUCTION 1

1.1 Nanotechnology 1

1.2 Nanoparticles 3

1.3 Nanotubes 10

1.4 Biomineralization 17

CHAPTER 2 DIRECT GROWTH OF SHAPE-CONTROLLED NANOCRYSTALS ON NANOTUBES VIA BIOLOGICAL RECOGNITION 25

2.1 Introduction 25

2.2 Experimental Section 28

2.3 Results and Discussion 29

2.4 Conclusion 37

CHAPTER 3 INCORPORATION OF SEQUENCED PEPTIDES ON NANOTUBES FOR PT COATING: SMART CONTROL OF NUCLEATION AND MORPHOLOGY VIA ACTIVATION OF METAL BINDING SITES ON AMINO ACIDS 39

3.1 Introduction 39

3.2 Experimental Section 43

3.3 Results and Discussion 44

3.4 Conclusion *51*

CHAPTER 4CU NANOCRYSTAL GROWTH ON PEPTIDE NANOTUBES BY BIOMINERALIZATION: SIZE CONTROL OF CU NANOCRYSTALS BY TUNING PEPTIDE CONFORMATION 52

4.1 Introduction *52*

4.2 Experimental Section *55*

4.3 Results and Discussion *57*

4.4 Conclusion *66*

CHAPTER 5 SIZE-CONTROLLED NI NANOCRYSTAL GROWTH ON PEPTIDE NANOTUBES AND THEIR MAGNETIC PROPERTIES 67

5.1 Introduction *67*

5.2 Experimental Section *69*

5.3 Results and discussion *70*

CHAPTER 6 ROOM-TEMPERATURE WURTZITE ZNS NANOCRYSTAL GROWTH ON ZN FINGER-LIKE PEPTIDE NANOTUBES BY CONTROLLING THEIR UNFOLDING PEPTIDE STRUCTURES 76

6.1 Introduction *76*

6.2 Experimental Section *78*

6.3 Results and Discussions. *80*

CHAPTER 7 FABRICATION AND APPLICATION OF ENZYME INCORPORATED PEPTIDE NANOTUBES 87

7.1 Introduction *87*

7.2 Experimental Section *90*

7.3 Results and Discussion *92*

7.4 Conclusion *100*

APPENDIX 102

REFERENCES: 104

LIst of Tables

Table 1 Nanoparticulate Metals Synthesis by Wet Chemical Methods 7

Table 2 Examples of some inorganic nanomaterials synthesized via biomineralization ..21

LIST OF FIGURES

Figure 1.1 (a) Chemical structure of the peptide monomer, bis(N-α-amido-glycylglycine)-1,7-heptane dicarboxylate. (b) Self-assembled structure of the peptide nanotube. (c) Illustration of potential ion-chelating sites of the peptide nanotubes. Yellow arrows indicate that the atoms bind neighboring peptide monomers via hydrogen bonds. 15

Figure 1.2 Scheme of protein-coating on peptide nanotube(Left) and Fluorescence micrograph of streptavidin-coated peptide nanotube(Right). 16

Figure 2.1 Scheme for Ag nanocrystal growth in the hexagonal shape on the template nanotubes. The sequenced AG4 peptide, incorporated on the nanotube surfaces, absorbs and reduces Ag ions to grow Ag nanocrystals. The AG4 peptide recognizes and effects the Ag growth on the (111) face and it controls the growth rate along different crystal axes and manipulates the shape of Ag nanocrystals.....27

Figure 2.2 Raman spectra of the AG4 peptide coated on the nanotubes (above), and the neat peptide (below) in aqueous solution. 29

Figure 2.3 (a) The correlation between the size of Ag nanocrystals and the nanocrystal growth time in the pH 7 growth solution. (b) TEM image of hexagon-shaped Ag nanocrystals on the nanotube after 14 h in the pH 7 growth solution. Scale bar = 100 nm. Inset: Highly magnified TEM image. Scale bar = 15 nm. (c) Tilted TEM image of the hexagon-shaped Ag nanocrystal on the nanotube after 14 h in the pH 7 growth solution. Scale bar = 10 nm. (d) TEM image of hexagon-shaped Ag nanocrystals on the nanotube after 72 h in the pH 7 growth solution. Scale bar = 50 nm. (e) TEM image of hexagon-shaped Ag nanocrystals on the smaller nanotube after 72 h in the pH 7 growth solution. Scale bar = 50 nm. Inset: the electron diffraction pattern showing (111), (011), and (100) faces. 31

Figure 2.4 UV/vis spectra of hexagon-shaped Ag nanocrystals on the nanotubes in the diameters of 5 nm (blue), 14 nm (red) 50 nm (black). 32

Figure 2.5 TEM images of Ag nanocrystals on the nanotubes (a) without incorporating the AG4 peptide on the surfaces after 14 h in the pH 7 growth solution. Scale bar = 100 nm. (b) with the HG 12 peptide on the surfaces after 72 h in the pH 7 growth solution. Scale bar = 100 nm.....34

Figure 2.6 TEM image of Ag nanocrystals on the nanotubes after 72 h in the pH 9 growth solution. Scale bar = 50 nm.....35

Figure 2.7 The correlation between the size of hexagonal Ag nanocrystals and the nanocrystal growth time in the pH 7 growth solution (•) in the pH 9 solution (Δ).....36

Figure 2.8 TEM image of Ag nanocrystals on the nanotubes after 72 hrs in the presence of an excess reducing agent, hydrazine hydrate, in the pH 7 growth solution. Scale bar = 40 nm. 37

Figure 3.1 Procedure to fabricate Pt nanotubes: (I) immobilization of the sequenced peptide on the template nanotubes. (II) Anchoring Pt ions on the sequenced peptide on the nanotubes. Pt ions bind one amino acid in pH< 8 solutions while Pt ions bind four amino acids in pH > 8 solutions. (III) Pt nanocrystal growth on the peptide nanotubes by reducing anchored Pt ions.....41

Figure 3.2 Raman spectra of (a) Pt^{2+}-immobilized peptide nanotubes in pH = 4 solution, (b) Pt^{2+}-immobilized peptide nanotubes in pH = 10 solution, (c) peptide nanotubes in the absence of Pt ions in pH = 4 solution and (d) peptide nanotubes in the absence of Pt ions in pH = 10 solution.....46

Figure 3.3 Illustration of the sequenced peptide binding Pt ions on the nanotubes. The dotted arrow indicates carboxylate oxygen in histidine as the Pt binding site on the peptide nanotube under acidic conditions. Solid arrows show imidazole nitrogens in

histidine and amide nitrogens in alanine and glycine as the Pt binding sites under basic condition. 47

Figure 3.4 TEM images of (a) Pt nanocrystals grown on the nanotubes at pH = 4 (inset: electron diffraction of the Pt nanocrystals), (b) Pt coating grown on the nanotubes at pH = 10 (inset: electron diffraction of the Pt coating). (c) The correlation between the surface coverage of Pt nanocrystals and pH of the growth solution. (d) TEM image of Pt nanocrystals grown on the non-functionalized nanotubes at pH = 4. 48

Figure 4.1 Scheme of the Cu nanotube fabrication. (a) Immobilization of the sequenced HG12 peptide at the amide-binding sites of the template nanotubes. (b) The Cu ion–HG12 peptide complexation on the nanotube surfaces. (c) Cu nanocrystal growth on the nanotubes nucleated at Cu ion-binding sites after reducing trapped Cu ions with $NaBH_4$. 55

Figure 4.2 (a) Cu nanocrystals grown on the nanotube at pH 6. (Left) TEM image. (Center) Electron-diffraction pattern. (Right) Size distribution. (Inset) The TEM image in higher magnification. (b) Cu nanocrystals grown on the nanotube at pH 8. (Left) TEM image. (Center) Electron-diffraction pattern. (Right) Size distribution. (Inset) The TEM image in higher magnification. (c) Cu nanocrystals grown on the nanotube without the HG12 peptide at pH 6. (Left) TEM image. (Center) Electron-diffraction pattern. (Right) Size distribution. (Scale bar = 100 nm.) 58

Figure 4.3 UV-visible spectra of the nanotubes coated with Cu nanocrystals in a diameter of 10 nm, grown in pH 6 solution (dotted line) (a) and Cu nanocrystals in a diameter of 30 nm, grown in pH 8 solution (solid line) (b). 60

Figure 4.4 TEM images of the Cu nanocrystals grown in the HG12 peptide solution without the template nanotubes at pH 6 (a) and at pH 8 (b). Arrows show the edges of aggregated HG12 peptides. (Scale bar = 100 nm.) 62

Figure 4.5 IR spectra of the HG12 peptide–Cu(II) complexes on the nanotubes at pH 6 (dotted line) and pH 8 (solid line). 65

Figure 4.6 A proposed structure of the Cu nanocrystal–HG12 peptide complex on the template nanotube..... 66

Figure 5.1 Scheme for the size-controlled Ni nanocrystal growth on the HG12 peptide-coated nanotube via pH change..... 68

Figure 5.2 TEM images of Ni nanocrystals generated on the nanotube (a) at pH 4. Inset: electron diffraction. (b) at pH 6 (c) at pH 8 (d) at pH 6 without the HG12 peptide coating on the nanotube. Scale bar = 200 nm. 72

Figure 5.3 Comparison of hysteresis curves of the peptide nanotubes coated with (a) the 30 nm-Ni nanocrystals and (b) the 100 nm-Ni nanocrystals. 74

Figure 6.1 Illustration of the ZnS nanocrystal growth on the unfolding M1 peptides on the template nanotubes as a function of pH..... 78

Figure 6.2 Structure of the Zinc salt used for the ZnS nanocrystal synthesis..... 79

Figure 6.3 (a) TEM image of ZnS nanocrystals on the M1 peptide nanotubes grown at pH 5.5, inset: in the high magnification. Scale bar = 70 nm. (b) TEM image of ZnS nanocrystals on the neat template nanotubes with no M1 peptides grown at pH 5.5. Scale bar = 100 nm. (c) Electron diffraction of the ZnS nanocrystals on the M1 peptide nanotubes grown at pH 5.5. 81

Figure 6.4(a) UV/vis spectra of the Zn(II)-bound M1 peptide nanotubes (blue line) and the M1 peptide nanotubes with no Zn(II) (red line). (b) Fluorescence spectrum of the ZnS nanocrystals on the M1 peptide nanotubes. (c) Raman spectra of the Zn(II)-bound M1 peptide nanotubes at pH 5.5 (pink) and at pH 10.0 (blue)..... 83

Figure 6.5 circular dichroism (CD) spectroscopy of M1 peptide with Zn ions at pH 5.0(solid line) and pH 7.0(dotted line) 85

Figure 7.1 Illustration of lipase nanotube fabrication and its enzymatic application..... 89

Figure 7.2 TEM images of peptide nanotubes incorporating *Candida rugosa* lipase at (a) [lipase] = 0.002 mg/mL (b) [lipase] = 0.006 mg/mL. Scale bar = 200 nm..... 92

Figure 7.3 Hydrolysis rate of lipases inside the nanotubes. A dotted line is a fit for experimental date points. 94

Figure 7.4 The product concentration versus reaction time, catalyzed by lipases (0.006 mg/mL) at room temperature, pH 7.0. The solid line and ■ represent lipases inside the nanotubes and the dotted line and ● represent the freestanding lipases. 96

Figure 7.5 Fluorescence spectra of lipases bound the inside wall of peptide nanotubes (a blue line) and free-standing lipases (a red line). Dotted lines are the Lorentzian fits for these spectra and the computed peak positions by these fittings are also marked in this plot. 97

Figure 7.6 Thermal stabilities of lipases. The solid line and ■ represent lipases inside the nanotubes and the dotted line and ° represent the freestanding lipases 99

Chapter 1 Introduction

1.1 Nanotechnology

Nanotechnology is the development of tools and techniques to create and use structures, devices and systems at the atomic or macromolecular levels, normally in the 1-100 nm range. The goal is to produce novel materials with properties and functions forming from these of their small or intermediate sizes. The decrease of the materials' size to nano-level unleashes some new characteristics, compared with their bulk counterparts, such as quantum confinement and Gibbs-Thomson effect. The quantum effect can result in different electromagnetic and optical properties of the material; the Gibbs-Thomson effect will lower the melting point of a material when it is nanometers in size. As interdisciplinary fields of science, nanoscience and nanotechnology are an extension of almost all of the current sciences. Departments of materials science, physics, mechanical engineering, bioengineering, and chemical engineering from different universities and institutes around the world are working in conjunction with each other and leading the discovery in novel technologies.(*1*) Any researcher entering the nanotechnology field should know Dr. Richard P. Feynman, a Nobel prize winner in 1965(*2*). In his famous lecture entitled "there is plenty of Room at the Bottom" at CalTech, he first mentioned some of the distinguishing concepts in nanotechnology. He predicted a process by which the ability to manipulate individual atoms and molecules might be developed, using one set of precise tools to build and operate another proportionally smaller set, and so on down to the needed scale.

Nano-scale features are mainly built up from their elemental constituents. In biosystems (e.g. protein), individual molecules are used as building blocks for the production of 3-D nanostructures and in chemical synthesis, simple reagents in solution can spontaneous self-assemble into molecular clusters. In industry, some micro- and nanolevel components, such as computer chips, can be fabricated using top-down lithographic and nonlithographic techniques and range in size from micro- to nanometers such as computer chips. After decades of development, research in nanotechnology has made promising advances in such areas as materials for nanoelectronics, energy, biotechnology, and information technology. The discovery of new materials, processes and phenomena at nanoscale, as well as the progress of new experimental and theoretical techniques provide opportunities for the development of innovative nanosystems and nanomaterials, the two fundamentals of nanotechnology. It is widely felt this technology will lead to the next industrial revolution.

Actually mother nature is the first skilled user of nanotechnology from billions of years ago. The key to understanding these processes in nature will allow us to mimic and produce nanodevices and nanomaterials with high efficiency. In the eyes of scientists, an abalone shell isn't much different from a semiconductor device: both are highly crystalline and macroscopically patterned with multilayers although the shell's layers are of calcium carbonate, not silicon. Meanwhile, semiconductor manufacturers approaching nanotechnology fabrication from the bottom up are keenly interested in self-assembly attributes reflected in much of nature, some proteins have an affinity for a variety of electronic materials including metals, semiconductors, and dielectrics. One approach is to

imitate the techniques of molecular biology in the synthesis and assembly of significant nanomaterials and nanodevices.

1.2 Nanoparticles

The development of nanomaterials, such as nanowires, nanotubes and nanoparticles is a fundamental focal point of the nanotechnology research. Physicists predicted that nanomaterials on the scale of 1-100 nm would display superior electronic, magnetic, optical, and mechanical properties as compared to their bulky counterparts (*3-8*). These propetries strongly depend on the particle size, interparticle distance, surface nature of the particle, and shape of the nanoparticles (*9*). Unlike bulk metals, there is a gap between the valence band and the conduction band in nanoparticles. This size-induced metal-insulator transition was first described in 1988 as the metal particle was small enough (about 20 nm) and this gap can result in the formation of standing electron waves with discrete energy levels. Also, some size-dependent quantization effects occur in particles because of their nanoscale size. *Single-electron transitions* occur between a tip and a nanoparticle, causing the observation of so-called Coulomb blockades if the electrostatic energy, $E_{el}= e^2/2C$, is larger than the thermal energy, $E_T = kT$. The capacitance C becomes smaller with smaller particles. This means that single-electron transitions can be observed at a given temperature only if C is very small, i.e., for nanoparticles ($C < 10^{-18}$ F). Large variations of electrical and optical properties are observed when the energy level spacing exceeds the temperature, and this flexibility is of great practical interest for applications

(e.g. transistors, switches, electrometers, oscillators, biosensors, catalysis; (*10-14*). Due to their exacting properties, various inorganic and carbon-based nanomaterials have been used as building blocks to assemble nanometer-scale devices. Some of these devices show significant improvements compared to existing devices (*15-18*). While these nanodevices are close to being applied in industry, there are still some problems to overcome. One of the biggest problems is how to decrease the cost of nanomaterial synthesis. Many inorganic and carbon-based nanotubes can be created by chemical vapor deposition (CVD) that is expensive, space-occupying and electric power consuming. Alternatively, wet chemical methods via coprecipitation procedure could be an important technique for nanoparticle synthesis which is cheaper, effective and easy to scale up. In this method clusters of metal atoms or semiconductor molecules are formed in the presence of a surface-capping ligand under aqueous and nonaqueous solvents. The capping ligand binds to the metal/semiconductor clusters, prevents aggregation of the particles into bulk materials, and controls the final dimensions of the nanoparticles. Many capping systems are available such as hydrophobic monolayers (*19*), positively or negatively charged hydrophilic monolayers (*20*), and polymer layers (*21*) and so on.

The precipitation of metals from water or organic solvents typically requires the chemical reduction of a metal cation. Reduction agents take many forms, the most common of which are gaseous H_2, solvated ABH_4 (A = alkali metal), hydrazine hydrate($N_2H_4 \cdot H_2O$), and hydrazine dihydrochloride ($N_2H_4 \cdot 2HCl$). For a typical reduction

reaction of a transition metal cation, there must be a reduction process of metal ions ($\mathbf{M}^{n+}$) and an oxidation process of reducing agent (**X**), as the equations below show:

$$M^{n+} + ne^- \longrightarrow M^0 \quad \text{and} \quad X^m - ne^- \longrightarrow X^{m-n}$$

For the oxidation/reduction reaction to occur, the free energy change, ΔG, must be favorable. As a matter of convention, the favorability of oxidation-reduction processes is reflected in the standard electrode potential, E°, of the corresponding electrochemical half-reaction.

Since the E° values of all reactions are stated relative to that of H_2, the half-reaction and E° for H_2 are, by definition, at standard temperature and pressure.

$$2H^+ + 2e^- \rightleftarrows H_2 \qquad E^\circ = 0.00V$$

Numerous metal ions can be reduced from aqueous solutions to the metallic state in the presence of gaseous H_2 with proper adjustment of pH.

The electrochemical half-reaction and E° for borohydride ions are given by

$$B(OH)_3 + 7H^+ + 8e^- \rightleftarrows BH_4^- + 3H_2O \qquad E^\circ = -0.48V$$

Borohydride ions, however, should be employed judiciously, as they are known to reduce some cations to metal borides, particularly in aqueous systems.

Hydrazine hydrate is freely soluble in water, but since N_2H_4 is basic, the chemically active free-ion is normally represented as $N_2H_5^+$,

$$N_2H_4 \bullet H_2O \rightleftarrows N_2H_5^+ + OH^-$$

or in the case of hydrazine dihydrochloride.

$$N_2H_4 \bullet 2HCl \rightleftarrows N_2H_5^+ + H^+ + 2Cl^-$$

The standard reduction potential for the hydrazinium ion, $N_2H_5^+$, is

$$N_2 + 7H^+ + 4e^- \rightleftarrows N_2H_5^+ \qquad E° = -0.25V$$

In theory, the reduction of any metal with an E° more positive than -0.481 V or -0.23 V should be possible at room temperature, given a sufficient excess of reducing agent and proper control of pH. The metals that fall in the reduction potential range would expect to precipitate from solution, this obviously includes many first-row transition metal ions, such as Fe^{2+}, Fe^{3+}, Co^{2+}, Ni^{2+}, and Cu^{2+}, but also many second (Pd^+) and third-row transition metals (Au^+, Pt^+) as well as most post-transition elements and a few nonmetals. Other reducing agents like $NaB(Et)_3H$ and ethylene glycol and dimethylformamide (DMF) were also commonly used depending on the reaction solvent and metal. A brief survey of nanoparticles prepared by reduction from solutions is provide in Table 1

Table 1 Nanoparticulate Metals Synthesis by Wet Chemical Methods

Metal	Reactant	Solvent	Reductant	Stabilizer	Conditions	Products size	Ref
Fe	$Fe(OEt)_2$	THF	$NaB(Et)_3H$	THF	16h at 67ºC	10-100(nm)	(*22*)
Ni	$Ni(OAc)_2$	Ethanol Glycol	Ethanol Glycol	Ethanol Glycol	150-160 ºC	25 (nm)	(*23*)
Ag	$AgNO_3$	methanol	$NaBH_4$	MSA	25 ºC	1-6(nm)	(*24*)
Au	$HAuCl_4$	formamide	formamide	PVP	30 ºC	30(nm)	(*25*)
Pt	H_2PtCl_6	water	potassium bitartrate	TDPC	60 ºC	<1.5(nm)	(*26*)
Ni	$NiCl_2$	water	$N_2H_4 \cdot H_2O$ +	CTAB	60 ºC	10-36(nm)	(*27*)

			NaOH			
Cu	$CuSO_4$	water	$N_2H_4 \cdot H_2O$	SDS	~35(nm)	(*28*)

THF = tetrahydrofuran; MSA= mercaptosuccinic acid; PVP = poly(vinylpyrrolidone); CTAB = cetytrimethylammonium bromide;SDS = sodium dodecyl sulfate TDPC = 3,3'-thiodipropionic acid

Association of molecular units to nanoparticles introduces chemical functionalities that can provide recognition or affinity interactions between different appropriately modified particles and thereby dictate the structure when aggregation occurs. These chemically functionalized nanoparticles can be used as building blocks to assemble 2D and 3D nanolevel architectures(*29, 30*). However, even after years of development, it's still a challenge to find simpler and more economical methods for scale-up production of nanoparticles.

Decades ago scientists noticed that a lot of biological nanomaterials could be synthesized under ambient conditions in a microscopic-sized laboratory. Much of the recent interest in biological nanoparticle syntheses is based on the molecular self-assembly of nanoparticles. Most of this work stems from the 1996 report by Mirkin et al. who demonstrated that functionalized DNA is capable of the directing the self-assembly

of Au nanostructures into regularly spaced 2-D arrays (*31*). Protein molecules can also undergo self-assembly processes to form nanometer-scale structures at room temperature and atmospheric pressure(*32, 33*). For example, Pt nanoparticles could be nucleated by single DNA and protein molecules(*34*) and also, the tobacco mosaic virus was used as the template for the growth of $<$10 nm Pt, Au, and Ag nanoparticles into cylindrical aggregates (*35*). Some bacteria exhibit the capability to reduce metals as well, particularly those exhibiting high reduction potentials, such as Fe(III), Cr(VI), Mn(IV) and Co(III). (*36-39*) Even the reduction and mineralization mechanisms in biological environments are still not well understood yet, but this method has resulted in a large yield of some inorganic nanocrystals which includes ferromagnetic, calcium, silicon, etc.(*40*). It's observed that some plants have the capability to uptake gold from soil, as mining companies take advantage of this phenomenon to aid in the exploration process. It was reported recently that scientists use alfalfa plants to harvest gold nanoparticles by adding aqueous gold salt to the nutrient solution. It's found that this live alfalfa plant can extract gold from grown media and 4-5 nm Au nanoparticles were observed in the leaf cells (*41, 42*). Nanomaterials created by biological synthesis usually undergo self-assembly processes in vivo or in vitro and when covered by the biomolecules on the surface such as proteins and peptides become water soluble, this character is very important for the applying of inorganic nanoparticles in biotechnological engineering and medicine. Many biological molecules like DNA and proteins are fascinating macromolecular structures in terms of their distinctive recognition, transport, and catalytic properties. This smart recognition function can address the biological

nanomaterials to exact locations or targets on the surface(*43-47*) where their complementary recognition groups are marked. This conjugation technique provides new opportunities for the fabrication of nanodevices.

1.3 Nanotubes

Recently, much attention to nanotubes has been based on theoretical predictions of their expected unique properties. Basically there are two kinds of nanotubes, organic and inorganic. Organic nanotubes include polymer, lipid, surfactant and peptide nanotubes. Inorganic nanotubes include different metal and semiconductor nanowires/nanotubes such as gold, platinum, silicon, semiconductor and the biggest branch in the nanotube family, carbon nanotubes. In this dissertation one kind of organic nanotube, self-assembled amphiphilic peptide nanotubes, was used as the template to grow inorganic nanoparticles and form metallic nanowires. More details of this kind of nanotube will be discussed later in this chapter.

As one of the first widely investigated nanotubes, carbon nanotube were discovered in 1991 by the Japanese electron microscopist Sumio Iijima who was studying the material deposited on the cathode during the arc-evaporation synthesis of fullerenes (*48, 49*). Carbon nanotubes are cylindrical carbon molecules with extraordinary strength and unique electrical properties, and are efficient conductors of heat, which makes them potentially useful in a wide variety of applications (e.g. nano-electronics, optics, materials applications, drugs, catalysts etc.). There are two main types of carbon nanotubes: single-

walled nanotubes (SWNTs) and multi-walled nanotubes (MWNTs), which means they may have a single cylinder or two or more concentric cylinders. These carbon nanotubes are composed entirely of sp^2 bonds between carbon atoms, similar to graphite, stronger than the sp^3 bonds found in diamond, this bonding structure provides them with their unique strength. Carbon nanotubes naturally align themselves into "ropes" held together by Van der Waals forces. Under high pressure nanotubes can merge together trading some sp^2 bonds for sp^3 bonds giving great possibility for producing strong, unlimited-length wires through high-pressure nanotube linking. Due to these great properties, carbon nanotubes have attracted much interest and demonstrated the reality of the world of nanotechnology. It was recently demonstrated that the electrical conductance of semiconductor carbon nanotubes is highly sensitive to the change in the chemical composition of the surrounding atmosphere at room temperature due to the charge transfer between the nanotubes and the molecules from the gases adsorbed onto the nanotube surface. The hollow inner cylinder and large surface area of carbon nanotubes may make it possible for them to be the next generation of hydrogen storage system for the hydrogen fuel cell. Carbon nanotubes also have an important role in nanotechnology engineering due to their strength and flexibility. They have already been used as composite fibers in polymer and concrete to improve the mechanical, thermal and electrical properties of the bulk product. Motorola Labs recently announced significant progress in carbon nanotube technology. They found a way to develop a process to grow carbon nanotubes at low temperatures (*50*). This capability is important because the commercial materials with which they must bond, such as glass or transistors, are heat

sensitive. Motorola has also created a method to precisely place carbon nanotubes individually on a surface material, in addition to controlling their length and diameter. This innovation gives manufacturers the ability to design products, on a molecular level for the enhancement of specific characteristics.

Although carbon nanotubes have amazing physical and chemical properties that make them ideal building blocks for nanodevice fabrication and other applications, they are not easily soluble in most solvents, have relative dull surface activity and are difficult and costly to produce. These disadvantages limit their applications in the real world, especially in biotechnology. Alternatively, peptide nanotubes can be unexpensive, soluble, and more tunable surfaces and can be developed by both natural and synthetic chemistry (*51-54*). Peptide nanotubes can be constructed by highly convergent noncovalent bonds by which monomer peptide molecules rapidly self-assemble and organize into ultra-large well ordered three-dimensional structures, upon an appropriate chemical- or medium-induced triggering. The properties of the outer surface and the internal diameter of peptide nanotubes can be adjusted simply by the choice of the amino acid side chain functionalities and the size of the peptide subunit employed. Just like carbon nanotubes, certain kinds of peptide nanotubes also display electrochemical properties, but they are more hydrophilic and easier to fabricate and functionalize.

Peptide nanotubes based on carbohydrate amphiphilic monomers are becoming attractive because this kind of monomer can self-assemble to generate various morphologies, including micelles, rods and nanotubes, and the variability of these

dimensions depends on the composition of monomers and reaction conditions , including pH, temperature and solvents. This makes them the ideal building blocks for the engineering of nanodevices. For example, Ghadiri and co-workers(*53*) have developed a peptide nanotube assembly from the stacking of cyclic peptide monomers, while the diameter of the nanotube is regulated by simply changing the ring diameters or the side chains of the cyclic peptide monomers. Self-assembly of molecular aggregates into supramolecules via non-covalent interactions, such as hydrogen bonding and hydrophobic/hydrophilic interactions, has been widely observed. Since the peptides and proteins can efficiently assemble into exact shapes with certain functionalities in biological systems by means of their smart recognition functions, they have been studied as model systems for advanced supramolecular self-assemblies. To understand the assembly mechanism that can lead to more control of the nanotube dimensions, many researchers have done a lot of detailed work. Lynn and co-workers used a fibril lamination peptide monomer to form nanotube structures and examined the interactions of aromatic amino acid sequences to understand which amino acid and sequence are responsible for the tubular aggregation and what conditions will affect tubular formation (*55*). Also, Zhang et al. recently observed branched nanotubes formed from surfactant-like peptides containing a hydrophilic headgroup of charged aspartic acids and a lipophilic tail (*56*). In addition, it's verified that the tail sequence and charges on the peptide terminus can change the nanotube self-assembly.

In this dissertation, one type of peptide monomer, bola-amphiphile, was used to form the peptide nanotube which was first synthesized by Matsui and co-workers (*57*). This monomer, bis(*N*-α-amidoglycylglycine)-1,7-heptane dicarboxylate, has two amide head groups connected by a hydrocarbon tail group (Figure 1.1) and shows pH dependence during the self-assembly in aqueous solution. When this heptane bolaamphiphile monomer is dispersed in room temperature water at pH 8 for one week, it assembles into a helical ribbon. At pH 4.5, however, a tubular structure is observed. Synthesis of the heptane bolaamphiphile is described in reference (*58*). and in the appendix. The Raman spectrum shows that the formation of the nanotube or helical ribbon is due to the intermolecular hydrogen bonds between C=O stretches and amide N-H group. The tubule diameter is much smaller than the width of the helical structure and the figures suggest that the tubules are hollow.(*54, 57, 59*) Figure 1.1 shows the structure of the monomer and the assembly method of the nanotube under acidic solution.

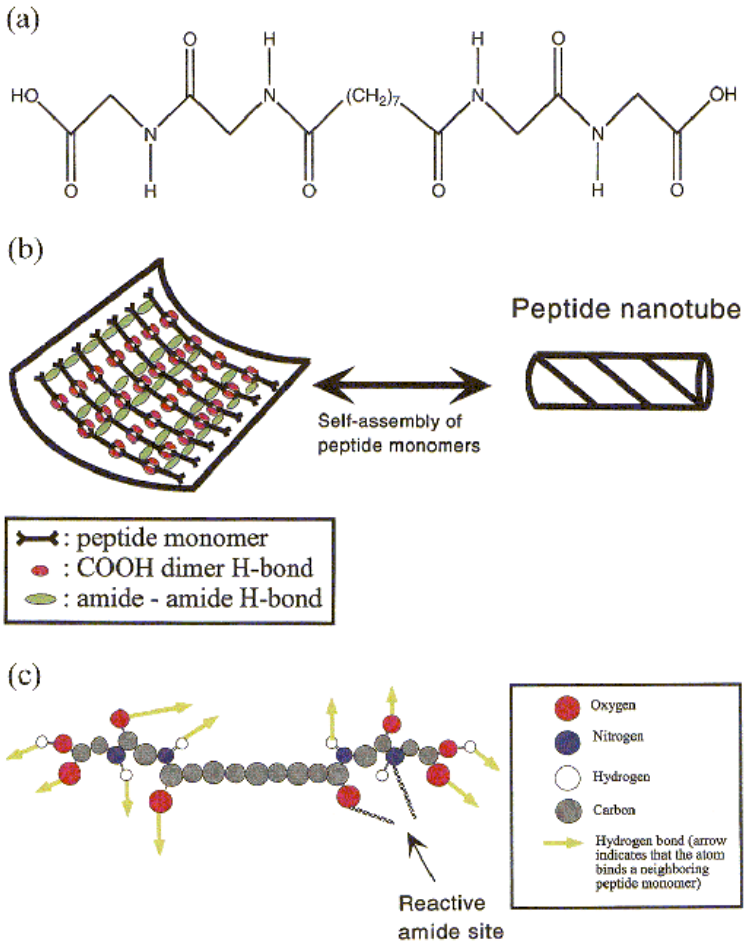

Figure 1.1 (a) Chemical structure of the peptide monomer, bis(N-α-amido-glycylglycine)-1,7-heptane dicarboxylate. (b) Self-assembled structure of the peptide nanotube. (c) Illustration of potential ion-chelating sites of the peptide nanotubes. Yellow arrows indicate that the atoms bind neighboring peptide monomers via hydrogen bonds.

Functionalization of this type of peptide nanotube can be achieved by anchoring functional molecules onto the nanotube surfaces via non-covalent bonding(*60*). The reason for the easy funtionalization of such peptide nanotube is that their free amide and carboxylate groups, which are not involved in nanotube self-assembly, can capture and

template biological molecules, such as DNA, synthetic peptides, proteins, porphyrins, azobenzenes, or other organic molecules via hydrogen bonding. (*43, 44, 60, 61*) As shown in Figure 1.2, a dye labeled Strepavidin was immobilized on this peptide nanotube via hydrogen bonding and as a result strong fluorescence was observed using the fluorescence microscopy.(*60*)

The free binding sites on the surface of the bola-amphiphile peptide nanotube allows them to be modified easily with antibodies/antigens, which could smartly navigate the nanotubes to antigen/antibodies-marked targets.(*62*) The nanotube surface could also be immobilized with synthetic sequenced peptides, known to biomineralize particular metals and semiconductors. The free binding sites make the amphiphile peptide nanotube a smart template for growing metals and semiconductor nanocrystals with tunable electronic and magnetic properties due to their controllable morphologies.(*63-67*)

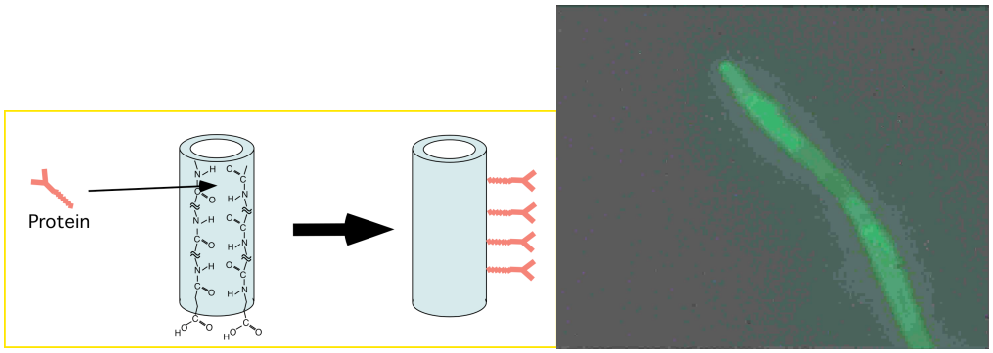

Figure 1.2 Scheme of protein-coating on peptide nanotube(Left) and Fluorescence micrograph of streptavidin-coated peptide nanotube(Right).

The functionalization of the bola-amphiphile peptide nanotube does not affect its structure and stability, which distinguishes this nanotube from other peptide nanotubes (*44, 60*). To apply this significant characteristic of the peptide nanotube in fabricating inorganic nanowires, different sequenced peptides are immobilized on the surface of template nanotubes to further grow the metal nanocrystals with specific morphology such as size, shape and packing density. It is commonly observed that many peptides and live cells are known to have the capability to mineralize specific types of metals and semiconductors (*52, 68-71*). For example, tobacco mosaic virus (TMV) is assembled from protein monomers with a stable viron nanostructure. The repeated polypeptide subunits in the TMV offer nucleation sites to produce highly crystalline semiconductor and metal coatings such as CdS, PbS, silica, iron oxides and Cu (*52, 72*). The biomineralization process will be discussed in the next section. Templated nanotubes with particular sequenced peptides therefore have the potential to be excellent templates for metal/semiconductor nanowire formation.

1.4 Biomineralization

In nature, biomineralization encompasses all mineral-containing tissues formed by organisms to fulfill a variety of different functions, such as in shells, skeletons and teeth, and these processes are usually carried out at near room temperature and in aqueous solutions. Crystal formation is often controlled in all its aspects, from their inception to their orientation, size, shape and assembly by functional proteins. The “active site” of a mineralized protein is the interface at which the biological macromolecules that control

mineral formation interact with the mineral surface. This control is achieved through the specialized proteins that recognize specific crystal surfaces during the growth of the crystals. It is known that histidine is one the key ligands in the metal-binding sites of the metalloproteinase, but the detailed mechanism of recognition processes during mineralization is still under exploration. The most well understood principle of the biomineralization process is that recognition is based on molecular complementarity between the protein and the defined phases of crystal structures. When the appropriate conditions occur, the nucleation and growth of the biomineral phase are almost always carefully and exquisitely controlled. These conditions include complex matrix biopolymers-preorganized supramolecular templates, which are associated to regulate a single, precise step in either the nucleation or the growth portion of the production of the mineral phase (*73*). The understanding of these processes is also relevant to research on advanced materials. Biomineralization processes can lead to the formation of precisely controlled inorganic-organic composites, in which the minute organic component exerts substantial control on the mineralization process, which results in the formation of particles with uniform size, novel crystal morphology, specific crystallographic orientation and interesting properties (*74, 75*). For example, seashells exhibit mechanical properties that are 1000 times greater than those of their inorganic component alone, due to the crystal structure and nucleation orientation (*76, 77*). CdS nanorods with controlled width and crystallographic orientation were synthesized by using negatively charged sugar-phosphate DNA as the biomineralization template resulting in the imprint of DNA molecules onto the inorganic crystal structures(*78*). The study of biomineralization offers

valuable insights into the scope and nature of materials chemistry at the inorganic-organic interface, which provides the basis for future innovations in the development highly efficient and/or unique materials synthesis strategies. Biomimetic design for the production of advanced composites with optimized properties has been explored and led to recent advances in materials design (*79, 80*). Some controlled nucleation and growth of nanocrystals was achieved based on molecular recognition at intrafaces or interfaces (*63*). These methods include template-directed crystallization under compressed Langmuir monolayers(*81*) on self-assembled monolayers or nanocomposite films, on particular peptides(*65*) and/or the membrane of bacteria (*82*). The simplest understanding of the binding mechanism between metal ions and synthetic or natural substrates is that the negative surface charge ensues from the COOH, N-H and PO(OH) groups on the biosubstrates at the neutral pH that can attract positively charged metal ions by electrostatic interactions. The presence of "matrix" proteins or other macromolecules (e.g. DNA) on the substrates are one of the keys for the crystal morphology, size and orientation. Morphological control can also be accomplished by adsorption of soluble additives onto specific faces of growing crystals, altering the relative growth rates of the different crystallographic faces leading to different crystal habits. A conventional approach called "selection from random sequences" has been used successfully for the selection of polypeptides with the function of mineralizing specific nanocrystals. In this approach, a molecularly diverse pool of peptides is first prepared by combinatorial polymerization of amino acids, after which clones possessing desired functions are selected from the pool (*83*). "Peptide-phage display," as one of the most popularly

employed applications of this methodology, and has helped scientists creat numerous polypeptides to specifically bind to a variety of inorganic materials such as Ag, Pt, Ti, Pd, Cr_2O_3, PbO_2, CoO, MnO_2, carbon nanotubes and zeolite. This technique provides plenty of resources for the construction of different inorganic nanomaterials for the purposes of research and further industrial applications.

Many researchers have realized that the design of templates is important for controlled mineralization of inorganic nanomaterials, especially for the biologic templates due to their mild experimental conditions and efficient reactions. The effects of pH, temperature, foreign inorganic ions, and the sequence of the peptides have been widely studied (*83, 84*). Current significant development of so-called "supermolecular chemistry" has shown great promise for the mineralization of nanomaterials. Jung and co-workers have used self-assembled superstructures of cyclohexane-based gelator as the template for the synthesis of new inorganic nanomaterials with controlled morphologies.(*85, 86*) DNA as the template for the mineralization and assignation of nanoparticles was also usually used for various inorganic materials (*31, 78*). Other than simplicity and rigidity, another advantage of DNA is it allows the convenient programming of artificial DNA receptors with any sequences. Alivisatos et al. have synthesized well-defined monoadducts from single nucleic acid moiety bonded gold nanoparticles by using the single-stranded DNA template that contains the complementary sequence stretches(*87*). A brief survey of nanomaterials produced by the biomineralization process is provided in Table 2.

Table 2 Examples of some inorganic nanomaterials synthesized via biomineralization

Materials	**Biotemplate**	**Material Size**	**Ref**
Au	Clostridium Botulinum	5-20 nm	(*88*)
Fe3O4	Shewanella putrifaciens	30-50 nm	(*89*)
Ag	AG4 peptide	100 nm	(*90*)
Silica sphere/ Rod	block copolypeptides	200μm	(*91*)
GaAs/InP	polypeptide	10-15 nm	(*92*)
ZnS	M13 bacteriophage	10-12 nm	(*93, 94*)
Zeolite	Polypeptide	14-21 nm	(*95*)
CdS	Polypeptide	Nanowire, 20 nm	(*96*)
FePt	M13 bacteriophage	Nanowire, 20 nm	(*94*)

The use of peptide nanotubes as templates also has the advantage of producing materials that cannot be produced by synthetic methods. For instance, Se nanotubes synthesized via a traditional solution-phase method possess a trigonal structure, whereas the protein cytochrome extracted from the bacteria *Desulfovibrio vulgaris* grew monoclinic Se nanotubes (*97, 98*). The prominence of this biomineralization with peptides can generally be accomplished under much more mild experimental conditions such as room temperature and atmospheric pressure, when compared to synthetic methods like CVD (*99*). These features are very important for industrial application in fabricating exotic nanowires, which are difficult and expensive to produce with existing technologies. If peptide nanotubes incorporate certain mineralizing peptide motifs at proper locations on the nanotube surface, efficient coating of the nanotubes with metal/semiconductor materials with controlled morphologies should be obtained. Peptide nanotubes assembled from synthetic peptide monomers with a diphenyalanine aromatic core grew Ag nanotubes inside their cavities, and then through the enzymatic degradation of the template Ag nanotubes were generated (*100*).

In this dissertation, peptide nanotube templates were synthesized by coating different sequenced peptides, which can specifically mineralize different metallic/nonmetallic ions. These sequenced peptides are chosen from phage display libraries or by other technologies. The synthesis of metal nanotubes by the peptide-nanotube templates are robust and useful. Due to their tunable morphologies, nanocrystal coatings on peptide

nanotubes have the potential to control physical properties of the resulting nanowires which could be used as building blocks in construction of electronic, optic and magnetic nanodevices. The next chapters will discuss the fabrication of Ag, Cu, Ni, Pt, ZnS nanowires by using bola-amphiphile peptide nanotubes as the template. All template nanotubes were first immobilized with specific sequenced peptides to mineralize the metal ions from the solution and then by changing the conditions of the solution such as pH, different morphologies of the metal nanoparticles were grown on the surface of template. The convergence of biotechnology and nanotechnology has resulted in the development of hybrid nanomaterials that incorporate the highly selective catalytic and recognition properties of biomaterials, such as proteins, enzymes and DNA, with the unique electronic, photonic, and catalytic features of nanoparticles. Biomaterials such as enzymes, antigens, antibodies, and biomolecular receptors have a similar size (2-20nm) compared with the dimensions of nanoparticles, making these two kinds of materials structurally compatible. The combination of nanoparticles or other nanoobjects with biomaterials could allow electronic or optical transduction of biological phenomena for the development of novel biosensors and other nanodevices (*101, 102*).

Depending on several fundamental features, bionanotechnologic approaches therefore be very important for nano-level architecture fabrication. Bionanomaterials could act as the framework for the nanostructures because of their specific and strong complementary recognition interactions. These biomaterials can provide binding sites for the nanoparticles assignment or can functionalize the surface of nanoparticles to make

them recognizable by the complementary partners. Biomolecules bonded to nanoparticles could then lead to biomolecule–nanoparticle recognition interactions and thus self-assemble into specific nanostructures and patterns. Due to the large surface-to-volume ratios and active surface, nanomaterials can serve as superior reactors and supporters for biologic and chemical reactions. Recently, peptide nanotubes have been used as the supports and reactor for enzyme catalysis.(*103*) The importance of functionalized nanoparticles for biotechnology applications cannot be overestimated, since they are already used for molecular imaging, drugs and drug delivery etc.

Chapter 2 Direct Growth of Shape-Controlled Nanocrystals on Nanotubes via Biological Recognition

2.1 Introduction

Nanocrystals have been studied extensively due to their tunability in electronic structures by adjusting their shapes, which naturally leads to significant interest in developing them as building blocks in catalytic, optical, and electronic applications.(*104*) While spherical/rod-shaped nanocrystals have received intensive attention, other interesting nanocrystal shapes are of special interest due to their novel physical properties. The shape control of nanocrystals has been achieved by inorganic approaches whereby the influence on the growth of particular nanocrystal faces at the nucleation stage controls the growth rate along different crystal axes and manipulates the shape of grown nanocrystals.(*105*) The influence toward particular faces of nanocrystals is mostly accomplished by capping these faces with organic surfactants. However, the binding specificity of organic surfactants toward particular crystalline faces is not well understood, and therefore it is still a challenge to choose appropriate capping agents to generate desired shapes of nanocrystals. Another challenge in applying nanocrystals to nanometer-scale devices is that it is necessary to assemble nanocrystals in certain matrices or on certain surfaces. Because multiple shapes of nanocrystals are frequently produced in this approach, this nanocrystal assembly requires an extra step to isolate the desired shape of nanocrystals. Whereas direct

growth of nanocrystals on surfaces will avoid those complications, the incorporation of nucleation sites and the shape control of nanocrystals are not trivial on surfaces.

Inspired by nature where various shapes of nanocrystals are produced accurately and reproducibly in biological systems, we report a biological approach to fabricate shape-controlled nanocrystals grown directly on surfaces. Here we demonstrate the direct growth of Ag nanocrystals in the hexagonal shape on sequenced peptide-coated nanotubes via biological recognition. The peptide sequence, Asn-Pro-Ser-Ser-Leu-Phe-Arg-Tyr-Leu-Pro-Ser-Asp (AG4), was found to recognize and effect the Ag nanocrystal growth on the (111) face via the combinatorial phage display peptide library (*90*).When this peptide was sequenced and incorporated onto template nanotube surfaces, the biomineralization of Ag ions on the nanotubes led the isotropic hexagon-shaped Ag nanocrystal coating under pH control (Figure 2.1).

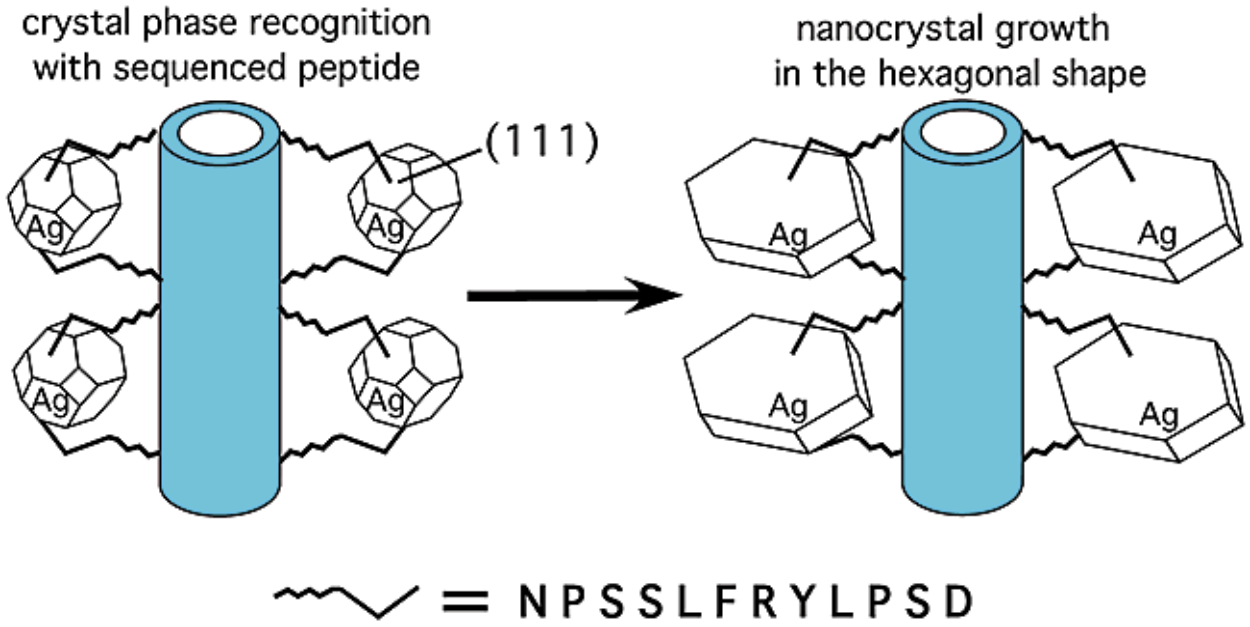

Figure 2.1 Scheme for Ag nanocrystal growth in the hexagonal shape on the template nanotubes. The sequenced AG4 peptide, incorporated on the nanotube surfaces, absorbs and reduces Ag ions to grow Ag nanocrystals. The AG4 peptide recognizes and effects the Ag growth on the (111) face and it controls the growth rate along different crystal axes and manipulates the shape of Ag nanocrystals.

In addition to the shape control of nanocrystals, nanocrystal-coated nanotubes are interesting in general due to their potential to serve as building blocks in optics, electronics, and sensor devices. Our strategy has an advantage that it does not require the self-assembling process of nanocrystals to organize them into the device configurations since the shape-controlled nanocrystals are grown directly on surfaces. Because the crystalline face recognition with peptides in particular sequences is much more specific than organic surfactants,(*90, 92*) the shape of resulting nanocrystals via this biological approach is also expected to be more controllable than the inorganic

approach once the peptide sequences, which can recognize specific faces of metals/semiconductors, are identified.

2.2 Experimental Section

Ag nanocrystals in the hexagonal shape were grown on template nanotubes, self-assembled from bis(*N*-α-amido-glycylglycine)-1,7-heptane dicarboxylate. The chemical process to synthesize and assemble the monomers into the template nanotube was described in the introduction (*57*). Those nanotubes in diameters of 20-200 nm were used as templates to grow shape-controlled Ag nanocrystals on the nanotube surfaces. After the template nanotubes were washed with distilled water twice, 0.5 mL of the template nanotube solution was incubated with 0.02 mL of the sequenced AG4 peptide (Asn-Pro-Ser-Ser-Leu-Phe-Arg-Tyr-Leu-Pro-Ser-Asp, 25 mM) in a buffer solution (pH = 7) for 24 h to immobilize it on the nanotubes. Since the template nanotube contains well-defined binding sites for proteins and peptides via hydrogen bonding, the AG4 peptide can be coated on the nanotubes in the simple incubation method. The immobilization of the AG4 peptide on the nanotube was verified by a confocal Raman microscope (LabRam, Jobin Yvon/Horiba). The AG4 peptide was sequenced by Applied Biosystems peptide synthesizer 432A and purified with Beckman 110 HPLC with the C-18 reverse phase column at the CUNY Gene Center. After the AG4 peptide immobilization on the nanotubes, 40 μL of $AgNO_3$ solution (30 mM) was incubated with the stirred peptide nanotube solutions between

pH 4 and 10 to grow Ag nanocrystals on the nanotubes. The Ag nanocrystal growth on the nanotubes was monitored via the Ag ion incubation time from 0.5 to 96 h by TEM and UV-vis spectroscopy.

2.3 Results and Discussion

When the template nanotubes were incubated with the AG4 peptide in a pH 7 buffer solution for 1 day, the AG4 peptide was immobilized on the nanotube surface, confirmed by a Raman microscope. As shown in Figure 2.2.

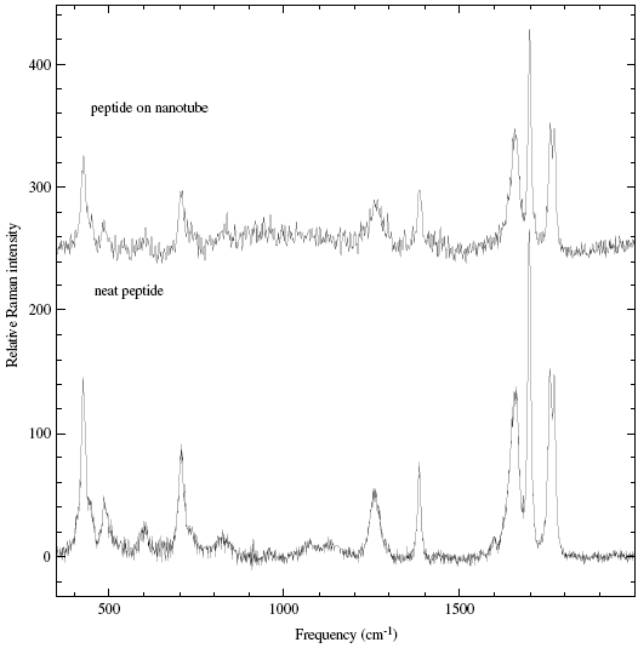

Figure 2.2 Raman spectra of the AG4 peptide coated on the nanotubes (above), and the neat peptide (below) in aqueous solution.

Ag ions were then absorbed and reduced simultaneously by the AG4 peptide on the nanotubes when $AgNO_3$ was incubated in the nanotube solution. The resulting Ag nanocrystals on the nanotubes were observed to be isotropic hexagonal plates at pH = 7. The Ag nanocrystals appeared on the nanotubes within 0.5 h after Ag ions were incubated in the nanotube solution, and the size of Ag nanocrystals increased as the ion incubation time increased (Figure 2.3a). Ag nanocrystals were grown to 14 nm in diameter after 14 h, as seen in transmission electron micrograph (TEM) in Figure 2.3b. The magnified TEM image in the inset of Figure 2.3b shows the isotropic hexagonal shape of Ag nanocrystals on the nanotube. Figure 2.3c and the tilted TEM image of Figure 2.3b indicate that those Ag nanocrystals are hexagonal plates, and the thickness is determined as 3 nm from the edge image shown in the right side of the Ag nanocrystal in Figure 2.3c. It should be noted that other Ag nanocrystal shapes were also observed when the AG4 peptide mineralized Ag ions without the template nanotubes in suspension (*90*). Therefore, the nanotube surface seems to have an influence on regulating the majority of Ag nanocrystals into the hexagonal shape, while the exact shape-controlling mechanism on the nanotubes is not clear at this point. Hexagon-shaped Ag nanocrystals were grown to 50 nm in diameter after 72 h (Figure 2.3d), and then further nanocrystal growth was not observed at longer ion incubation, as shown in Figure 2.3a. Hexagon-shaped Ag nanocrystals were also observed to grow on the nanotubes whose diameters were equivalent to the diameter of Ag nanocrystals after 72 h of the Ag ion incubation (Figure 2.3e). The electron diffraction pattern of Ag nanocrystals in the hexagonal shape (inset in Figure 2.3e)

shows the highly crystalline structure. While the plasmon band of hexagon-shaped Ag nanocrystals on the nanotubes red-shifted as the size of nanocrystals increased (Figure 2.4), those spectra indicate the distinctive electronic structures of hexagon-shaped Ag nanocrystals compared to spherical Ag nanocrystals in the similar size domains (*106*).

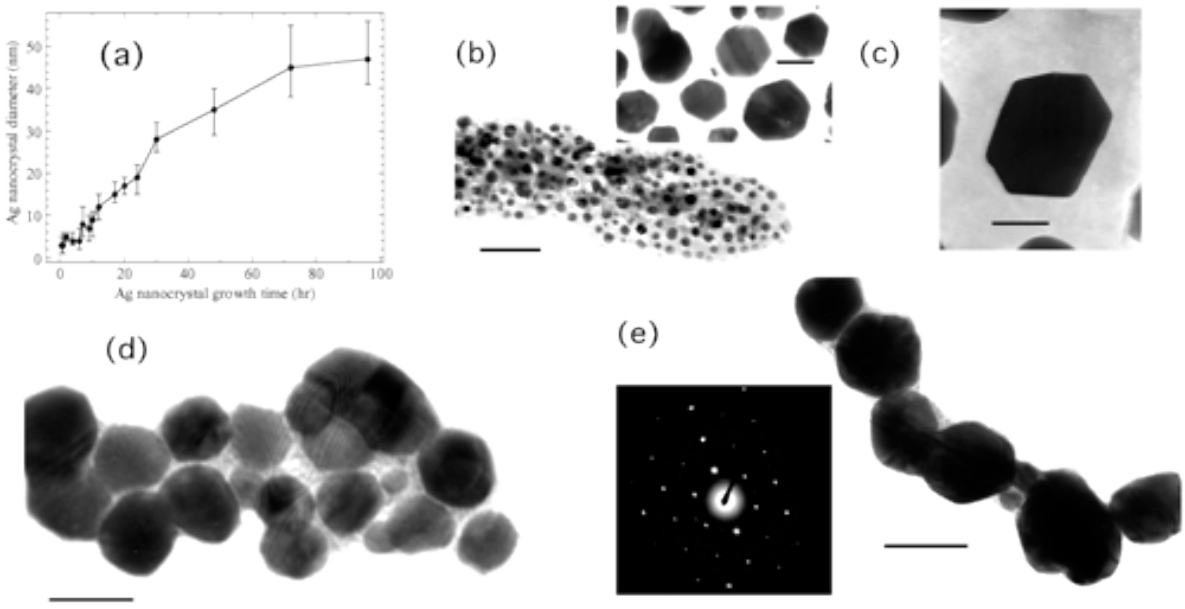

Figure 2.3 (a) The correlation between the size of Ag nanocrystals and the nanocrystal growth time in the pH 7 growth solution. (b) TEM image of hexagon-shaped Ag nanocrystals on the nanotube after 14 h in the pH 7 growth solution. Scale bar = 100 nm. Inset: Highly magnified TEM image. Scale bar = 15 nm. (c) Tilted TEM image of the hexagon-shaped Ag nanocrystal on the nanotube after 14 h in the pH 7 growth solution. Scale bar = 10 nm. (d) TEM image of hexagon-shaped Ag nanocrystals on the nanotube after 72 h in the pH 7 growth solution. Scale bar = 50 nm.

(e) TEM image of hexagon-shaped Ag nanocrystals on the smaller nanotube after 72 h in the pH 7 growth solution. Scale bar = 50 nm. Inset: the electron diffraction pattern showing (111), (011), and (100) faces.

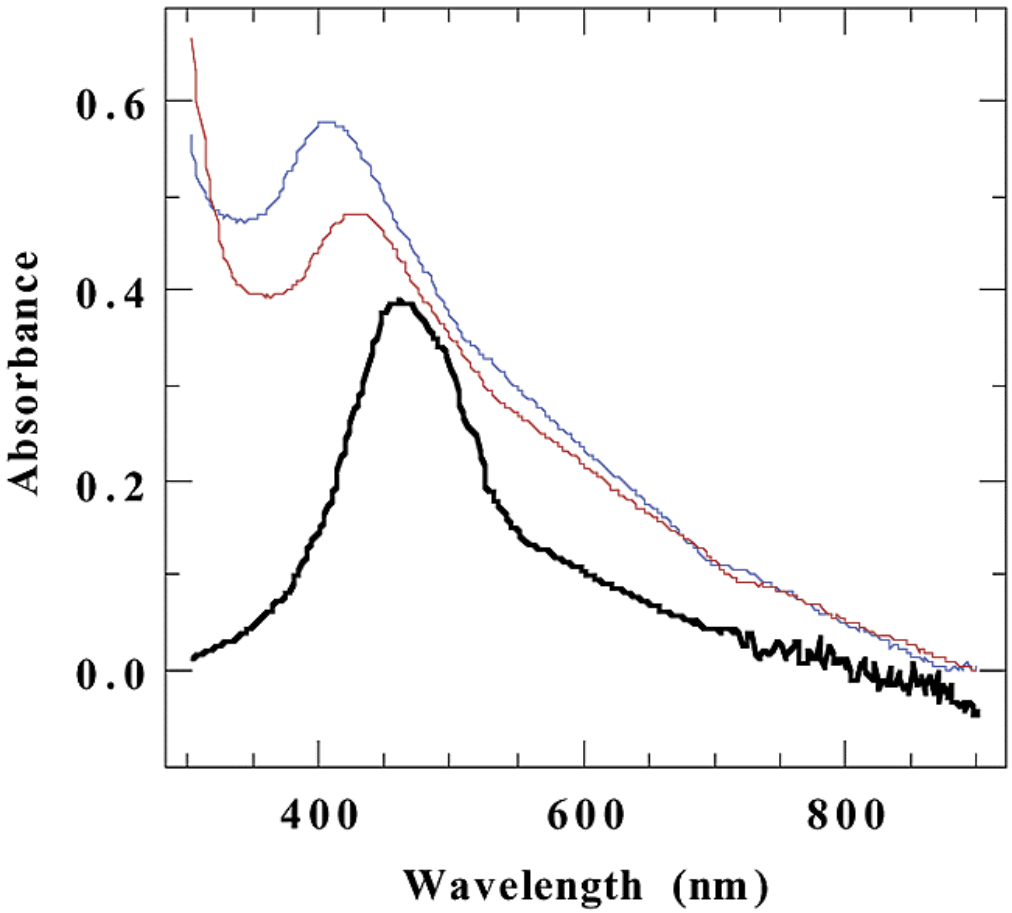

Figure 2.4 UV/vis spectra of hexagon-shaped Ag nanocrystals on the nanotubes in the diameters of 5 nm (blue), 14 nm (red) 50 nm (black).

To confirm the effect of the AG4 peptide nanotube on the shape control of Ag nanocrystals, two control experiments were examined. As the first control experiment, Ag nanocrystals were grown on the template nanotubes without the AG4 peptide, reduced by hydrazine hydrate for 14 h at pH = 7. Under this condition, Ag nanocrystals were observed to coat the nanotube surfaces only partially (Figure 2.4a), whereas Ag nanocrystals fully coated the AG4 peptide-functionalized nanotubes at pH = 7 in the same Ag ion incubation time (Figure 2.3b). For the second control experiment, a different peptide with the same number of amino acids as the AG4 peptide whose sequence is not designed to recognize the (111) face of Ag nanocrystals was immobilized on the template nanotubes, and the shape of Ag nanocrystals on those nanotubes was compared to that of nanocrystals grown on the AG4 peptide nanotubes. When the HG12 peptide (His-Gly-Gly-Gly-His-Gly-His-Gly-Gly-Gly-His-Gly) was sequenced and immobilized on the template nanotubes in the same condition as the AG4 peptide coating, both spherical and hexagonal shapes of Ag nanocrystals were observed on the HG12 peptide nanotubes after the 72 hr-incubation of Ag ions and reduction with hydrazine hydrate (Figure 2.5b), while the shape of Ag nanocrystals was regulated to hexagonal shapes on the AG4 peptide nanotubes in the same experimental conditions (Figure 2.3d). It should be noted that the longer incubation did not affect the shape and the size of the Ag nanocrystals. Therefore, these comparisons indicate that the AG4 peptide certainly has a significant effect on the growth and the shape of Ag nanocrystals on the nanotubes. Because the free-standing AG4 peptide without the nanotube produced multiple Ag nanocrystal

shapes (*90*), the shape control on the nanotube may be observed by the reduction of the AG4 peptide aggregation due to the peptide immobilization at the discrete binding sites on the nanotube.

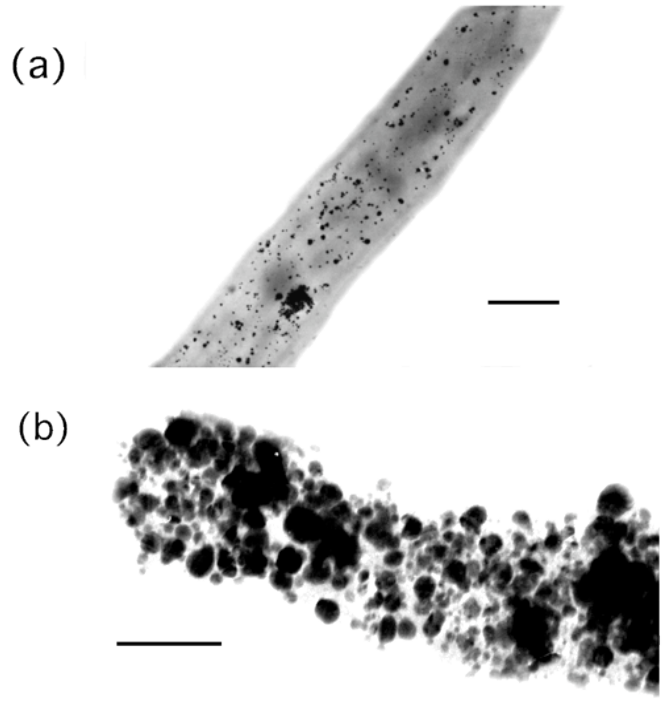

Figure 2.5 TEM images of Ag nanocrystals on the nanotubes (a) without incorporating the AG4 peptide on the surfaces after 14 h in the pH 7 growth solution. Scale bar = 100 nm. (b) with the HG 12 peptide on the surfaces after 72 h in the pH 7 growth solution. Scale bar = 100 nm

When Ag nanocrystals were grown on the peptide nanotubes in pH < 7 growth solutions, hexagon-shaped nanocrystals were still grew with more polydispersity. However, a striking difference was observed when the pH of growth solutions was over 7. Under this basic condition, Ag nanocrystals grew faster and smaller on the

nanotubes, and their diameters were around 15 nm after 9 h of the Ag ion incubation (Figure 2.6), Further growth of Ag nanocrystals was not observed for the longer growth period (Figure 2.7).

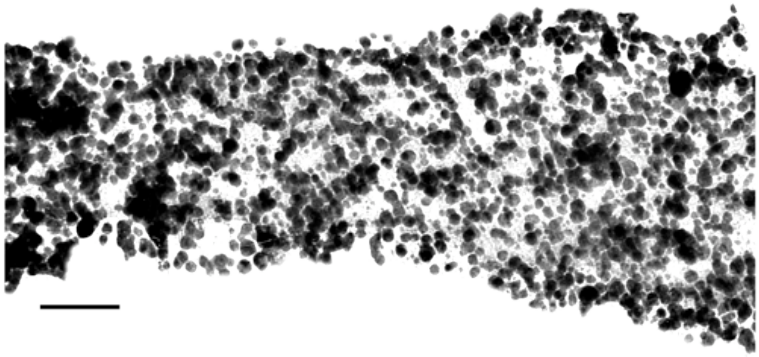

Figure 2.6 TEM image of Ag nanocrystals on the nanotubes after 72 h in the pH 9 growth solution. Scale bar = 50 nm.

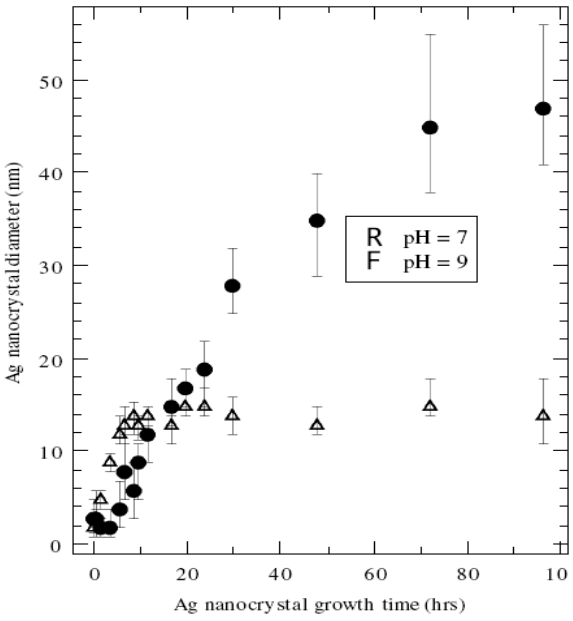

Figure 2.7 The correlation between the size of hexagonal Ag nanocrystals and the nanocrystal growth time in the pH 7 growth solution (•) in the pH 9 solution (Δ).

Because the efficiency of electron donation from the amino acids in the AG4 peptide toward Ag ions generally increases as pH increases, the shape and the size of Ag nanocrystals are not under control due to the faster growth rate in basic conditions. The hexagon-shaped nanocrystal formation around pH = 7 is also explained by the crystal growth kinetics that Ag nanocrystals grow slowly enough to form into larger hexagonal plates around the isoelectric pH = 6.09 under the influence of the AG4 peptide. This mechanism is supported by a control experiment to accelerate Ag nanocrystal growth in the presence of an excess reducing agent in the growth solution. When Ag nanocrystals were grown at pH = 7 for 72 h with hydrazine hydrate, hexagon-shaped Ag nanocrystals in the diameter of 50 nm were no longer observed.

Instead, Ag nanocrystals were limited to grow only up to 15 nm in diameter under this growth condition (figure 2.8). This outcome suggests that the acceleration of Ag ion reduction rate due to the addition of the reducing agent decreases the size of Ag nanocrystals on the nanotubes via the faster growth rate, which is consistent with the proposed growth mechanism.

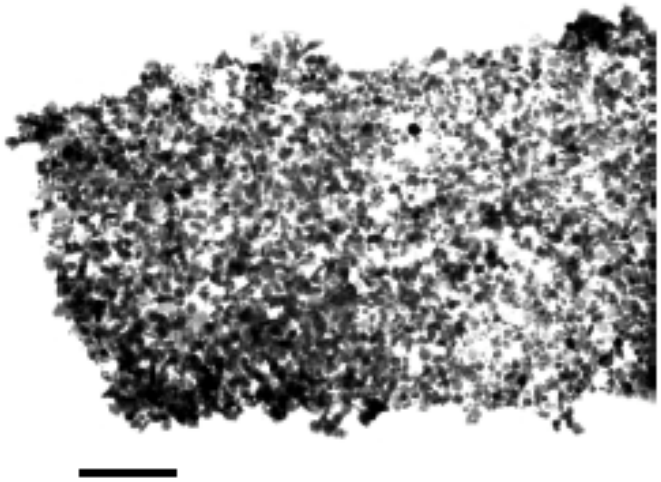

Figure 2.8 TEM image of Ag nanocrystals on the nanotubes after 72 hrs in the presence of an excess reducing agent, hydrazine hydrate, in the pH 7 growth solution. Scale bar = 40 nm.

2.4 Conclusion

Hexagon-shaped Ag nanocrystals were grown directly on the peptide nanotubes by means of biological recognition and biomineralization against Ag ions with the

sequenced AG4 peptide on the nanotube, which has a significant influence in the Ag nanocrystal growth on the (111) face. The pH value of the growth solution is necessary to be controlled around 7 to form isotropic Ag nanocrystals in the hexagonal shape on the nanotubes because the pH value has a significant effect on the growth rate of Ag nanocrystals.

Chapter 3 Incorporation of sequenced peptides on nanotubes for Pt coating: smart control of nucleation and morphology via activation of metal binding sites on amino acids

3.1 Introduction

Non-lithographic and bottom-up approaches for nanometer-sized device fabrication are of considerable interest, and the development of smart building blocks for such nanodevices will contribute significantly to advances in nanotechnology (*107*). Applying biological molecules as the building blocks is a promising approach in nanodevice fabrications due to their biomolecular recognition function, which can be used for their targeted immobilization and selective semiconductor/metal coatings (*84, 90, 92*). For example, DNAs have been immobilized at specific locations with the complementary sequences patterned on surfaces to interconnect multiple electrodes, and subsequent metallization of the bridging DNA nanowires configured simple electric circuits (*47*). A similar fabrication technique was also demonstrated by metallized protein nanotubes bridging electrodes *via* protein acceptor–ligand receptor interactions (*108, 109*). The biomolecular recognition incorporated in nanocomponents can also be applied to efficient chemical sensors and catalysts because of the high surface-to-volume ratio of the nanocomponent assembly, which allows target molecules to contact with the surfaces effectively (*5, 16*). In all cases, it

is necessary to control the biomineralization of biological nanocomponents to obtain desired electrical, magnetic, optical, and catalytic properties.

While various DNA, peptide, and protein nanowires were recently biomineralized to produce metallic nanowires (*96, 110, 111*), morphology control of these metallic coatings has not been well established yet. If the morphology of a metallic coating can be regulated by controlling the surface coverage of coated nanocrystals on the biological nanowires, it will be possible to produce nanowires with tunable electronic properties from semiconducting to metallic by varying the packing densities of nanocrystals (*112*). Since biological systems routinely control size, shape, and morphology of nanocrystals with high reproducibility and efficiency due to the high specificity of peptide sequences toward specific biomineralization(*90, 113*) , a smart choice of the peptide sequence on nanotubes could allow one to control the morphology of metal coatings under controlled external conditions such as pH, temperature, and salt concentration.

Here, we demonstrate that a short histidine-rich peptide, His-Pro-Gly-Ala-His, incorporated on the peptide nanotube, anchored Pt ions and produced Pt nanocrystals on the nanotubes after reducing the Pt ions. Histidine is one of the most important amino acids in metal–protein binding systems because many metalloenzymes contain histidine as active sites to bind metal ions.(*114*) The interaction between noble metal ions and histidine-containing peptides has also been studied extensively as model systems to understand functions of metalloproteins in nerve diseases such as

Parkinson's disease (*115*) . The peptide sequence, His-Pro-Gly-Ala-His, was previously reported to have high affinity toward Pt ions (*116*), and we synthesized and incorporated this histidine-containing peptide on the nanotubes in this study to anchor Pt ions efficiently for Pt nanocrystal nucleation. The procedure to produce the Pt nanocrystal coatings on the peptide nanotubes is illustrated in Figure 3.1. After the sequenced peptide was immobilized on the peptide nanotubes *via* amide–amide hydrogen bonding (step I in Figure 3.1), Pt(II) ions formed complexes with specific amino acids on the nanotubes as a function of pH (step II in Figure 3.1).

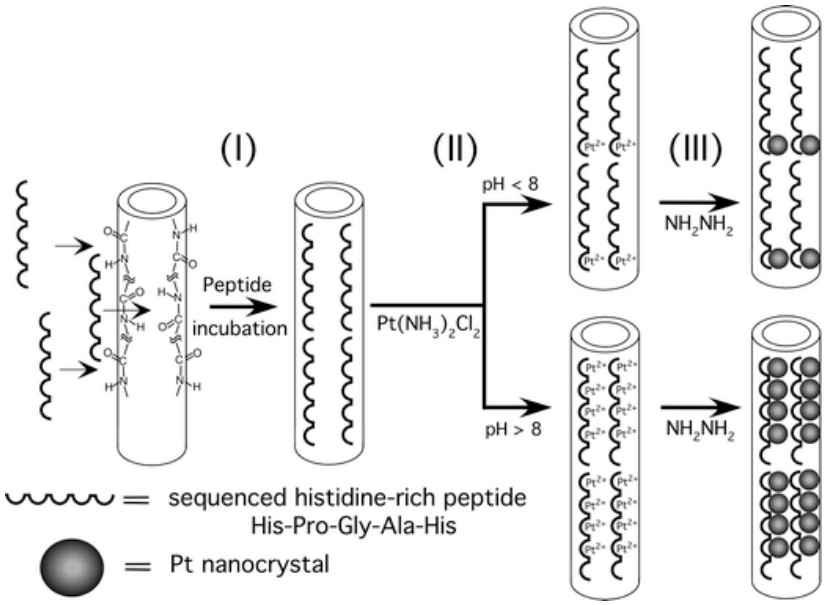

Figure 3.1 Procedure to fabricate Pt nanotubes: (I) immobilization of the sequenced peptide on the template nanotubes. (II) Anchoring Pt ions on the sequenced peptide on the nanotubes. Pt ions bind one amino acid in pH< 8 solutions while Pt ions bind four amino acids in pH > 8 solutions. (III) Pt nanocrystal growth on the peptide nanotubes by reducing anchored Pt ions

It has been reported that the affinity between Pt ions and amino acids depends on pH values of peptide solutions (*117*). For example, carboxylate oxygens in histidine bind Pt ions under acidic conditions while imidazole nitrogens in histidine and amide nitrogens in alanine and glycine have higher affinity toward Pt ions under basic conditions(*116*) . Therefore, the surface coverage of Pt nanocrystals, or the morphology of the Pt coating, on the nanotubes is expected to be controllable as a function of pH because the peptide nanotubes have higher density of Pt nucleation sites under basic conditions, as shown in Figure 3.1. These Pt ions on the peptide nanotubes were then reduced by hydrazine hydrate to generate Pt nanocrystals (step III in Figure 3.1). While narrow dispersed Pt nanocrystals of average diameter of 12 nm were grown on the peptide nanotubes in pH < 8 solutions, the Pt coating became nearly continuous when Pt ions were incubated and reduced in pH > 8 solutions. This type of dynamic transition in morphology between discrete and continuous nanocrystal coatings *via* pH change was not observed in the case of Au nanocrystal growth on the peptide nanotubes(*64*) . The distribution of Pt ion-binding sites in the sequenced peptide seems to play an important role for the morphology change of Pt nanocrystals on the peptide nanotubes between acidic and basic conditions after reducing Pt ions. The growth mechanism of Pt nanocrystals on the peptide nanotubes as a function of pH is proposed in the discussion section.

3.2 Experimental Section

Template nanotubes for immobilization of the sequence peptide were self-assembled from the bolaamphiphile peptide monomer, the same as what we used in Chapter 1. The bolaamphiphile peptide monomers (10 mM) were self-assembled into nanotubes in a pH 4.5 citric acid–NaOH solution after 2 weeks. After the template nanotubes were washed thoroughly with distilled water, 0.5 mL of the nanotube solutions were mixed with buffer solutions between pH 4–10 in centrifuge tubes respectively, and then 25 μL of the sequenced peptide, His-Pro-Gly-Ala-His, (25 mM) was added to each solution and allowed to stand for 48 h. The immobilization of peptide on the nanotubes was confirmed by Raman microscopy (LabRam, Jobin Yvon/Horiba). Then 25 μL of *cis*-(diamine)platinum(II) dichloride, $Pt(NH_3)_2Cl_2$ (50 mM), was added to the peptide nanotube solution to immobilize Pt ions on the nanotube surface *via* Pt–peptide complexation. After 24 h of the Pt ion incubation, 25 μL of a reducing agent, hydrazine hydrate, ($NH_2NH_2 \cdot H_2O$ 50 mM) was added and the samples vortexed for 1 h. After the samples were allowed to stand for 24 h, Pt nanocrystals grown on the peptide nanotubes were studied by transmission electron microscopy and electron diffraction (JOEL Model 1200 EX). As a control experiment, a Pt coating was also examined on non-functionalized nanotubes without incorporating the sequenced peptide. The peptide, His-Pro-Gly-Ala-His, was made at an Applied Biosystems Peptide Synthesizer 432A and purified with Beckman 110

HPLC with C-18 reverse phase column at the CUNY Gene Center. Other chemicals were obtained from Sigma–Aldrich.

3.3 Results and Discussion

Previously, the freestanding histidine-rich peptide, His-Pro-Gly-Ala-His, was reported to bind Pt ions at distinct binding sites, which depend upon pH (*116*) . For example, carboxylate oxygens in histidine bind Pt ions in acidic solutions, while imidazole nitrogens in histidine bind Pt ions in basic solutions. To probe the binding mechanisms between Pt^{2+} and the peptide on the nanotubes, the peptide nanotubes incubated with Pt^{2+} at various pH values were investigated by Raman microscopy. Figure 3.2(a) shows a Raman spectrum of Pt^{2+}-immobilized peptide nanotubes in a pH = 4 solution while Figure 3.2 (b) shows a Raman spectrum of Pt^{2+}-immobilized peptide nanotubes in a pH = 10 solution. It should be noted that all Raman spectra of the Pt^{2+}–peptide nanotube complexes in pH 4–7 solutions are identical to that of Figure 3.2(a) while the Raman spectra in pH 8–10 solutions correspond to Figure 3.2(b). In Figure 3.2(a), a sharp peak at 1596 cm^{-1} is assigned as a carbonyl stretch mode of COO^{-} –Pt (*118*). Peaks at 1037, 1148, 1161 and 1377 cm^{-1} are assigned as δC–H, νNCN, δN–H and ring breathing modes of imidazole in histidine free from Pt binding, respectively (*119*). Based on those vibrational assignments, under acidic conditions, the carboxylate oxygen in histidine on the peptide nanotube binds Pt^{2+} while the imidazole nitrogen in histidine on the nanotube does not bind Pt^{2+}. This

binding scheme is consistent with the previous observation for the Pt^{2+}–peptide complex in suspension at lower pH values (*116*). On the other hand, the binding mechanism between Pt^{2+} and the peptide nanotubes is quite different under basic conditions. In pH > 8 solutions, Pt ions bind imidazole nitrogens in histidine instead of the carboxylate oxygens, as observed in the appearance of the in phase C=O/C–N stretch mode of N(amide)–Pt–N(His) at 1435 cm^{-1} and in the disappearance of the 1596 cm^{-1} carbonyl peak in Figure 3.2 (b) (*120, 121*). While all imidazole peaks observed under acidic condition are absent in Figure 3.2(b), a new COO^- peak free from Pt binding appears at 1092 cm^{-1} in this spectrum (*119*). This observation indicates that Pt ions bind the imidazole nitrogens but they no longer bind carboxylate oxygens under basic conditions. Appearance of an amide III peak at 1264 cm^{-1}, red-shifted due to Pt binding, also suggests that Pt ions bind amide nitrogens in alanine and/or glycine.(*119*) However, when the peptide nanotubes are in pH 4 or 10 solution without Pt ions, neither the carbonyl stretch mode of COO^-–Pt (pH 4) nor the in phase C=O/C–N stretch mode of N–Pt–N (pH 10) was observed in the corresponding Raman spectra in Figure 3.2(c) and (d). Therefore, those control experiments also support the vibrational assignments in Figure 3.2(a) and (b). The conclusions derived from these Raman spectra are summarized in Figure 3.3. In this illustration, a dotted arrow indicates the Pt binding site on the peptide nanotube under acidic conditions and solid arrows show the Pt binding sites under basic conditions. Figure 3.3 shows that there are more nucleation sites for the Pt nanocrystal growth on the peptide nanotube under basic conditions.

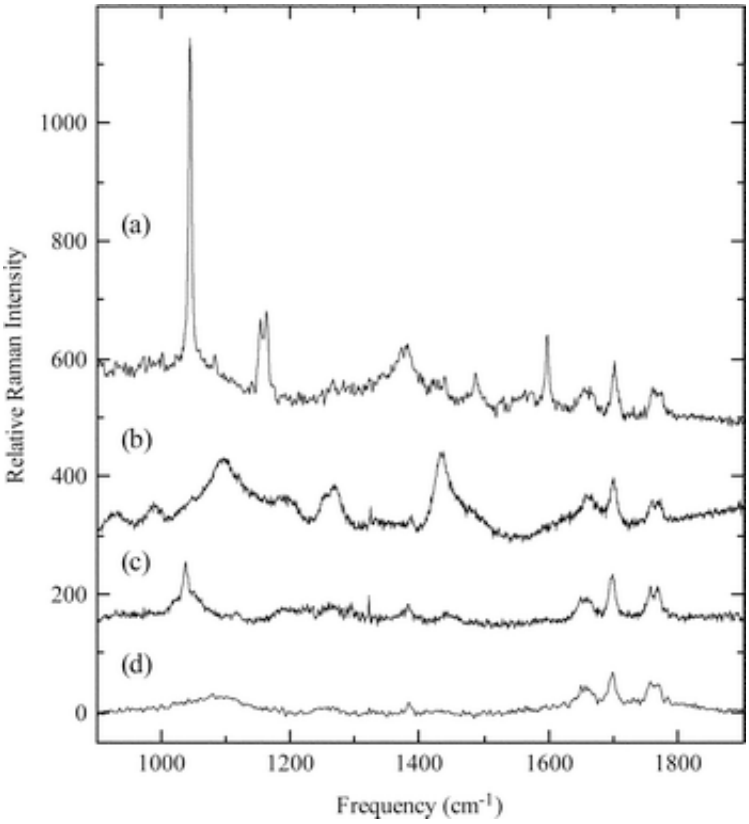

Figure 3.2 Raman spectra of (a) Pt^{2+}-immobilized peptide nanotubes in pH = 4 solution, (b) Pt^{2+}-immobilized peptide nanotubes in pH = 10 solution, (c) peptide nanotubes in the absence of Pt ions in pH = 4 solution and (d) peptide nanotubes in the absence of Pt ions in pH = 10 solution

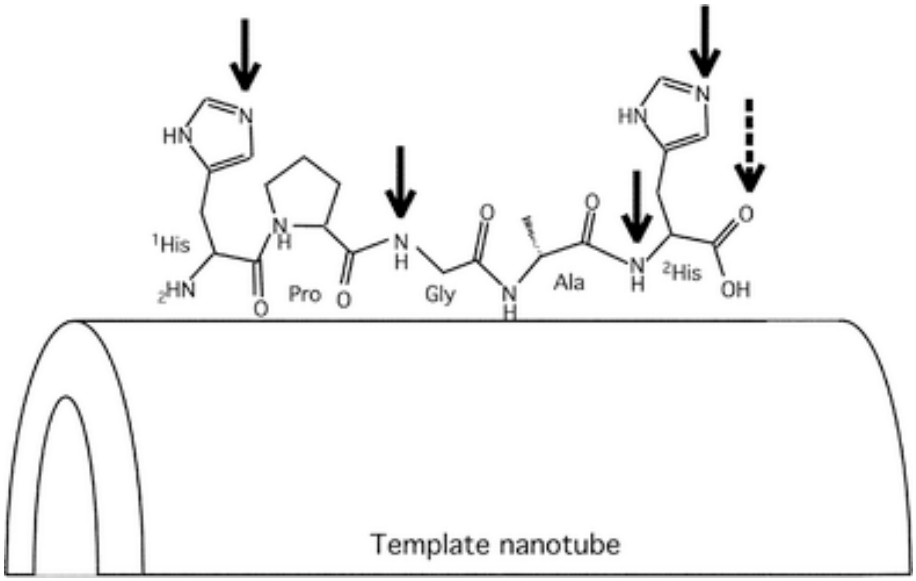

Figure 3.3 Illustration of the sequenced peptide binding Pt ions on the nanotubes. The dotted arrow indicates carboxylate oxygen in histidine as the Pt binding site on the peptide nanotube under acidic conditions. Solid arrows show imidazole nitrogens in histidine and amide nitrogens in alanine and glycine as the Pt binding sites under basic condition.

When Pt ions on the peptide nanotubes were reduced by hydrazine hydrate, Pt nanocrystals were observed on the nanotube surfaces as shown in Figure 3.4. Under acidic conditions, the TEM image shown in Figure 3.4(a) reveals that Pt nanocrystals grown on the peptide nanotubes at pH = 4 and these nanoparticles dispersed in very narrow range with an average diameter of 12 nm. The nanocrystal size and the surface coverage (~65%) are consistent among the Pt nanotubes grown in the pH 4–7 solutions. The electron diffraction pattern of Pt nanocrystals on the peptide nanotube, inset in Figure 3.4(a), shows (100), (200) and (210) phases for a face-centered cubic crystal. When Pt coatings were developed on the peptide nanotubes under basic

conditions, the Pt coating was nearly continuous, as shown in TEM image in Figure 3.4(b). The surface coverage change of Pt nanocrystals as a function of pH is summarized in Figure 3.4(c). The lattice structure of the Pt coating on the peptide nanotubes under basic conditions (inset in Figure 3.4(b)) is identical to that under acidic conditions (inset in Figure 3.4(a)). It needs to be noted that all the incubation time at different conditions are constant.

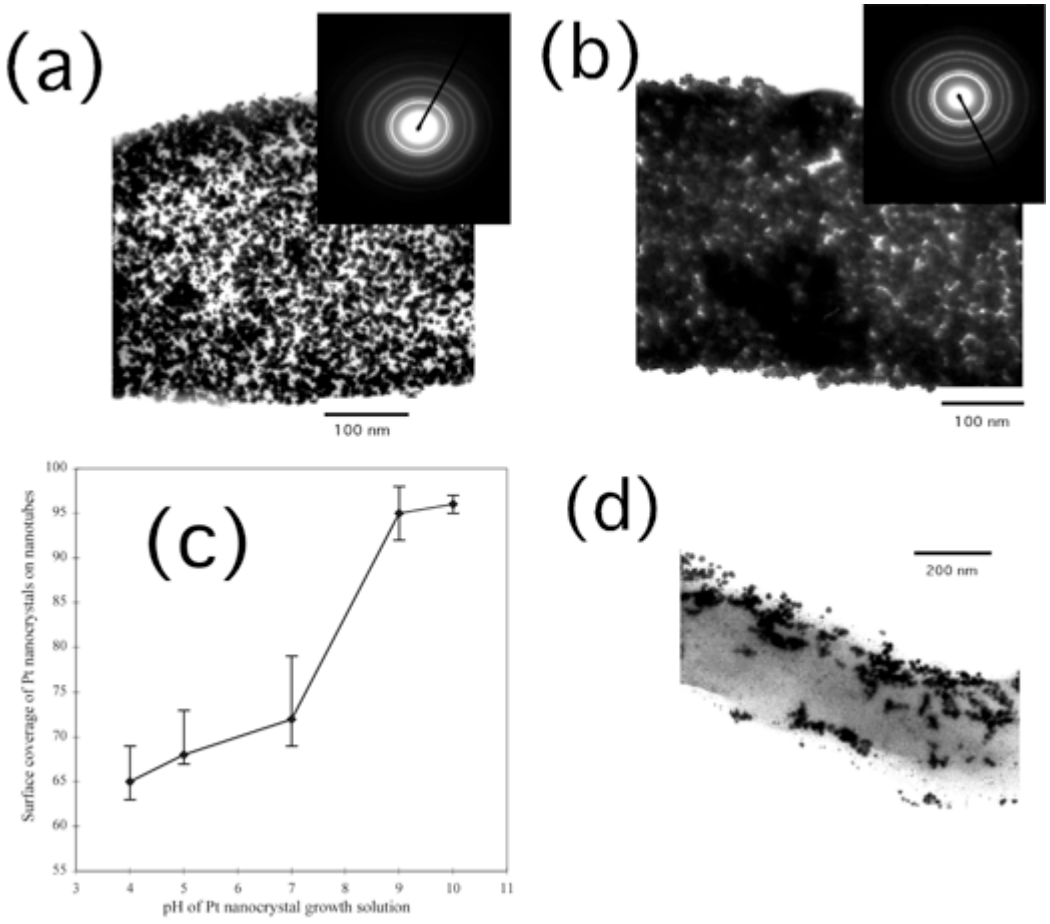

Figure 3.4 TEM images of (a) Pt nanocrystals grown on the nanotubes at pH = 4 (inset: electron diffraction of the Pt nanocrystals), (b) Pt coating

grown on the nanotubes at pH = 10 (inset: electron diffraction of the Pt coating). (c) The correlation between the surface coverage of Pt nanocrystals and pH of the growth solution. (d) TEM image of Pt nanocrystals grown on the non-functionalized nanotubes at pH = 4.

To confirm that the sequenced peptides on the nanotubes have significant influence on the morphology of Pt coating, a control experiment to grow Pt nanocrystals on the nanotubes without incorporating the sequenced peptide was examined. When Pt ions were incubated in the non-functionalized nanotube solution at pH = 4 and reduced by hydrazine hydrate, the coverage of Pt nanocrystals on the nanotubes was significantly diminished (Figure 3.4(d)), as compared to the Pt nanocrystals grown with the sequenced peptide (Figure 3.4(a)). This reduced coverage of Pt nanocrystals on the non-functionalized nanotubes was also observed in the pH = 10 solution. While the diminished Pt coating on the nanotubes suggests that glycines of the neat nanotubes still bind Pt ions, the reduced area of the Pt coating on the non-functionalized nanotubes seems consistent because generally histidine has a higher affinity toward Pt ions. This control experiment indicates that the amino acid, His-Pro-Gly-Ala-His, is necessary to be incorporated on the nanotubes to produce uniform and narrow dispersed Pt nanocrystal coatings on the nanotubes.

Under basic conditions, more amino acids were observed to bind Pt ions as compared to acidic conditions in the Raman spectra. As more nucleation sites are available for Pt nanocrystal growth under basic conditions, it is reasonable to observe much denser Pt nanocrystal coatings on the peptide nanotubes in the pH > 8 solutions.

We hypothesize that the continuous phase is likely observed due to the diffusion of Pt nanocrystals on the peptide nanotube surfaces. This hypothesis is supported by the electron diffraction patterns in Figure 3.4(a) and (b) that crystalline structures of Pt coatings developed under both acidic and the basic conditions are identical. While we still do not have concrete evidence for the mechanism to control the morphology of the Pt coating on the peptide nanotubes as a function of pH, the Pt growth mechanism is proposed based on the comparison with the previous outcome in Au nanocrystal coatings on peptide nanotubes (*64*). When Au nanocrystals were grown on the template nanotubes incorporating a sequenced peptide, Ala-His-His-Ala-His-His-Ala-Ala-Asp, after reducing Au ions, Au nanocrystals were grown with a uniform diameter of 6 nm in the entire pH range from 4 to 10. The Au nanocrystal coating did not become continuous even under basic conditions in this system because Au nanocrystals grow between the incorporated peptides on the nanotube, which bind the nanotube surfaces periodically at a distance of 6.4 nm. In other words, this periodic spacing of peptides prevents the diffusion of Au nanocrystals on the peptide nanotubes. In the case of the Pt coating, the sequenced peptide is likely laid down on the nanotube surface as illustrated in Figure 3.3 and it does not maintain the discrete binding geometry as observed in the case of the Au nanocrystal growth because this geometry will allow Pt nanocrystals to diffuse on the nanotube surface in order to aggregate in to a continuous phase. This peptide binding conformation may be induced by the shorter peptide sequence for the Pt nanocrystal growth.

3.4 Conclusion

The sequenced peptide, His-Pro-Gly-Ala-His, was immobilized on template nanotubes, and the biomolecular recognition efficiently anchored Pt ions to nucleate Pt nanocrystals on the nanotubes. When Pt ions were incubated in the peptide nanotube solutions at pH < 8, Pt ions bound carboxylate oxygens of histidine and subsequent reduction of the complexes produced narrow dispersed Pt nanocrystals with an average diameter of 12 nm on the peptide nanotubes. When Pt ions were incubated in the peptide nanotube solutions at pH > 8, Pt ions were anchored to imidazole nitrogens in histidine and amide nitrogens in alanine and/or glycine and the reduction of those Pt ions led to a continuous Pt coating on the peptide nanotubes. The higher Pt ion concentration on the peptide nanotubes under basic conditions seems to nucleate Pt nanocrystals more efficiently, and then the diffusion of Pt nanocrystals on the nanotube surfaces may induce a continuous phase. This simple biological method to control the morphology of Pt coatings from discrete to continuous phases *via* pH change may be used to tune band gaps of the nanotubes, which can be applied as smart building blocks in nanometer-scaled electronics and sensor devices. This type of biomineralization technique will also provide a clean and reproducible manner to produce metallic/semiconductor nanowires due to efficient nanocrystal formation

Chapter 4 Cu Nanocrystal Growth on Peptide Nanotubes by Biomineralization: Size Control of Cu Nanocrystals by Tuning Peptide Conformation

4.1 Introduction

The size and shape of nanocrystals have significant effects on catalytic, optical, and electronic properties (*105, 122-125*). To apply nanocrystals as building blocks for practical electronic, magnetic, and optical devices, nanocrystals must be assembled. Although various nanocrystals have been assembled on flat substrates(*7, 126*), the self-assembly of nanocrystals on cylindrical nanotube surfaces has also been reported recently (*69, 109, 127, 128*). When the coupling strength of overlapped wave functions between neighboring nanocrystals is tuned by compressing the lattice of nanocrystals, the range of tuning the electronic structures is considerable because the overlap depends exponentially on the interdot distance and the size(*129*). If nanocrystals can be formed on nanotube geometry in controlled diameters and packing densities, one may be able to produce nanotubes with tunable electronic properties from one type of nanocrystal. Although this type of material is expected to serve as a smart building block to interconnect nanometer-sized electronic components in microelectronics and biological/chemical sensors, the controls of nanocrystal size and packing density are not straightforward on nanotubes.

Biological systems control mineralizations and nanocrystal synthesis of various metals in exact shapes and sizes with high reproducibility and accuracy (*33, 84, 130*). Therefore, it is logical to use biological nanotubes as templates on which to grow narrow dispersed nanocrystals by biomineralization. Complexation of metals and histidine-containing peptides has been studied extensively because their high affinities to metal ions damage central nervous systems by altering peptide conformations into abnormal forms, and this protein deformation may cause Parkinson's disease and Alzheimer's disease. Therefore, a nanotube form of sequenced histidine-rich peptides has potential to serve as an efficient template for metallic nanotube synthesis, because the specific sequences of peptides mineralize specific metals/semiconductors to produce highly crystalline nanocrystals (*70, 90*). In addition, the peptide conformations and charges on nanotubes, which can be controlled by experimental conditions such as pH, ion concentration, and temperature, determine the size and packing density of nanocrystals (*92, 131*). Therefore, the size and packing density of nanocrystals on histidine-rich peptide nanotube surfaces are potentially controlled by simply tuning those experimental conditions. Because metallic nanocrystals in diameters <10 nm are in the size domain to observe a significant conductivity change by tweaking the nanocrystal size (*7, 132*), this system may be developed to a conductivity-tunable nanotube-building block.

By applying this principle, we have mineralized Au nanocrystals on the sequenced peptide [Ala-His-His-Ala-His-His-Ala-Ala-Asp (HRE)]-functionalized

nanotubes, and the packing density of Au nanocrystals was controlled by pH of the growth solution. Although the charge-distribution change of the sequenced HRE peptides by pH change controlled the Au nanocrystal-packing density, the Au nanocrystal size was constant over various pH values, because the conformation of HRE peptide could not be altered by pH change because of the stiffness of HRE peptide backbone.

Here we present Cu nanocrystal growth on the nanotubes functionalized by a histidine-rich peptide, whose sequence is His-Gly-Gly-Gly-His-Gly-His-Gly-Gly-Gly-His-Gly (HG12). The fabrication process is illustrated in Figure 4.1. In brief, the sequenced HG12 peptides were immobilized onto amide groups of the template nanotubes, self-assembled from bolaamphiphile peptide monomers(*57*), by hydrogen bonding Figure 4.1a (*60*). Then, the HG12 peptides coordinate Cu(II) as the nucleation site Figure 4.1b for further Cu nanocrystal growth by reduction of trapped ions Figure 4.1c. This peptide sequence has been reported to fold into multiple conformations by coordinating Cu ions at various positions, dependent on pH values (*115*). Therefore, the HG 12 peptide, immobilized on the nanotube surfaces, has potential to control the size of Cu nanocrystals due to the flexible conformations by way of pH change. Indeed, we observed that the pH change altered the HG12 peptide conformation and the grown Cu nanocrystal size on the nanotube, shown by Fourier transform IR spectroscopy and transmission electron microscopy (TEM). Although the self-assembly of Cu nanocrystals on flat substrates has been studied extensively

for microelectronic, sensor, and catalytic applications (*124, 133*), this study is a previously uninvestigated example of growing narrow range disperse and isotropic Cu nanocrystals on the nanotube surfaces by biomineralization.

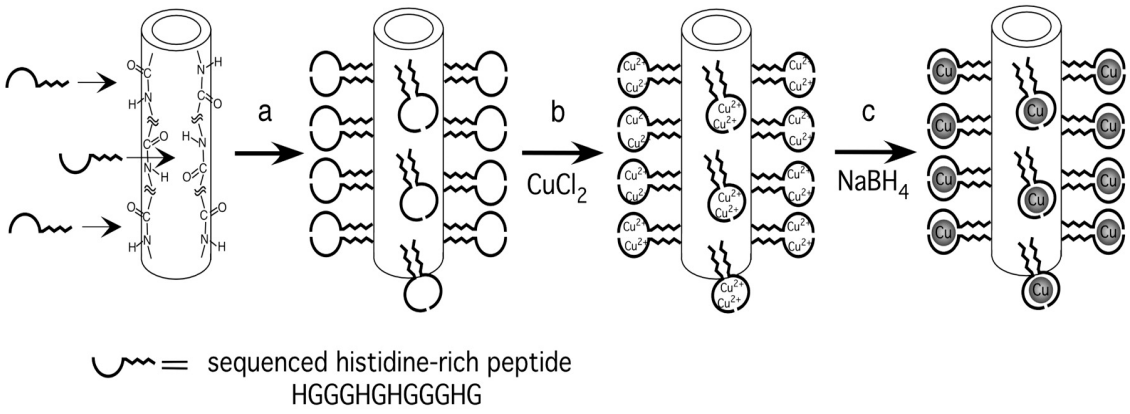

Figure 4.1 Scheme of the Cu nanotube fabrication. (a) Immobilization of the sequenced HG12 peptide at the amide-binding sites of the template nanotubes. (b) The Cu ion–HG12 peptide complexation on the nanotube surfaces. (c) Cu nanocrystal growth on the nanotubes nucleated at Cu ion-binding sites after reducing trapped Cu ions with $NaBH_4$.

4.2 Experimental Section

To prepare templates for the Cu nanocrystal coating, bis(*N*-α-amido-glycylglycine)-1,7-heptane dicarboxylate molecules (10 mM) were self-assembled into nanotubes in a citric acid/ NaOH (pH 5.5) solution. Details of this bolaamphiphile peptide monomer synthesis and the nanotube self-assembly have been described in previous chapters (*57, 134*). The HG12 peptide was synthesized by Applied Biosystems Peptide Synthesizer 432A and purified by using Beckman 110

HPLC equipped with a C-18 reverse-phase chromatographic column at the Center for Study of Gene Structure and Function, City University of New York. To immobilize the HG12 peptide on the template nanotubes, 50 µl of the HG12 peptide solution (25mM) in buffer was incubated to 100 µl of the nanotube solution, and the HG12 peptides were bound on amide sites of the nanotube surfaces by means of hydrogen bonding Figure 4.1a. The reaction mixture was then stirred slowly for 24 h, the coated nanotubes were washed with deionized water to remove any unbound HG12 peptides, and then centrifuged for 30 min (14,500 rpm) to collect the HG12 peptide-coated nanotubes. The HG12 peptide coating on the nanotubes was confirmed by using a Raman microscope and atomic force microscope. To grow Cu nanocrystals on the HG12 peptide nanotubes, 50 µl of 50 mM $CuCl_2$ solution was added to the peptide nanotube solution to form Cu(II)–HG12 complexes on the nanotubes to create Cu nanocrystal nucleation sites Figure 4.1b. The concentration of Cu(II) was maintained at a metal-to-ligand ratio of 1:1 [0.0012 mM Cu(II)], and the pH was varied between 4 and 10 to study the pH effect on Cu nanocrystal growth. In all cases, the reaction mixtures were allowed to sit undisturbed overnight under nitrogen to complete Cu-ion immobilization on the nanotubes. The Cu(II) on the peptide nanotubes was then reduced by 50 µmol of $NaBH_4$ to produce Cu nanocrystals Figure 4.1c. This reduction step was carried out under nitrogen, and the resulting solutions were aged for 24 h after reduction with sodium borohydride. After 24 h, the nanotubes were washed with nanopure water and then centrifuged twice to remove the excess reducing agent and nanocrystals that were not coated on the nanotubes. The nanotube

solutions (3–5 μl) were then dropped on TEM grids for further analysis by TEM (model JEOL 1200 EX). Two sets of control experiments were carried out as follows. In the first set, Cu nanocrystals were grown directly on the neat nanotubes at pH 6 with no HG12 peptides coating on the nanotubes. The experimental condition was the same as above except that no HG12 was coated on the nanotubes before incubating Cu ions. In the second set, 50 μl of 50 mM $CuCl_2$ solution was incubated with 50 μl of the peptides in buffer solutions of pH 6 and pH 8 under nitrogen in the absence of the nanotubes. These solutions were then reduced by sodium boronhydride and washed in the same procedure as above. These samples were analyzed by TEM.

4.3 Results and Discussion

Because the charge distribution of histidine changes dramatically at about pH 6, the HG12 is expected to undergo a significant conformation change below and above pH 6. When Cu nanocrystals were grown on the HG12 peptide nanotubes between pH 4 and pH 6, the Cu nanocrystals were dispersed very narrowly and packed in high density as shown in the TEM image in Figure 4.2a Left. Inset, a magnified TEM image, shows the isotropic Cu nanocrystal shape at pH 6. In this pH range, the Cu nanocrystals were grown in an average diameter of 10 nm(Figure 4.2b Right), determined by the TEM images. The electron-diffraction pattern of Cu nanocrystals on the nanotubes shows (111) and (220) planes for a face-centered-cubic crystal (Figure 4.2a Center). The diffraction pattern of copper oxide was not observed in

Figure 4.2a, and the HG12 peptide seems to protect the Cu nanocrystals on the nanotubes from oxidation (*131, 133*).

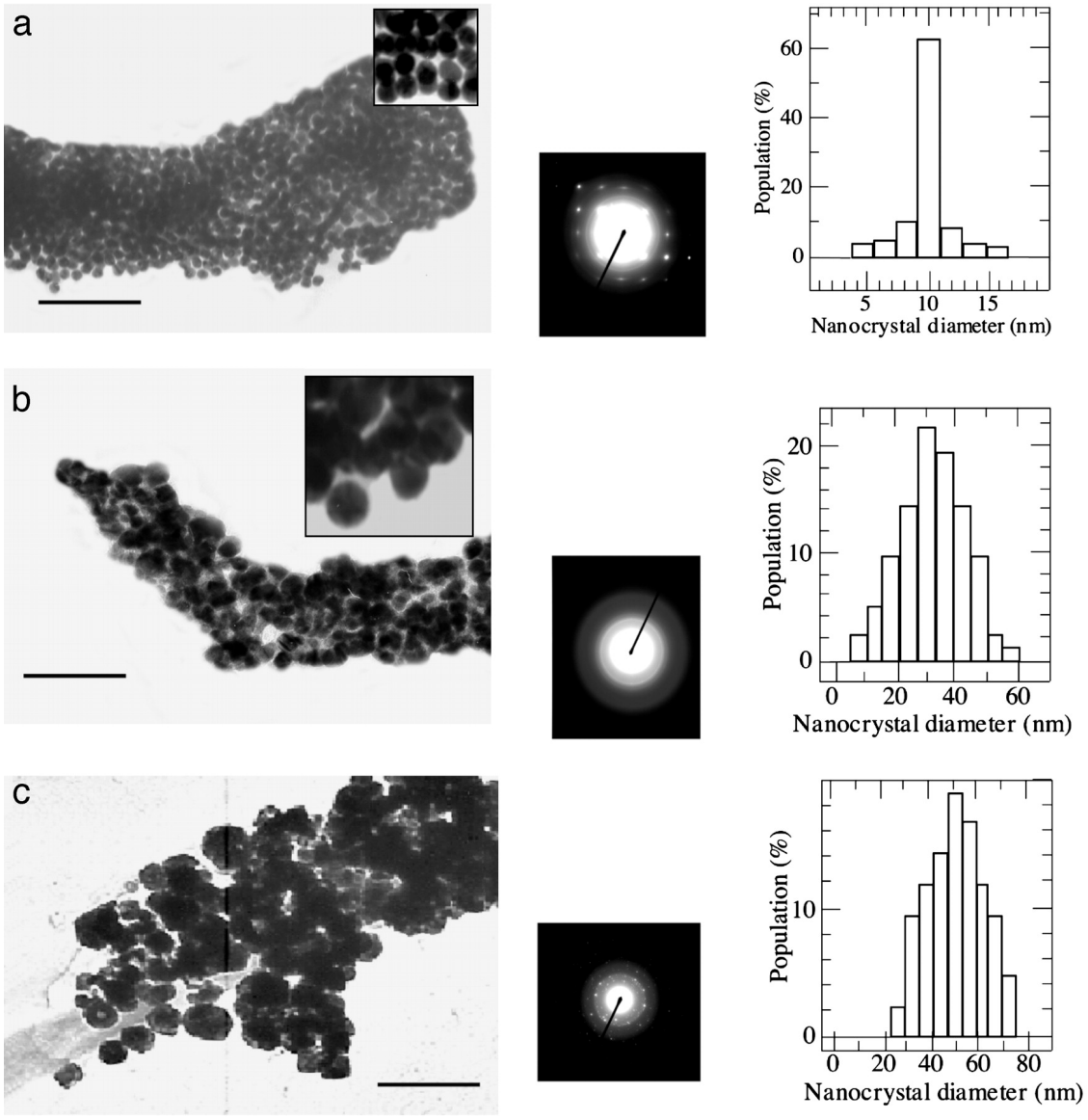

Figure 4.2 (a) Cu nanocrystals grown on the nanotube at pH 6. (Left) TEM image. (Center) Electron-diffraction pattern. (Right) Size distribution. (Inset) The TEM image in higher magnification. (b) Cu

nanocrystals grown on the nanotube at pH 8. (Left) TEM image. (Center) Electron-diffraction pattern. (Right) Size distribution. (Inset) The TEM image in higher magnification. (c) Cu nanocrystals grown on the nanotube without the HG12 peptide at pH 6. (Left) TEM image. (Center) Electron-diffraction pattern. (Right) Size distribution. (Scale bar = 100 nm.)

A striking difference in Cu nanocrystal growth was observed when the HG12 peptide nanotubes with Cu(II) were reduced between pH 7 and pH 10. In this pH range, the average diameter of Cu nanocrystals was increased to 30 nm (Figure 4.2b Left). Although the statistical size distribution of Cu nanocrystals in the basic condition is dispersed in narrow range in general (Figure 4.2b Right), those Cu nanocrystals were less monodisperse than the Cu nanocrystals grown in the pH range between 4 and 6. The electron-diffraction pattern of Cu nanocrystals grown on the HG 12 peptide nanotubes at pH 8 (Figure 4.2b Center) shows that the crystallinity of those Cu nanocrystals is equivalent to the Cu nanocrystals in the acidic condition except for the orientation of nanocrystals, which is more aligned in the acidic condition. The significant difference of electronic structures between the 10-nm Cu nanocrystal-coated nanotube and the 30-nm Cu nanocrystal-coated nanotube was also observed in UV-visible absorption spectra (Figure 4.3). The absorption maximum of the 30-nm Cu nanocrystal-coated nanotube, 620 nm (Figure 4.3b), was shifted to 585 nm for the 10-nm Cu nanocrystal-coated nanotube (Figure 4.3a). This comparison indicates that the Cu nanocrystal size on the nanotubes, controlled by the pH change, may result in altering the electronic property of nanotube.

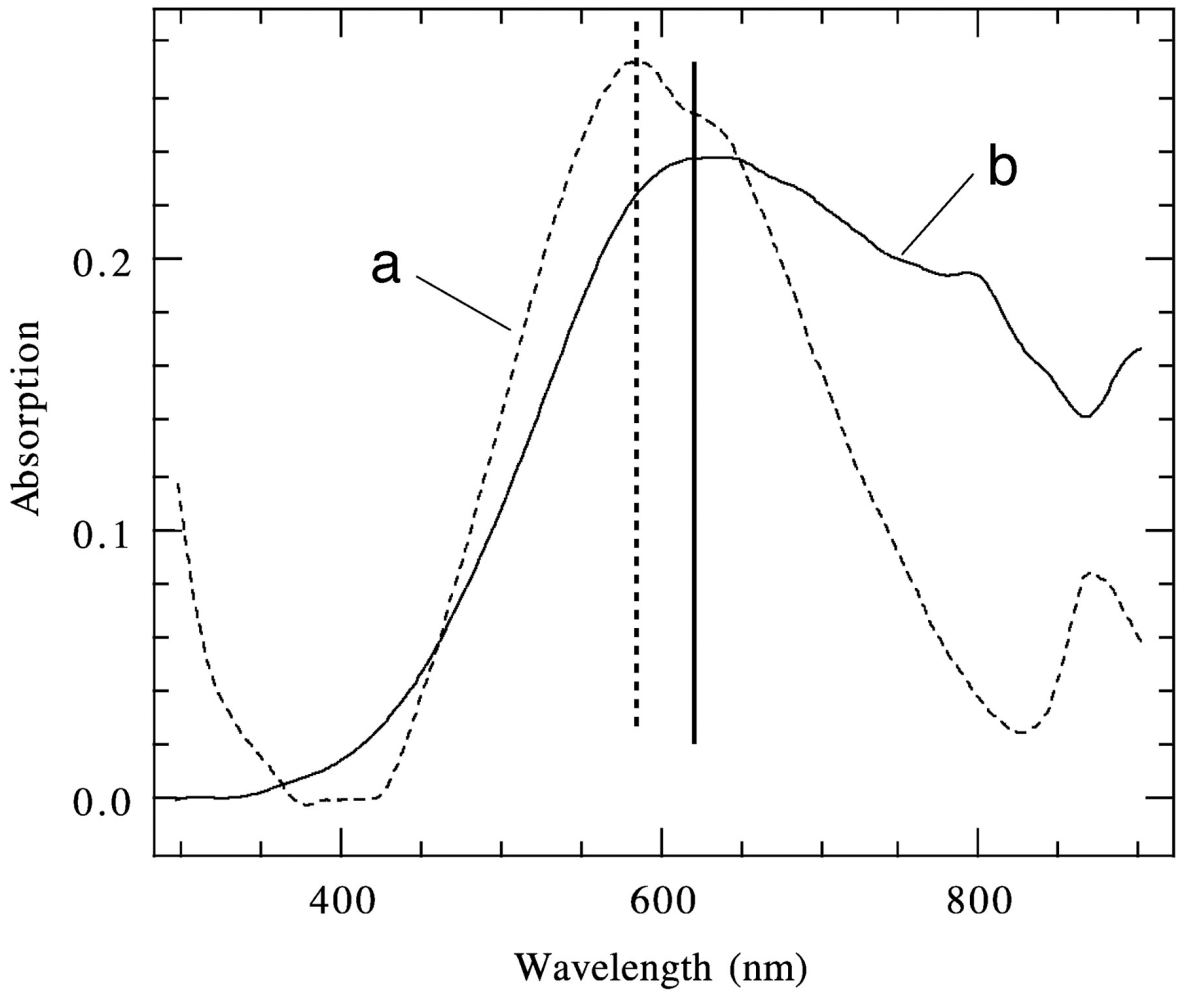

Figure 4.3 UV-visible spectra of the nanotubes coated with Cu nanocrystals in a diameter of 10 nm, grown in pH 6 solution (dotted line) (a) and Cu nanocrystals in a diameter of 30 nm, grown in pH 8 solution (solid line) (b).

To confirm that the HG12 peptide plays a role in controlling the size of Cu nanocrystals on the nanotube, we examined a control experiment to grow Cu nanocrystals on the template nanotubes without the HG12 peptide at pH 6 in the same procedure described above. The Cu nanocrystals were grown in much larger sizes, 50

nm in an average diameter, and they were polydisperse, as shown in Figure 4.2c Left and Right. The Cu nanocrystals grown without the HG12 peptide are less oriented, as shown in the diffraction pattern (Figure 4.2c Center). The comparison between Figure 4.2 a and c indicates that the HG12 peptide on the nanotube certainly regulates the size and the dispersity of Cu nanocrystals.

Another control experiment was examined to confirm the role of template nanotubes in the Cu nanocrystal growth. This time, we produced Cu nanocrystals in the HG12 peptide solution without the template nanotubes. The TEM image in Figure 4.4a shows Cu nanocrystals grown in the HG12 peptide solution at pH 6. The average diameter of Cu nanocrystals was 14 nm grown in the pH 6 growth solution, which is similar to the size of Cu nanocrystals formed on the HG12 peptide nanotubes. But the particle-size distribution of Figure 4.4a is more polydisperse than the one observed on the HG12 peptide nanotubes. This comparison indicates that the dispersity of Cu nanocrystals is regulated by the template nanotubes. When we reported Au nanocrystal growth on the sequenced HRE peptide-coated nanotubes, the regular spacing of the HRE peptide binding on the nanotube was observed to be crucial to control the monodispersity and size of Au nanocrystals. Therefore, it is reasonable that the dispersity of Cu nanocrystals on the HG12 peptide nanotubes in the lower pH range is also regulated with the same growth mechanism that Cu nanocrystals are grown between the regularly spaced HG12 peptide chains on the nanotubes. When the same non-nanotube experiment was examined at pH = 8, Cu nanocrystals were grown

in an average diameter of 50 nm (Figure 4.4b), which shows the trend similar to the Cu nanocrystal size observed on the HG12 peptide nanotubes. In this basic condition, the HG12 peptides were found to aggregate, shown between arrows in Figure 4.4b. This observation suggests that the HG12 peptides also aggregate on the nanotubes to induce the larger Cu nanocrystal growth in the higher pH range.

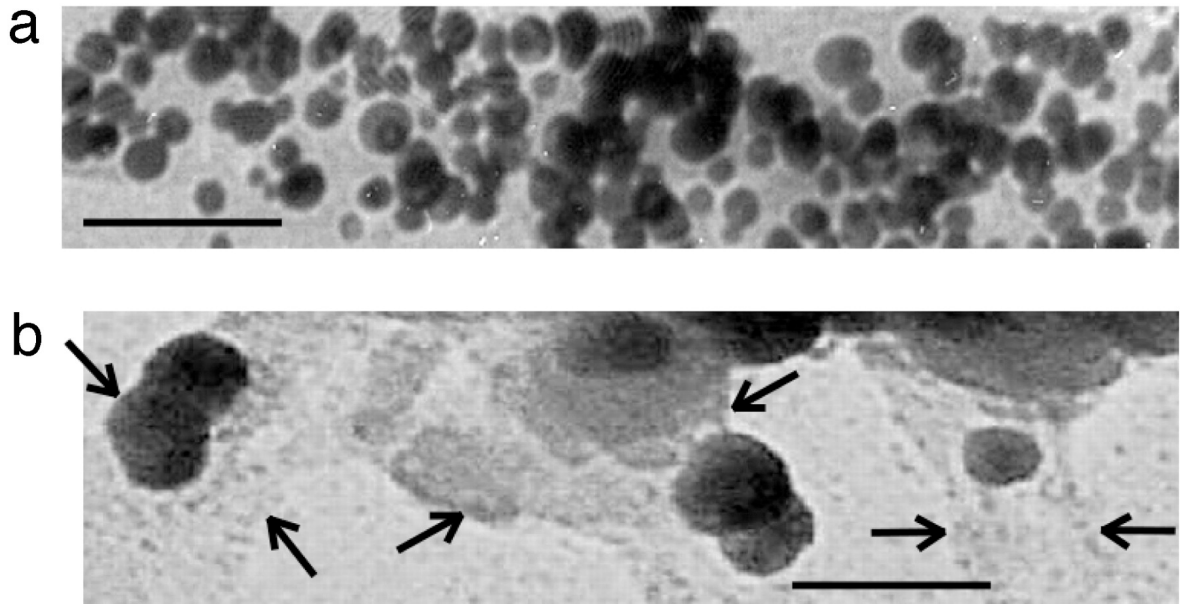

Figure 4.4 TEM images of the Cu nanocrystals grown in the HG12 peptide solution without the template nanotubes at pH 6 (a) and at pH 8 (b). Arrows show the edges of aggregated HG12 peptides. (Scale bar = 100 nm.)

When Au nanocrystals were grown on the sequenced HRE peptide-coated nanotubes, the Au nanocrystal size was unchangeable with pH change because of the rigidity of HRE peptide backbone. Because the size of Cu nanocrystals was changed on the HG12 peptide nanotubes by pH change, it is likely that the HG12 peptide–

Cu(II) complex undergoes the conformation change on the nanotubes between the lower pH range and the higher pH range. This conformation change is supported by the report that the free HG12 peptide molecules in aqueous solution formed complexes with Cu(II) and folded into the compact form by means of ligation between histidines and Cu(II) in the lower pH range, whereas the HG12 peptide–Cu(II) complexes were aggregated in the higher pH range (*115, 118*). To confirm that this peptide conformation change by pH change also occurs on the nanotubes, Fourier transform IR spectra of the HG12 peptide–Cu(II) complexes on the nanotubes at pH 6 and pH 8 were compared in Figure 4.5 The glycine amide I mode of the N(Gly)–Cu(II)–N(His) complex at 1,657 cm^{-1} in pH 6 (Figure 4.5, dotted line) is blue-shifted to 1,674 cm^{-1} in pH 8 (figure 4.5, solid line), indicating that fewer Cu ions bind the glycine amides in the basic condition (*120*). The 1,625 cm^{-1} peak is the amide vibration of β-sheet conformation of peptide backbone aggregation by hydrogen bonding (*118, 135*), and the increase of this IR intensity by increasing pH indicates that the HG12 peptide chains on the nanotubes were aggregated in the higher pH range. The increase of IR intensity at a 1,604 cm^{-1} peak by pH increase is due to the formation of intermolecular N(His)–Cu(II)–N(His) bonds between the peptide chains by means of the aggregation (*118, 120*). This observation is consistent with the loss of IR intensity at a 1,550 cm^{-1} peak, the imidazole side chain vibrational mode of histidine without the Cu(II) ligation, by way of pH increase (*121*). Although this vibrational analysis does not reveal the complete Cu growth mechanism vs. pH change on the nanotubes, the combination of this analysis and the control experiments

in Figure 4.4 strongly supports the hypothesis that the peptide aggregation is one of the major factors controlling the size of Cu nanocrystal. This hypothesis is summarized in Figure 4.6 In the lower pH range, Cu(II) is coordinated with histidines and glycines to fold the HG12 peptides on the nanotubes, and Cu nanocrystals nucleate on the folded peptide chains (Figure 4.6 Left). This folded conformation of the HG12 peptide–Cu(II) complex is adapted from the complex conformation observed in the free suspension (*115, 118*). The compacted HG12 peptide chain by folding may also contribute reduction of the aggregation between the regularly spaced peptide chains on the nanotubes. In the higher pH range, intermolecular His–Cu(II)–His bonds are formed between the neighboring aggregated HG12 peptides on the nanotube to nucleate Cu nanocrystals between the HG12 peptide aggregates (Figure 4.6 Right). The peptide configuration in Figure 4.6(right) may increase the space to grow Cu nanocrystals, which induces larger Cu nanocrystal growth in the basic condition. The degree of peptide chain aggregation seems not to be uniform on the entire nanotube surface, and the variation in the peptide chain aggregations likely induces the uneven HG12 peptide chain spacing for the Cu nanocrystal nucleation on the nanotubes, which makes Cu nanocrystals less monodisperse in the higher pH range.

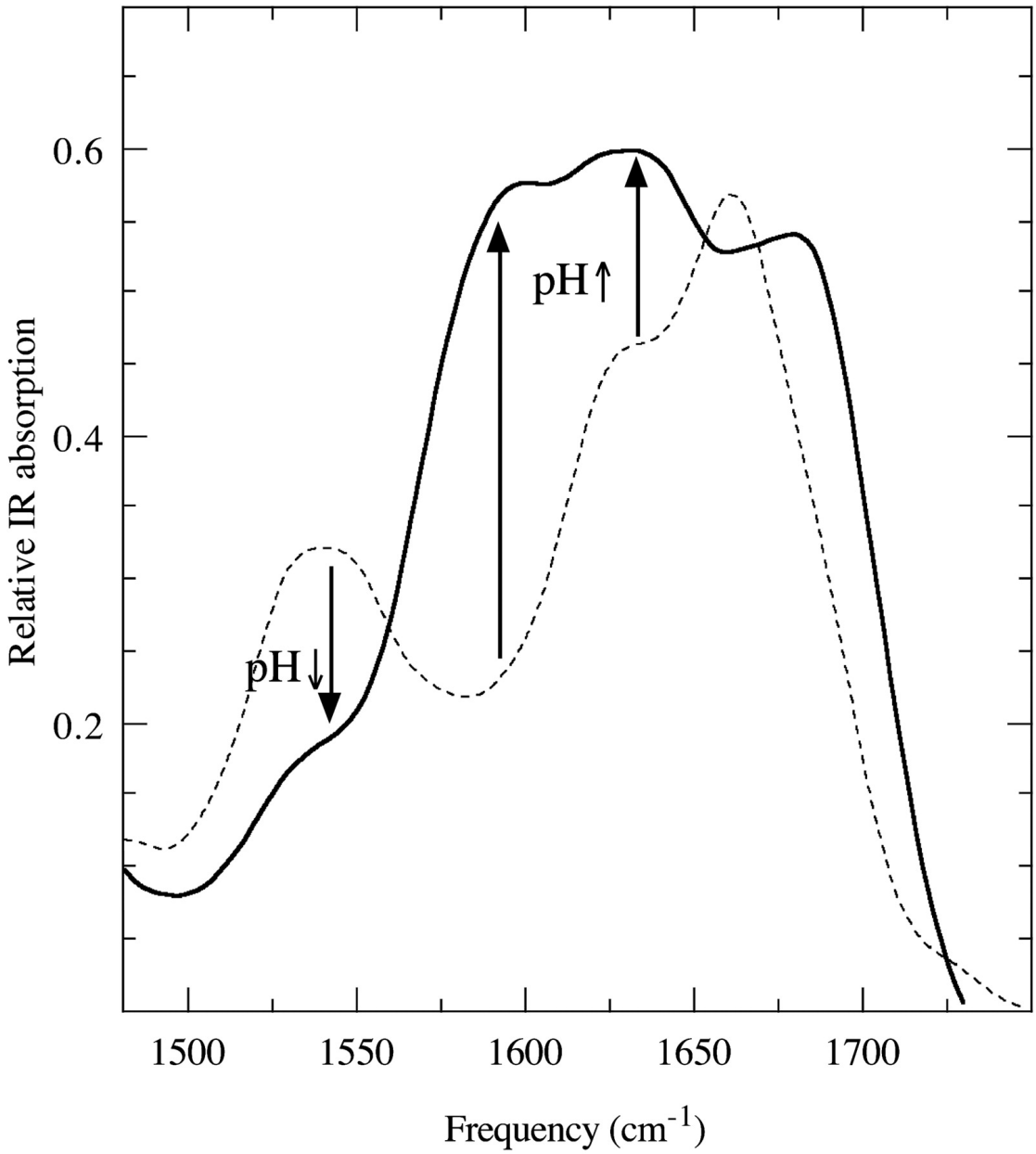

Figure 4.5 IR spectra of the HG12 peptide–Cu(II) complexes on the nanotubes at pH 6 (dotted line) and pH 8 (solid line).

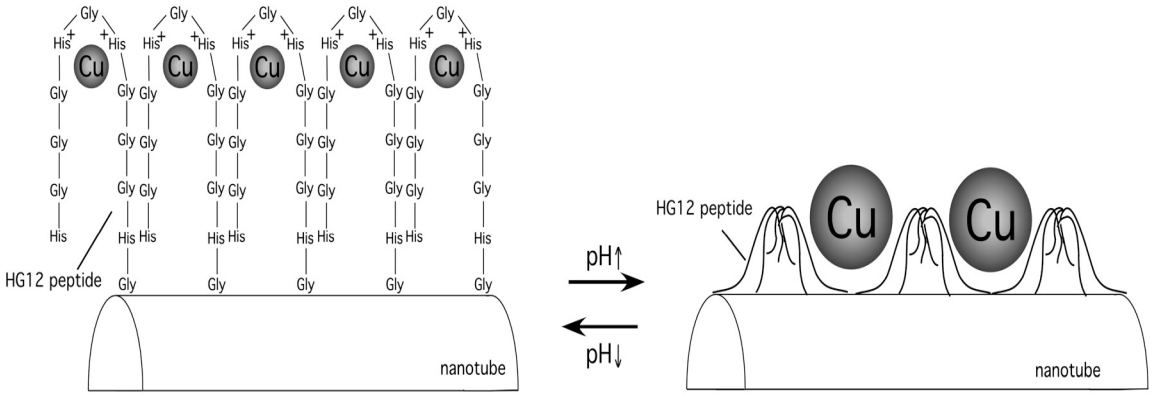

Figure 4.6 A proposed structure of the Cu nanocrystal–HG12 peptide complex on the template nanotube

4.4 Conclusion

Cu nanocrystals can be mineralized in different sizes via the HG12 peptide conformation changes on the nanotubes, controlled by pH values. This system may be developed as smart nanotubes that can tune their electronic properties by simple environmental controls and applied as smart building blocks for microelectronic, sensor, and catalytic applications.

Chapter 5 Size-Controlled Ni Nanocrystal Growth on Peptide Nanotubes and Their Magnetic Properties

5.1 Introduction

The project of this chapter is very similar to the chapter 4, we made Size controlled Ni Nanocrystal other than Cu by using same sequenced peptide, HG12, to immobilize on the bola-amphiphile template nanotube. The sequenced peptide can also mineralize Ni on the biological nanotubes. The major advantage of this approach is the efficient and reproducible control of the Ni nanocrystal size on the template nanotube, which adds tenability of the magnetic properties to the resulting nanotube. A schematic of growth of Ni nanocrystals on the nanotube was shown in Figure 5.1.

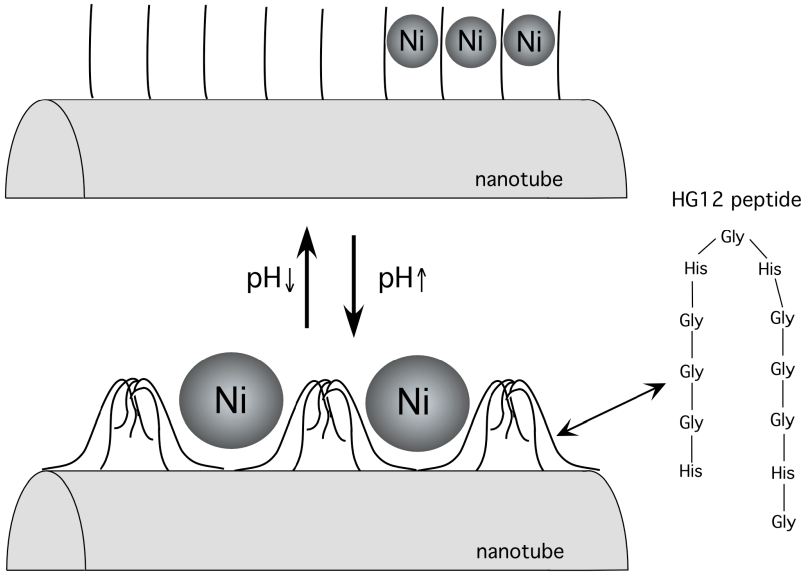

Figure 5.1 Scheme for the size-controlled Ni nanocrystal growth on the HG12 peptide-coated nanotube via pH change.

Previously, the packing densities and the shapes of nanocrystals were controlled by tuning peptide conformations and charges of the nucleation sites on the nanotubes via pH changes of growth solutions and the electronic properties of the resulting nanotubes were influenced by the packing densities and the shapes (*136, 137*). In the present study, we synthesized a more flexible peptide for Ni mineralization that allowed a significant conformation change by changing pH in solution. When this flexible peptide was incorporated onto the template nanotube, the pH change induced dramatic peptide conformation change that influenced the size of Ni nanocrystal grown on the nanotube. Magnetic properties of the resulting nanotubes were changed, depending upon the sizes of Ni nanocrystals. This outcome may be useful not only for

magnetic device fabrications but also for understanding of biomineralization processes *in vivo* (*138, 139*).

5.2 Experimental Section

Synthesis of the template nanotube was described in chapter 4. The nanotubes were washed with deionized water and a microcentrifuge (13,400 rpm) for 4 minutes. In order to break up the aggregates, the nanotubes were sonicated in deionized water. The immobilization of the synthetic HG12 peptides on the template nanotubes was also described in chapter 4.

Mineralization of Ni nanocrystals on the nanotubes: In order to mineralize Ni nanocrystals on the HG12 peptide nanotubes, 50 μL of 50 mM $NiCl_2$ solution was added to the nanotube solution. The concentration was kept constant (M:L =1:1) and the pH was varied between 4 and 10 in order to study the pH effect on the size of Ni nanocrystal grown on the nanotube. In all cases, the reaction mixtures were allowed to sit undisturbed overnight under nitrogen to complete immobilization of Ni ions on the nanotube. This was followed by the addition of $NaBH_4$, 75 μmol as a reducing agent to mineralize Ni nanocrystals on the nanotube.

Magnetic measurement: Magnetic properties of the Ni nanocrystals on the nanotubes were characterized using an alternating gradient magnetometer (AGM) under varying magnetic fields of up to 0.2 T at room temperature. Hysteresis loops for the samples

were obtained by AGM to determine magnetic parameters such as coercivity H_c, a field required to reverse the net magnetization, and squareness M_r/M_s, a ratio of the remanent magnetization M_r to saturation magnetization M_s.

5.3 Results and discussion

The oligopeptide, His-Gly-Gly-Gly-His-Gly-His-Gly-Gly-Gly-His-Gly (HG12), we used here is designed to mineralize Ni nanocrystals. After the HG12 peptides were immobilized on the template nanotubes by incubating the peptides in the nanotube solution for 24 hours under pH values between 4 and 10, the resulting HG12 peptide nanotubes were examined to grow Ni nanocrystals on the nanotube surfaces. Previously the HG12 peptides were shown to aggregate in basic solutions (*140-142*), and we hypothesized that the degree of the peptide aggregation controls the size of Ni nanocrystal on the nanotube as proposed in Figure 5.1. If Ni nanocrystals are grown between the pH-controlled peptide aggregates on the nanotubes, the larger degree of the aggregation provides more space for the Ni nanocrystal growth and produces larger Ni nanocrystals on the nanotubes in higher pH range, as shown in Figure 5.1. Based upon this concept, the sizes of Ni nanocrystals generated on the HG12 peptide nanotubes were studied as a function of pH by a transmission electron microscope (TEM). Ni nanocrystals were mineralized on the HG12 peptide nanotubes after incubating $NiCl_2$ for 24 hours and reduced by $NaBH_4$ at various pHs. When Ni nanocrystals were generated on the nanotubes at pH 4, the diameter of Ni nanocrystal

was 30 ± 4 nm (Figure 5.2-a). The electron diffraction pattern of these nanocrystals in the inset of Figure 5.2-a shows (111), (200). (220), and (222) faces of face-centered cubic Ni nanocrystals. At pH 6, Ni nanocrystals were grown in the diameter of 50 ± 5 nm, as shown in Figure 5.2-b. In this TEM image, the darker line in the center of nanotube appeared due to the Ni nanocrystal growth inside the nanotube. The experimental condition at pH 6 seems to match these criteria for the interior growth of Ni nanocrystals. The electron diffraction pattern in this condition was consistent with the one at pH 4. When Ni nanocrystals were generated on the nanotubes at pH 8, the diameter of Ni nanocrystal was 100 ± 23 nm (Figure 5.2-c). The equivalent electron diffraction pattern was also obtained in this sample, indicating that the crystalline structure was unchanged between pH 4 and 8. Those results show that the size of Ni nanocrystal on the HG12 peptide nanotube increases as the pH in the growth solution increases. While currently there is no direct observation to probe the exact Ni nanocrystal growth mechanism on the nanotube, the growth of Ni nanocrystals without incorporating the HG12 peptides on the nanotube surfaces was examined as a control experiment. In the absence of the HG12 peptides, Ni nanocrystals were still deposited on those template nanotubes, but the Ni nanocrystal coating was not uniform and polydisperse in the range of 10-100 nm in diameter at pH 6 (Figure 5.2-d). Ni nanocrystals were observed on the nanotubes with the same degree of polydispersity at pH 4 and pH 8. These comparisons are indicative that the HG12 peptide plays a vital role in regulating the Ni nanocrystal size and the degree of the HG12 peptide aggregation on the nanotube determines the size of Ni nanocrystal.

Recent FTIR study of the HG 12 peptides on the nanotubes also supports that higher pH values induce more aggregation of the HG12 peptides and this transformation seems to provide more space to grow nanocrystals between the HG12 peptide aggregations in the higher pH range (*142*). These outcomes support our hypothesis for the Ni nanocrystal growth process on the nanotube.

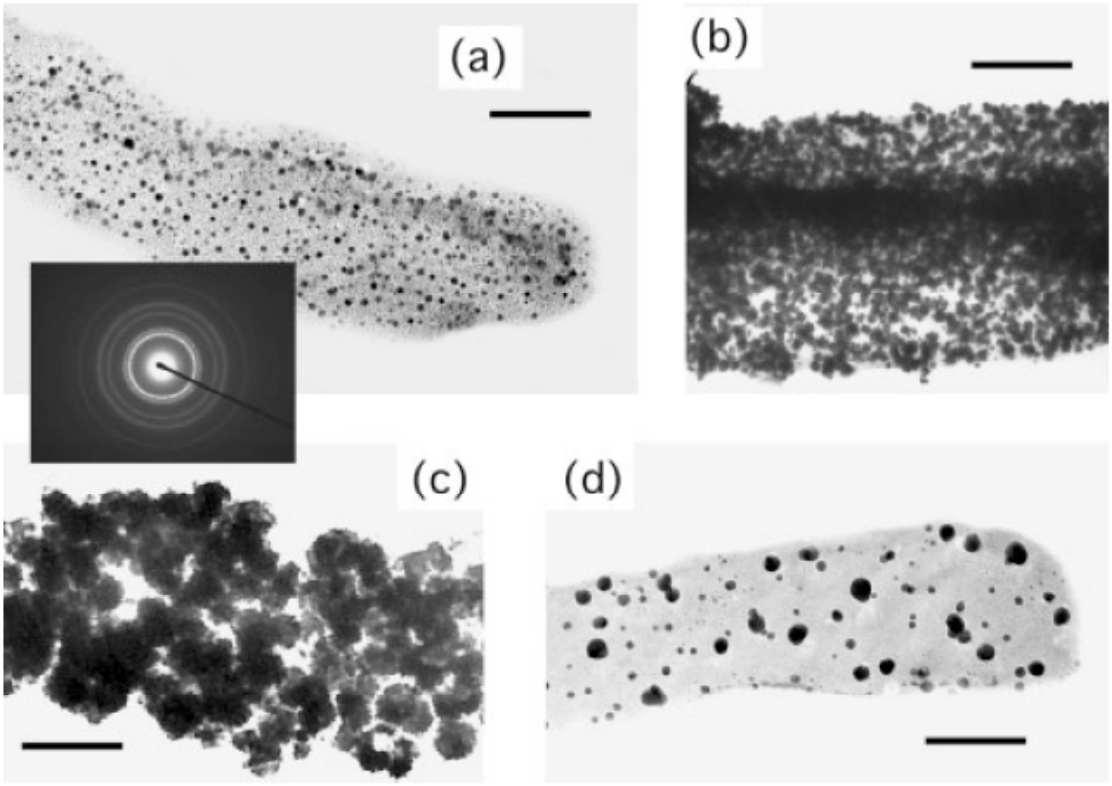

Figure 5.2 TEM images of Ni nanocrystals generated on the nanotube (a) at pH 4. Inset: electron diffraction. (b) at pH 6 (c) at pH 8 (d) at pH 6 without the HG12 peptide coating on the nanotube. Scale bar = 200 nm.

The magnetic properties of the Ni nanocrystal-coated nanotubes at various pH values were studied by an alternating gradient magnetometer (AGM). Figure 5.3-a

shows a magnetic hysteresis loop obtained from the 30 nm Ni nanocrystal-coated peptide nanotubes (Figure 5.2-a) measured at room temperature in varying magnetic fields up to 0.2 T. From the hysteresis loop, the coercivity of H_c = 2.9 mT and the squareness of M_r/M_s = 0.20 were obtained, showing that the Ni nanocrystal-coated nanotubes are ferromagnetic. Therefore, the peptide nanotubes coated with the 30 nm-Ni nanocrystals can be treated as an assembly of finite-sized ferromagnetic Ni nanocrystals, indicated by the sheared hysteresis loop shape and the small squareness. The hysteresis loop of 50 nm Ni nanocrystal-coated peptide nanotubes was consistent with the one obtained for the 30 nm Ni nanocrystal-coated peptide nanotubes. Figure 5.3-b represents a hysteresis curve of the 100 nm Ni nanocrystal-coated peptide nanotubes. The coercivity H_c = 6.2 mT and the squareness M_r/M_s = 0.19 were determined from this hysteresis curve. The higher H_c value for these nanotubes can be consistently explained by the long-range dipolar interaction between the larger Ni nanocrystals on the nanotubes (*143*). Enhanced magnetostatic interactions between the larger Ni nanocrystals on the nanotubes may be responsible for reducing the M_r/M_s value. It should be noted that this mineralization method did not provide full control in the magnetic property of the nanotube by tuning the Ni nanocrystal sizes over 100 nm in diameter because the conformation of HG12 peptide affected not only the nanocrystal size but also the morphology of nanocrystal in this size range. For example, when Ni nanocrystals were generated on the peptide nanotubes at pH > 8, the Ni nanocrystals were grown in the diameters of 150-200 nm. But the structure of Ni nanocrystal became amorphous in this pH range and this structural change also

resulted in decreasing the coercivity and the squareness. Hence, Ni nanocrsytals larger than 150 nm on the nanotubes did not exhibit higher H_c values compared to the crystalline Ni nanocrystals smaller than 100 nm.

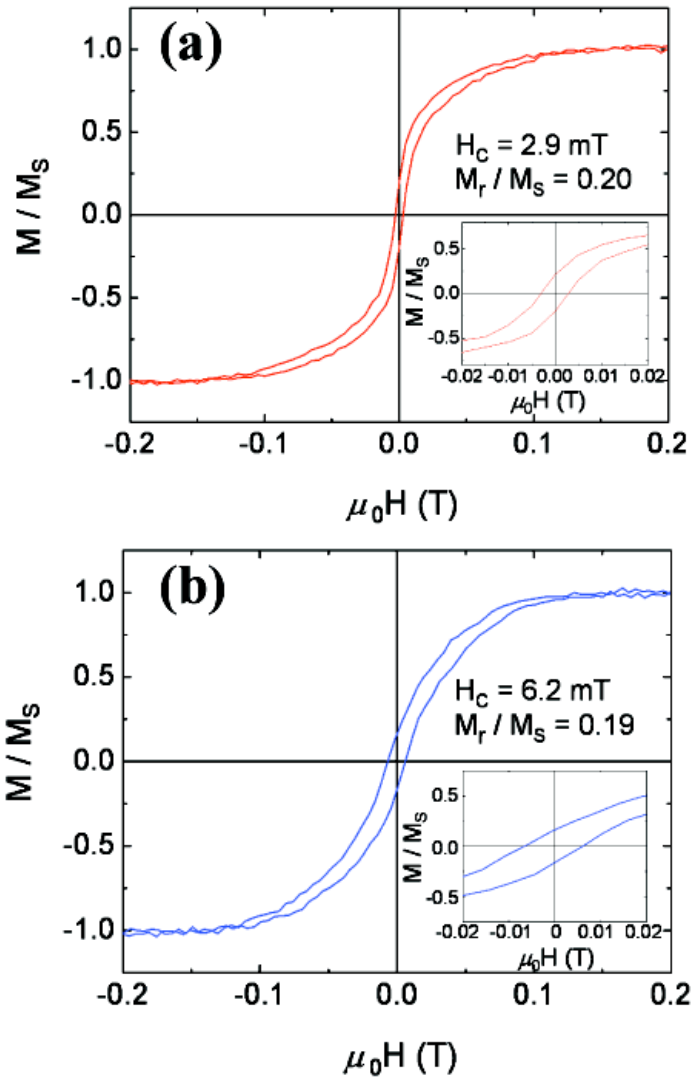

Figure 5.3 Comparison of hysteresis curves of the peptide nanotubes coated with (a) the 30 nm-Ni nanocrystals and (b) the 100 nm-Ni nanocrystals.

In summary, we have demonstrated that the Ni-mineralizing HG12 peptide-coated nanotubes led to the efficient Ni nanocrystal growth on the nanotube surfaces. The higher pH values of the growth solutions increased the size of Ni nanocrystal on the HG12 peptide nanotube. The conformation of the HG12 peptide seems to play a significant role to control the resulting Ni nanocrystal size on the peptide nanotube via pH change. In the absence of the HG12 peptides on the template nanotubes, Ni nanocrystals were formed on the nanotubes with no size control. The nanotubes coated with Ni nanocrystals in the diameters of 30-50 nm behaved as the assembly of finite-sized ferromagnetic nanocrystals while the magnetic property of the nanotube coated with the 100 nm-Ni nanocrystals was closer to the bulk. We believe that this magnetic nanotube fabrication method can be extended to other magnetic species with peptides whose amino acid sequences are known to mineralize specific ions. This type of smart nanotube with the tunable magnetic property may be useful as a building block for magnetic devices such as spintronics and recording media. Those magnetic peptide nanotubes also provide potential for *in vivo* sensing and separation applications.(*144-147*)

Chapter 6 Room-Temperature Wurtzite ZnS Nanocrystal Growth on Zn Finger-Like Peptide Nanotubes by Controlling Their Unfolding Peptide Structures

6.1 Introduction

A class of wide-gap II-VI semiconductor nanomaterials has shown interesting optical, electrical, and optoelectric properties via quantum confinement.(*148, 149*) ZnS nanocrystals have attracted considerable attention due to its applications in flat-panel displays, electroluminescent devices, infrared windows, sensors, and lasers.(*150*) For those applications, phase controls of ZnS nanocrystals were critical to tune their physical properties to the appropriate ones. From the industrial point of view, the wurtzite ZnS nanocrystal fabrication at room temperature is extremely practical, however the most stable ZnS structure in nanoscale is the zinc blende (cubic) structure(*151*) and scientists have just begun exploring the room-temperature synthesis of the wurtzite structure of ZnS nanocrystals. One promising approach for the room-temperature nanocrystal synthesis is to use biological templates because biomineralization in nature crystallizes many types of nanoparticles at room temperature by using proteins and peptides (*152-156*). For example, peptide sequences were identified by phage display libraries to grow the wurtzite ZnS nanocrystals and the zinc blende ZnS nanocrystals respectively (*148*). Histidine, which binds Zn ions in Zn finger peptides, was also used to grow wurtzite ZnS

nanocrystals at room temperature (*157*). While those approaches could mimic biological systems to grow the targeted nanocrystal structure at room temperature, how peptides control nucleations and crystalline phases is not clear enough to apply them to synthesize specific nanocrystal structures in general.

Recently, in the high-temperature synthesis of ZnS nanobelts, sizes of seed crystals could control their final crystalline structures (*150*). For example, Au catalyst particles smaller than 50 nm nucleated the zinc blende structure while particles larger than 100 nm nucleated the wurtzite structure via vapor deposition techniques. In this chapter, we combined the peptide template approach and the nucleation-site controlling approach to control the phase of ZnS nanocrystals to the wurtzite structure at room temperature. Peptide nanotubes, consisting of the M1 peptide (VAL-CYS-ALA-THR-CYS-GLU-GLN-ILE-ALA-ASP-SER-GLN-HIS-ARG-SER-HIS-ARG-GLN-MET-VAL) that is synthesized based on the peptide motif of the Influenza Virus Matrix Protein M1, could grow the wurtzite ZnS nanocrystals on the nanotube templates in solution. The M1 protein controls ribonucleoprotein (RNP) coatings on the virus as a function of pH, which plays a crucial role in the virus replication (*158*).In the M1 protein, the unfolding process of the helical M1 peptide backbone motif via pH change creates a linker region between N- and C-terminated helical domains that contains a Zn finger-like Cys_2His_2 motif. Because the higher pH increases the uptake of Zn ions in the Cys_2His_2 motif of the M1 peptide by unfolding more helical domains, the pH change can essentially control the size and the number

of the nucleation sites in the M1 peptides to grow ZnS nanocrystals with desired phases. Here we optimized the nucleation sites in the M1 peptides by unfolding them with pH to obtain monodisperse and crystalline wurtzite ZnS nanocrystals on the template nanotubes at room temperature (Figure 6.1).

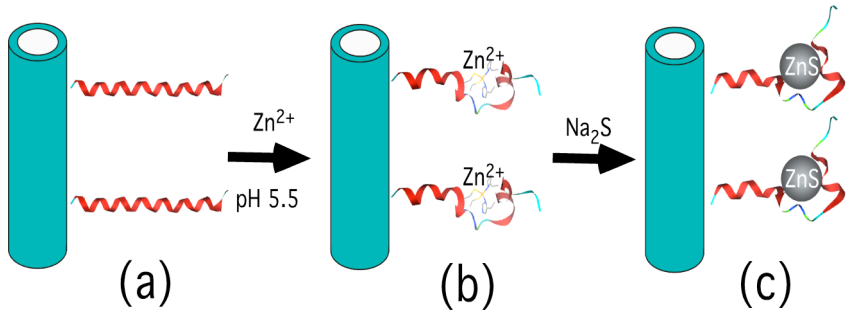

Figure 6.1 Illustration of the ZnS nanocrystal growth on the unfolding M1 peptides on the template nanotubes as a function of pH

6.2 Experimental Section

To prepare templates for the ZnS nanocrystal coating, the bola-amphiphile monomer (10 mM) were self-assembled into nanotubes in a pH 4.5 citric acid/NaOH solution. In order to immobilize the 20-mer M1 peptide, VAL-CYS-ALA-THR-CYS-GLU-GLN-ILE-ALAASP-SER-GLN-HIS-ARG-SER-HIS-ARG-GLN-MET-VAL (>90% purity, Genescript Co.), on the template nanotubes, 50 μL of the M1 peptide solution in a pH 7 buffer was incubated with 100 μL of the nanotube solution (10 mM). After the mixture was stirred slowly for 24 hours, the coated nanotubes were washed with deionized water to remove any unbound M1 peptides in solutions and

then centrifuged for 60 minutes (14,500 rpm) to collect the M1 peptide-coated nanotubes. The M1 peptide coating on the nanotubes was confirmed by Raman microscope and atomic force microscope (AFM) before growing ZnS nanocrystals.

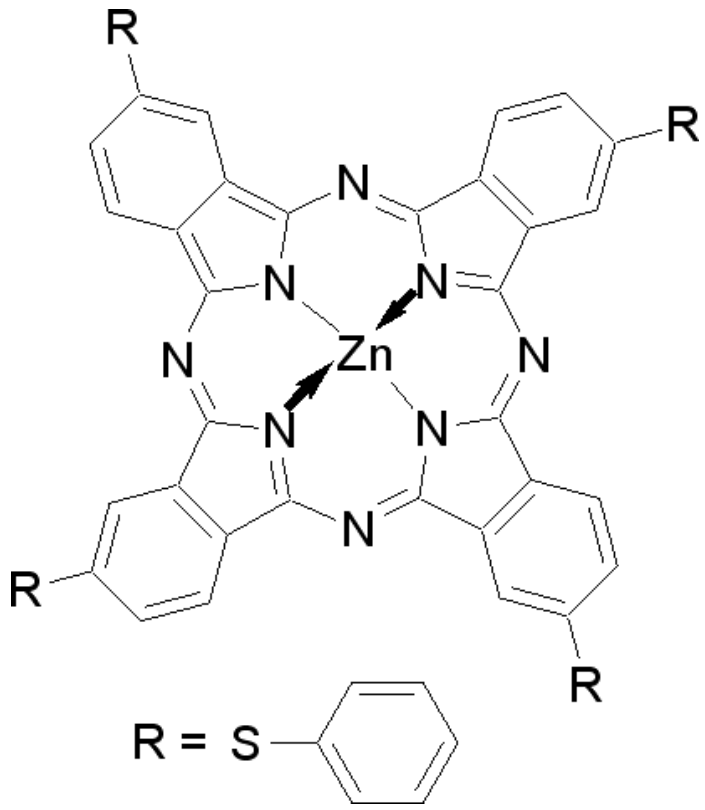

Figure 6.2 Structure of the Zinc salt used for the ZnS nanocrystal synthesis

For the growth of ZnS nanocrystals on the M1 peptide nanotubes, 20μL of 50μM zinc 2,9,16,23-tetrakis(phenylthio)-29*H*,31*H*-phtanlocyanine solution (in 70% THF),as showed in figure6.2, was added to the peptide nanotube solution to bind Zn(II) ions to the linker region between N and C-terminated helical domains of the

M1 peptides that contains the Zn finger-like Cys_2His_2 motif (Figure 6.1-b The concentration of the Zn(II) precursor was maintained as a metal to ligand ratio =1:1, and the pH of the growth solution was varied between 5 and 10 to study the pH effect on the ZnS nanocrystal growth. In all cases, the reaction mixtures were allowed to sit undisturbed overnight under nitrogen to complete the Zn ion immobilization on the nanotubes. Then 0.1 mL of 0.5 M Na_2S solution was added to the peptide nanotubes at 10□C, and the solution was purged with nitrogen aged for 24 hours at 10□C to grow ZnS nanocrystals on the nanotubes (Figure 6.1-c). After 24 hours, the resulting nanotubes coated by ZnS nanocrystals were washed with nanopure water and then centrifuged twice to remove excess Na_2S as well as nanocrystals that were not bound to the nanotubes.

6.3 Results and Discussions.

Figure 6.3-a shows transmission electron micrograph (TEM) of ZnS nanocrystals grown on the nanotubes at pH 5.5. Those nanocrystals were relatively monodisperse with an average diameter of 4 nm when they were grown in pH 5.5 - 7.4. When the same coating procedure was applied to the template nanotubes without the M1 peptide, the coverage of ZnS nanocrystals on the nanotube was significantly diminished and the polydisperse nanocrystals were aggregated on the nanotube surfaces, as shown in Figure 6.3-b. This comparison indicates that the M1 peptide play a significant role to regulate the size and the surface coverage of ZnS

nanocrystals. When the ZnS nanocrystals were grown on the M1 peptide nanotubes in pH 5.5, the electron diffraction pattern of resulting ZnS nanocrystals shows (002), (110) and (112) phases of the wurtzite structure, as shown in Figure 6.3-c. In the higher pH conditions (pH > 8), the crystalline ZnS could not be obtained on the nanotubes. When ZnS nanoparticles were grown with the M1 peptides without the template nanotubes in the pH range of 5.5 – 7.4, large aggregates of ZnS particles and the M1 peptides were observed.

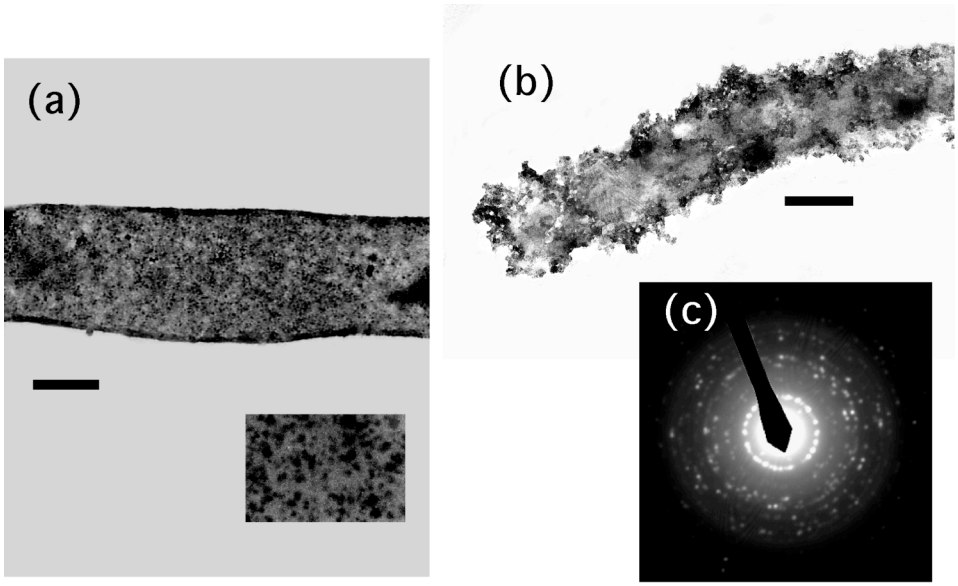

Figure 6.3 (a) TEM image of ZnS nanocrystals on the M1 peptide nanotubes grown at pH 5.5, inset: in the high magnification. Scale bar = 70 nm. (b) TEM image of ZnS nanocrystals on the neat template nanotubes with no M1 peptides grown at pH 5.5. Scale bar = 100 nm. (c) Electron diffraction of the ZnS nanocrystals on the M1 peptide nanotubes grown at pH 5.5.

The UV-vis spectrum and the fluorescence spectrum (excited at 288 nm) of ZnS nanocrystals on the M1 peptide nanotubes (pH 5.5) show absorption λ_{max} at 280 nm (blue line in Figure 6.4-a) and a fluorescence peak at 439 nm (Figure 6.4-b), respectively. Since no absorption from the M1 peptide nanotubes around 280 nm was observed (red line in Figure 6.4-a), the 280 nm absorption of the blue line in Figure 6.4-a is attributed to the ZnS nanocrystals. A small shoulder at 470 nm in Figure 6.4-b corresponds to the defect-related emission of ZnS nanocrystals (*121*) . These absorption and fluorescence peaks indicate that the band gap of these ZnS nanocrystals in the diameter of 4 nm is 4.4 eV, and the peak positions in both UV/vis and fluorescence spectra are consistent with the ones for ZnS nanocrystals, whose diameter is about 4 nm (*149, 151*).

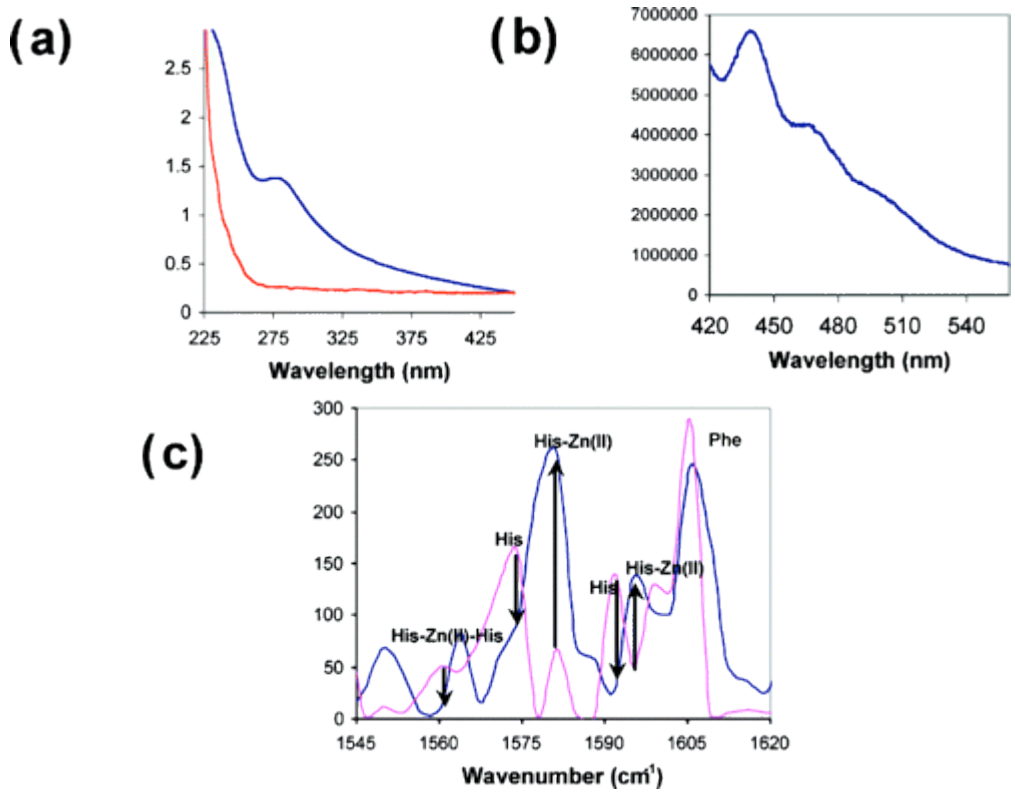

Figure 6.4(a) UV/vis spectra of the Zn(II)-bound M1 peptide nanotubes (blue line) and the M1 peptide nanotubes with no Zn(II) (red line). (b) Fluorescence spectrum of the ZnS nanocrystals on the M1 peptide nanotubes. (c) Raman spectra of the Zn(II)-bound M1 peptide nanotubes at pH 5.5 (pink) and at pH 10.0 (blue).

The binding conformation between Zn ions and M1 peptide was showed in figure 6.4. When Zn ions were mixed with the M1 peptides at pH 5.5 (red line in Figure 6.4-c), the N(His)-Zn^{2+}-N(His) bond formation was observed at 1561 cm^{-1} (*121*). However, as Zn ions were incubated in the pH 10.0 nanotube solution (blue line in Figure 6.4-c), this His-Zn^{2+}-His peak intensity was much weaker and instead the peak intensities for the N(His)- Zn^{2+} bond at 1581 cm^{-1} and 1595 cm^{-1} were increased (*159, 160*) . This spectral comparison indicates that the unfolding of the M1 peptide on the

nanotubes via pH increase induces the extension of the linker region in the helical backbone, which favors the His-Zn^{2+} chelation over the His-Zn^{2+}-His chelation. The decrease of the imidazole peak of the neat histidine via pH increase shows that more Zn ions were taken up by histidines of the M1 peptide at higher pHs, which is consistent with previous observations (*161*). The crystallinity difference of ZnS nanocrystals between acidic and basic conditions may be explained by two chelation structures between Zn ions and histidines. When sulfide ions substitute nitrogens of the Zn(II)-N(His) bonds to grow ZnS in the nucleation stage, the exchange kinetics and the directionality of resulting Zn-S bonds should differ between these two chelating structures. This difference in the nucleation process can influence the crystallinity and the final crystalline structure of nanocrystals. In the case of the M1 peptide nanotube, the Zn(II)-Cys_2His_2 motif was the right nucleation structure to grow the wurtzite ZnS nanocrystals at room temperature.

The folding M1 peptide conformation and the binding conformations between Zn ions and the M1 peptides were also probed by circular dichroism (CD) spectroscopy, as showed in Figure 6.5.

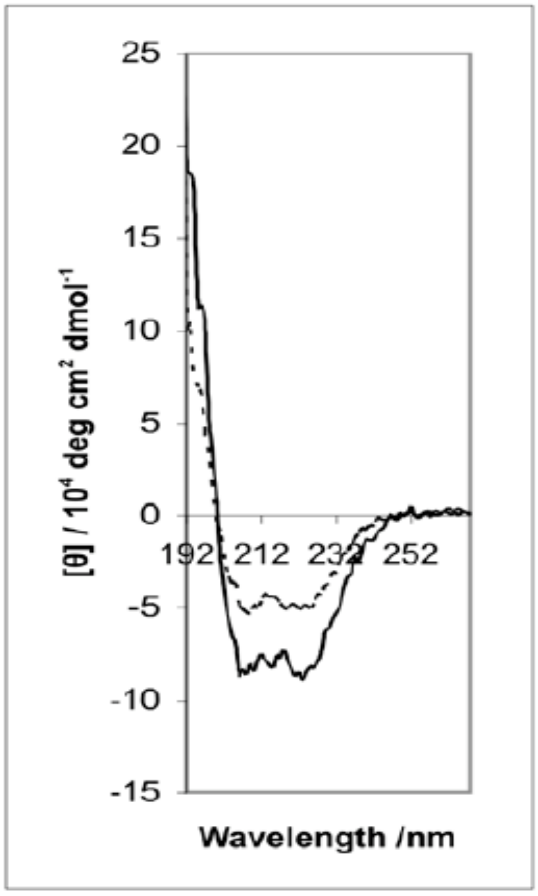

Figure 6.5 circular dichroism (CD) spectroscopy of M1 peptide with Zn ions at pH 5.0(solid line) and pH 7.0(dotted line)

In CD spectra, the structure change of the M1 peptides on the nanotubes were examined at pH = 5.0 and pH =7.0 in the presence of Zn ions in 50 % 2,2,2-Trifluoroethanol(TFE) solution spectroscopy. A solid line represents pH = 5.0 and a dotted line represents pH = 7.0. We could observe in these CD spectra that the M1 peptides on the nanotubes are not in random coils and there is a negative peak at 222 nm, which is in the region of α-helical propensity of the M1 peptide. This 222 nm peak decreased as the pH increased from 5.0 to 7.0, which indicates that the M1

peptide on the nanotube undergoes more unfolding in the higher pH. The difference in the CD spectra between the freestanding M1peptides and the M1 peptides on the nanotubes also suggests that the nanotube surface may have an effect on the secondary structure of the M1 peptides, however the definitive structural analyses of the M1 peptide on the nanotubes are still under investigation. therefore the change in CD spectra of the M1 peptides on the nanotubes in the presence of Zn ions as a function of pH indicates that the M1 peptide undergoes more unfolding in higher pHs.

In conclusion, monodisperse ZnS nanocrystals were grown on the M1 peptide-coated nanotubes at room temperature. When pH of the growth solution was adjusted to 5.5, ZnS nanocrystal was grown as the highly crystalline wurtzite and the structure became more amorphous as pH was raised to 10.0, controlled by the unfolding conformation of the M1 peptides. This concept should be widely applicable to other crystal growths to control their structures by optimizing peptide sequences and conformations.

Chapter 7 Fabrication and Application of Enzyme Incorporated Peptide Nanotubes

7.1 Introduction

Enzymes are versatile biocatalysts that catalyze specific chemical reactions effectively in *vivo* and in *vitro* (*162*). However, most enzymes have been used in the form of crude and free protein extracts, which usually increases the reaction time and/or decrease the selectivity (*163, 164*) . In order to make enzymes cost-effective, long-lived, and highly active, many supports, including sol-gels, (*165*) polymer membranes, (*166*) silica (*167, 168*), and zeolites (*169, 170*), have been utilized to immobilize the enzymes. In most cases, while when enzymes immobilized on the surface of above-mentioned supports have higher enzymatic activity, longer lifetime, and higher thermal stability as compared to the freestanding enzyme(*166, 170, 171*) , but there are some support also decrease the lifetime and activity of enzymes(*168, 172*) . So many researchers are still exploring new supports to immobilize and protect the enzymes that would work at of higher temperatures without loss of activity.(*173*)

Recently, enzymes immobilized on magnetic nanoparticles possessed higher catalytic activity and thermal stability as compared to freestanding enzymes (*171, 174*) .These studies indicated that nanoscale particles can serve as superior supports for the

immobilization of enzymes due to their distinctive functionalized surface properties and large surface-to-volume ratios in comparison with traditional macroscale materials. However, reduction of substrate size could increase the possibility of deactivating and the desorption of enzymes in the processes of enzymatic reactions, (*67*) and this phenomena will become more characteristic as the reaction temperatures rise. To evaluate the effectiveness of nanoscale enzymatic supports, more studies in various types of nanosupports are desirable.

One direction to accomplish this is to incorporate enzymes in nanometer-scale tubules that can protect enzymes within the hollow structure. The disadvantage of tubular substrates may be the reduction of surface area and lower probability for reactants to enter the nanometer-scale hole as compared to nanoparticle substrates, but these difficulties may be overcome by creating attraction forces inside the nanotube substrates such as hydrophobic / hydrophilic interactions, hydrogen bonding, and capillary forces. This nanotube enzyme substrate is worth examining its performance because it has potential to improve the thermal stability of enzymes dramatically due to the immobilization in the hollow structure.

In this chapter, we applied peptide nanotubes as supports for enzymes. The incorporation of proteins on the nanotube to mineralize various metal nanoparticles on the nanotube surface with controlled size, packing density, and shape was discussed in previous chapters (*175*). In this work, when nanoparticles was grew on the nanotube, it was found that the nanoparticle growth starts inside the nanotube first

and then they grow the outside, and the inside coating can be accomplished by controlling the growth time or the ion concentration due to the capillary effect and the hydrophobic interaction (*67*). Therefore, if we can limit the adsorption of enzymes to inside the peptide nanotubes with the same strategy, our hypothesis on effective tubular substrate can be examined.

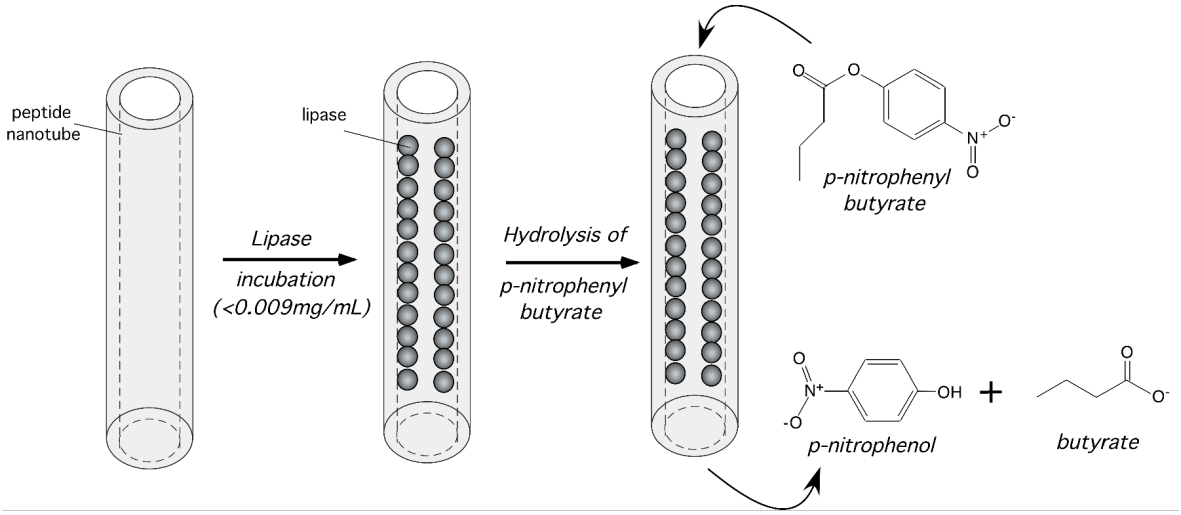

Figure 7.1 Illustration of lipase nanotube fabrication and its enzymatic application.

We encapsulated a model enzyme, *Candida rugosa* lipase, within peptide nanotubes (Figure 7.1) and examined its catalytic activity. Lipase is one of the most versatile enzymes applied as catalysts, medical therapy, degradation of food, detergent additives, and industrial synthesis of specialty chemicals, and we used lipase as a model enzyme because they are quite stable in various nonaqueous solvents (*176-178*). While the ideal porous diameter of nanotube for lipase

incorporation is unknown, we used the peptide nanotube with the inner diameter of 160 nm because we considered that the porous diameter is large enough to introduce reactants and lipases. We observed that the activity of lipase inside the nanotube was 33% higher as compared to the freestanding lipase at room temperature. At elevated temperature, 65˚C, the activity of lipase inside the nanotube was 70% higher as compared to the freestanding lipase. It is advantageous to apply these peptide nanotubes as enzyme supports because enzymes can be immobilized on the nanotube surfaces with appropriate conformations for high enzymatic activities(*179, 180*) , which is beneficial to develop sensors and high-throughput catalysts. Since the peptide nanotubes can be decorated by magnetic particles(*181*) , the nanotubes may also be applied as recyclable substrates by using magnetic fields. Further optimization in experimental conditions may even increase the enzymatic activity and the thermal stability.

7.2 Experimental Section

First, 10 mM of bis(*N*-α-amido-glycylglycine)-1,7-heptane dicarboxylate, bolaamphiphile peptide, was self-assembled into peptide nanotubes in a pH 4.5 citric acid/NaOH solution. Methods for the bolaamphiphile peptide synthesis and the nanotube self-assembly are described in appendix and references(*57, 58*) . After the peptide nanotubes were washed with deionized water several times, 200 μL of nanotube solution was mixed with various 1~20 μL of *Candidan rugosa* lipase

solution (1 mg/mL) and the resulting solutions were allowed to stand still at 4 °C for one week. Then, these samples were washed twice after centrifuging for 3 hours to remove excess lipases in the supernatant solutions. The immobilization of lipases inside the peptide nanotubes was confirmed by transmission electron microscopy (TEM, JEOL 1200EX). To study the activities of the immobilized-lipases inside the peptide nanotubes, 30 μL of *p*-nitrophenol butyrate solution (13.8 mg/mL in 2-propanol solvent) was added to 200 μL of the lipase-nanotube solutions (Figure 7.1). The hydrolysis rates of *p*-nitrophenol butyrate solutions were monitored by the product concentration, [*p*-nitrophenol], by means of UV-Vis spectra (Varian Cary 300 Bio) at room temperature. The thermal stability of lipases was also investigated at various reaction temperatures from 25 °C to 75 °C. In this thermal experiment, 6 μL of lipase solution (1 mg/mL) was mixed with 200 μL of the nanotube solution for one week to produce the lipase nanotubes. After one week, the resulting solution was diluted to 1 mL by deionized water for further analyses. All control experiments without the nanotube substrates were done under the same experimental conditions stated above. Fluorescence intensities of freestanding and nanotube-bound lipase solutions, balanced to 1000 mL, were measured by a fluorometer (Jobin Ybin-SPEX, FL3-11). The excitation wavelength was 310 nm. The amount of lipases immobilized inside the nanotubes was determined by measuring the free protein content in the supernatants after the incubation process with a colorimetric method using a Bio-Rad reagent for the protein assay. For this measurement, bovine serum albumin was applied as a standard. This assay determined percentages of lipase molecules

absorbed on the nanotubes as compared to the original lipase concentration after the nanotubes were incubated in the lipase solutions.

7.3 Results and Discussion

After the lipases were incubated in the nanotube solutions for one week, the lipases were observed to bind inside the nanotubes, as shown in Figure 7.2. Figure 7.2a is TEM image of the lipase nanotube produced at 0.002 mg/mL lipase concentration.

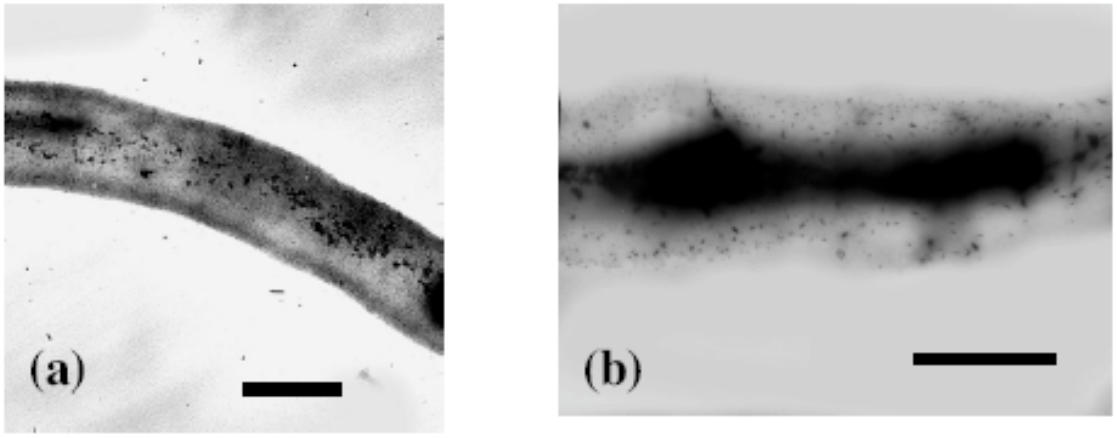

Figure 7.2 TEM images of peptide nanotubes incorporating *Candida rugosa* lipase at (a) [lipase] = 0.002 mg/mL (b) [lipase] = 0.006 mg/mL. Scale bar = 200 nm.

In this TEM image, lipases were appeared as darker areas because they were crystallized inside the nanotubes when the samples were dried on TEM grids(*182*) .

Figure 7.2b shows TEM image of the lipase nanotube produced at 0.006 mg/mL lipase concentration. This TEM image shows that the inner wall of nanotube was fully coated by lipases. When the lipase concentration exceeded 0.009 mg/mL, the lipases were coated outside the nanotubes because the saturation of lipase binding on the inner wall induces the outside coating with the excess amount of lipases. While we do not have direct evidence to explain this inside coating mechanism, various nanoparticles were observed to coat inside the peptide nanotubes at lower nanoparticle concentrations via capillary effect(*183, 184*) and the trend of the lipase incorporation is consistent with these outcomes. Another possible mechanism is hydrophobic interactions. In general, the hydrophobic non-polar residues of lipase spread on the outer shell while the enzymatic active sites are clustered(*173, 177*) . As a result, lipases were observed to aggregate on hydrophobic surfaces(*182*) and the incorporation of lipases inside the peptide nanotubes may indicate that the inner surface of the peptide nanotube may be more hydrophobic than the outer surface.

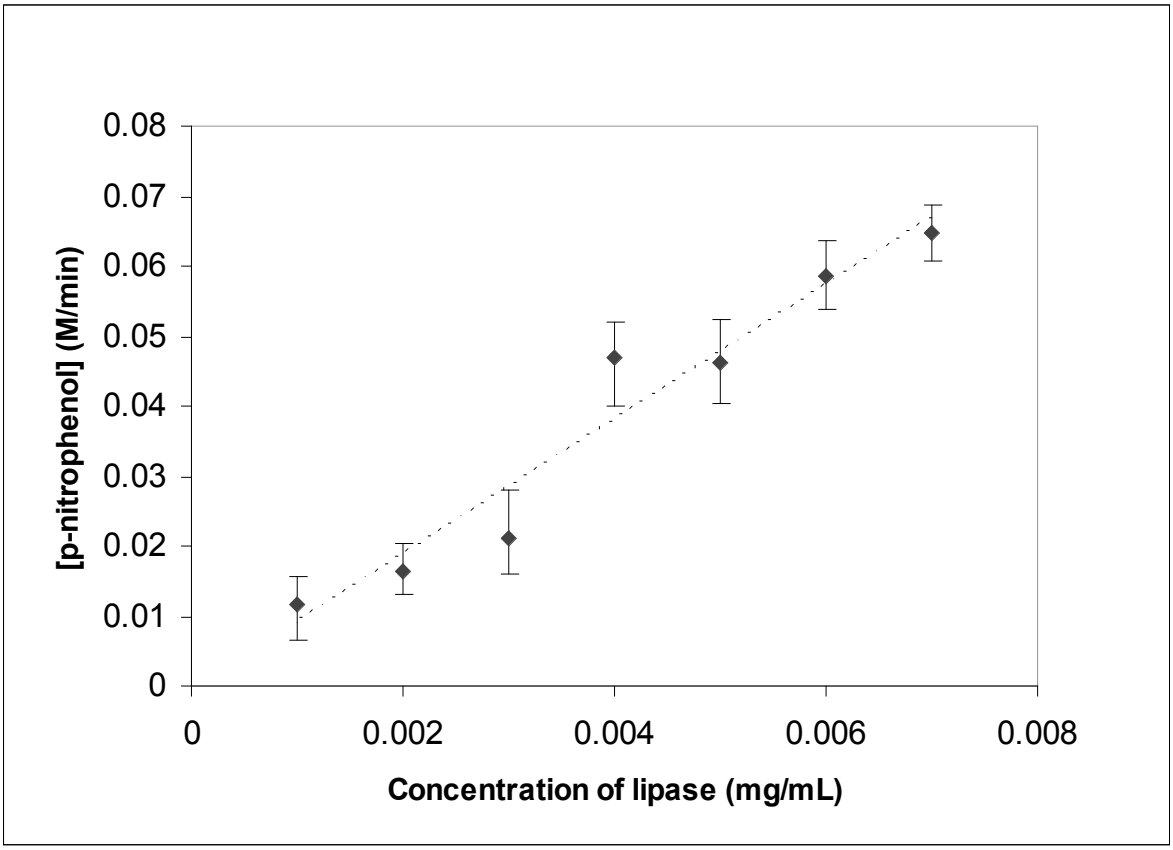

Figure 7.3 Hydrolysis rate of lipases inside the nanotubes. A dotted line is a fit for experimental date points.

Enzymatic activities of lipases immobilized inside the peptide nanotubes were studied by monitoring hydrolysis rates with the concentration change of the product, *p*-nitrophenol (Figure 7.3). The activities of the immobilized-lipases were obtained by initial slopes of *p*-nitrophenol concentration changes over the reaction time. Figure 7.3 shows the hydrolysis rate of lipases inside the peptide nanotubes increased linearly as a function of lipase concentration, which is consistent with the freestanding lipases.(*58*) This outcome indicates that the peptide nanotube support

could maintain the enzymatic function of lipase and the binding inside the nanotube did not hinder the catalytic reaction.

The product concentration changes catalyzed by the lipases inside the nanotubes and freestanding lipases were monitored over of the enzymatic reaction time at various temperature. as shown in a solid line in Figure 7.4. The concentration of lipases was 0.006 mg/mL for freestanding and inside the nanotube. The production of *p*-nitrophenol was observed to rise sharply and reached plateau after 3 minutes of the reaction. While freestanding lipases also showed the same trend (a dotted line in Figure 7.4), the nanotube bound lipases produced *p*-nitrophenol approximately 33% higher than freestanding lipases. Kinetic parameters, K_{cat} and K_m, were obtained as 0.329 S^{-1} and 2.4724 x 10^{-4} M respectively by the Lineweaver-Burk plot for the nanotube-bound enzyme. K_{cat} and K_m for the freestanding lipases were obtained as 0.215 S^{-1} and 3.3951 x 10^{-4} M respectively. The K_m of the nanotube-bound lipases was consistently smaller as compared to the freestanding lipase.

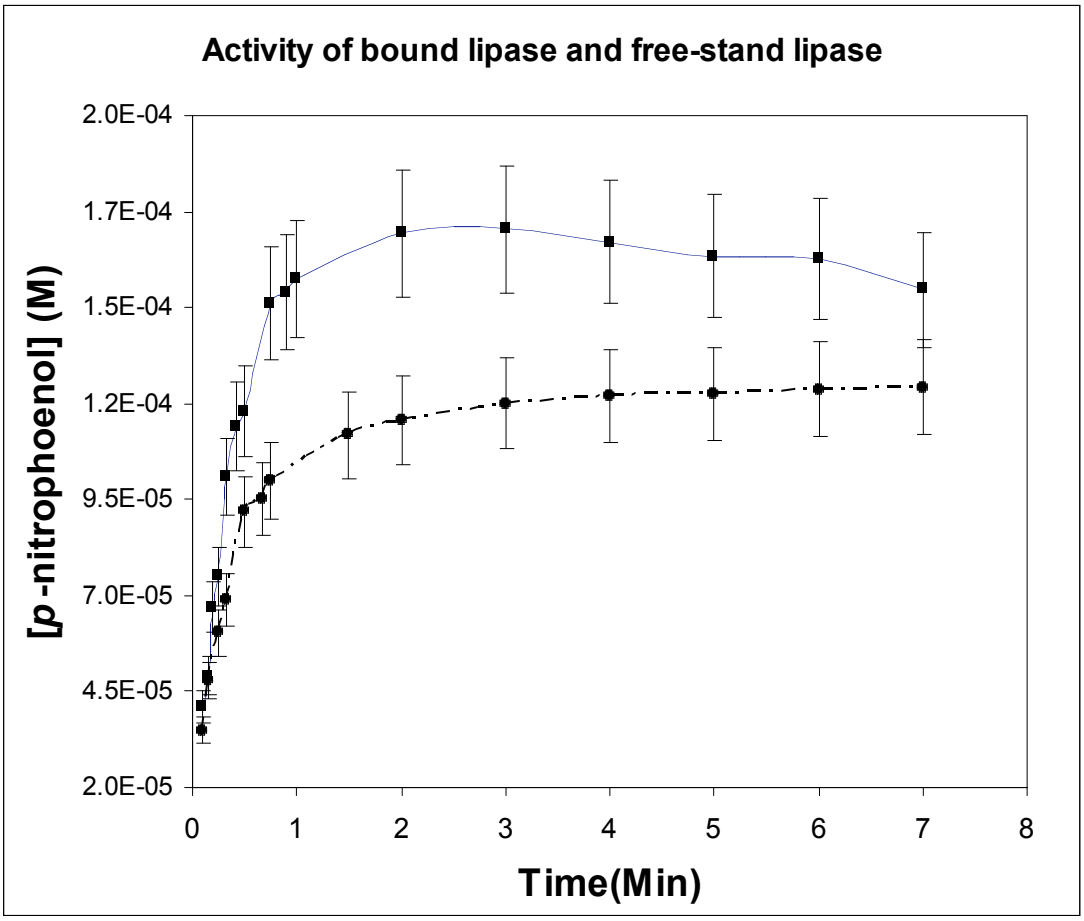

Figure 7.4 The product concentration versus reaction time, catalyzed by lipases (0.006 mg/mL) at room temperature, pH 7.0. The solid line and ■represent lipases inside the nanotubes and the dotted line and ●represent the freestanding lipases.

This result indicates that lipases in the nanotubes have sufficient contact with the reactants and the lipases are well dispersed on the inner wall of nanotubes. It means that the non-covalent binding between the peptide nanotube inner surfaces and lipases are strong enough to hold lipases during the enzymatic reaction. The increase of lipase activity may also be contributed by the conformation change of lipases as

lipase molecules were attached to the peptide nanotubes. When lipases were attached on an oil-water interface, their catalytic activity was enhanced dramatically because lipases could undergo the conformation change from the closed form (i.e., enzymatically inactive) to the more open form (i.e., enzymatically active) (*182*) . This type of conformation change has been detected by monitoring intrinsic fluorescence intensity

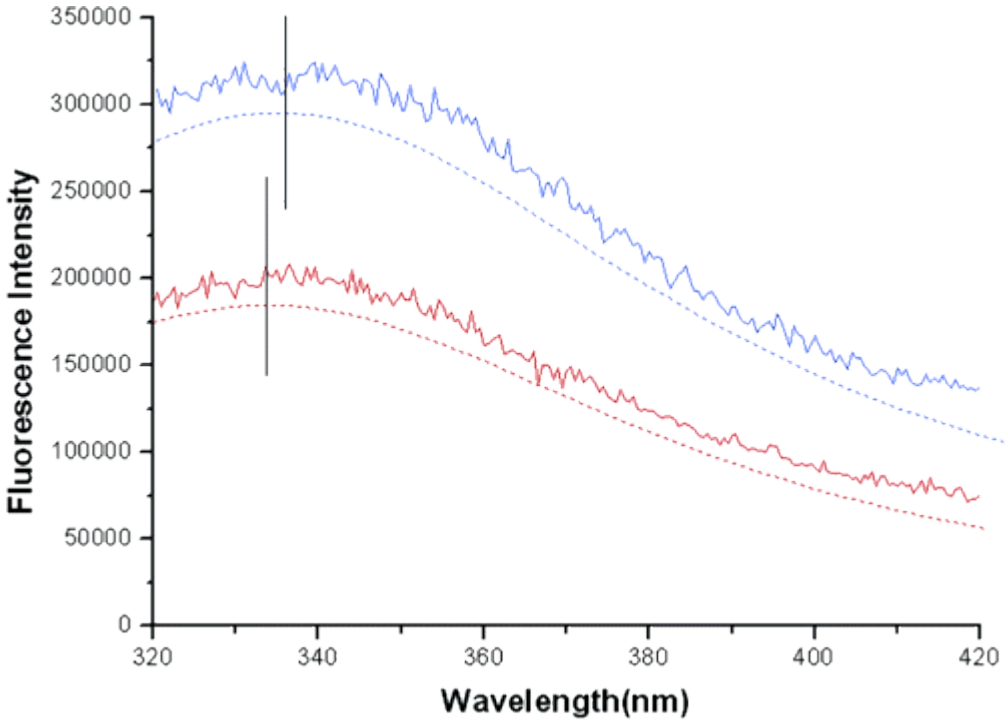

Figure 7.5 Fluorescence spectra of lipases bound the inside wall of peptide nanotubes (a blue line) and free-standing lipases (a red line). Dotted lines are the Lorentzian fits for these spectra and the computed peak positions by these fittings are also marked in this plot.

of tryptophan in lipases(*184*) . When lipases were unfolded to the open conformation, the hydrophobic pockets of lipases were exposed, which increased the fluorescence intensity of tryptophan. If the activity of lipases on peptide nanotubes is increased with the same mechanism via the conformation change induced by the nanotube-water interface, the increase of Trp fluorescence intensity of nanotube-bound lipases can be observed as compared to the freestanding lipases. Figure 7.5 shows the fluorescence intensity change of tryptophan in lipases before and after adding the peptide nanotube solution. The exact peak positions of these spectra was determined by the Lorenztian fits, as shown in dotted lines in figure 7.5. Indeed, the increase of lipase fluorescence intensity at 339 nm (blue) was observed after binding the nanotubes is observed, which is consistent with the enhancement mechanism observed in the lipase system at the oil-water interface. The red shift of the tryptophan peak from 333 nm (a peak of red line in figure 7.5) to 339 nm (a peak of blue line in figure 7.5) after the nanotube solution was added to lipase, is also consistent with the red-shift of the tryptophan's fluorescence spectra in polar environments. When we added the substrate to a solution of the peptide nanotubes without lipase and measured the amount of substrate remaining in solution by UV-vis absorption, the resulting substrate concentration was identical to the initial concentration of the substrate. Since there is no partitioning of substrates in the nanotubes over 24 hours, the observed enhancement of lipase activity in the peptide nanotubes is not due to simply local increase of the substrate concentration inside the nanotube. The conformation change of lipases inside the nanotubes may also indicate that the inner

surface of the peptide nanotube facilitates on the nanotube surface to adopt a favorable orientation to maximize the contact with the reactant, *p*-nitrophenol butyrate (*169, 178*) . The thermal stabilities of lipases inside the nanotubes and the freestanding lipases were compared between the temperature ranges, 25 ˚C – 75 ˚C, as shown in Figure 7.6.

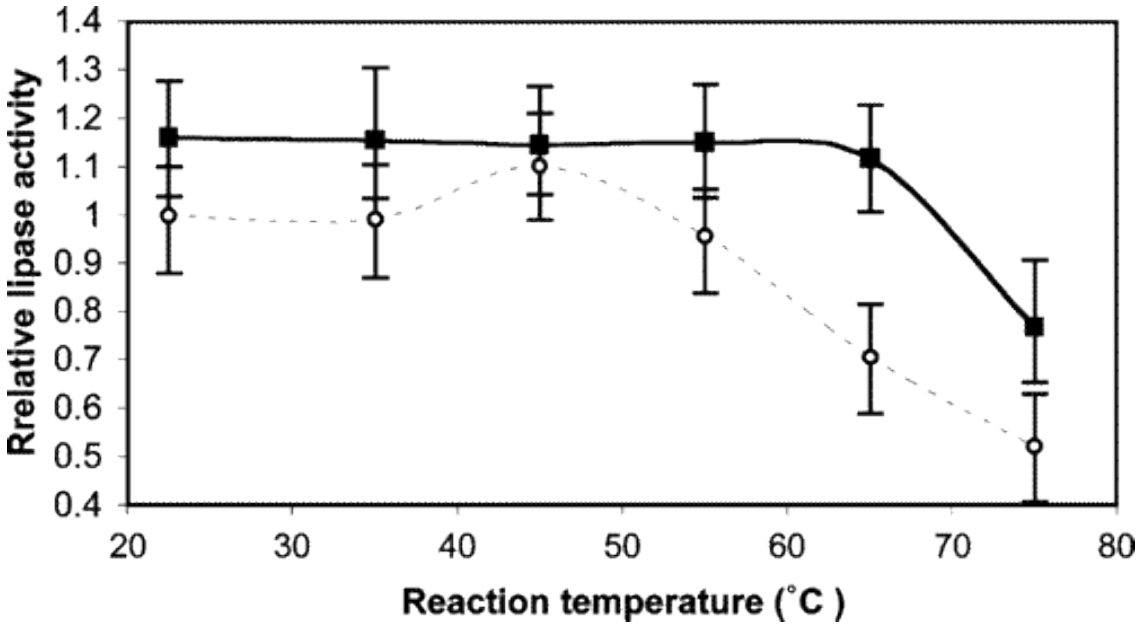

Figure 7.6 Thermal stabilities of lipases. The solid line and ■ represent lipases inside the nanotubes and the dotted line and ° represent the freestanding lipases

The relative lipase activity was calculated by normalizing the hydrolysis rates of *p*-nitrophenol butyrate with the hydrolysis rate of freestanding lipase at 22 ˚C. Below 45 ˚C, lipase activities were not affected by temperature and the activity of the nanotube-bound lipases (a solid line in Figure 7.6) was about 20 % higher than the

activity of freestanding lipases (a dotted line in Figure 7.6). However, there is a striking difference above 45 ˚C. At this higher temperature range, the nanotube-bound lipases still maintained its activity up to 65 ˚C but the freestanding lipases lost its activity rapidly. The activity of the nanotube-bound lipases was observed to be 70 % higher compared to the activity of the freestanding lipases at 65 ˚C. This activity enhancement was also held at 75 ˚C while the absolute activity of the nanotube-bound lipases starts falling at this temperature. All the activities of the lipases at different temperatures were obtained by initial slopes of *p*-nitrophenol concentration changes over the reaction time. This considerably improved thermal stability of the nanotube-bound lipases may be caused by the lipase stability and the geometrical protection in the peptide nanotube. The stable binding between the nanotubes and lipases may also contribute to maintain the open form of lipases, which keeps high catalytic activity at elevated temperature.

7.4 Conclusion

Peptide nanotubes were applied as supports for enzymes. We encapsulated a model enzyme inside peptide nanotubes, and the catalytic activity of the nanotube-bound enzymes was 33 % higher as compared to the freestanding lipase at room temperature. It was remarkable that the peptide nanotubes behaved as even better supports for enzymes at higher temperature. At the elevated temperature, 65 ˚C, the activity of lipases inside the nanotubes was 70 % higher as compared to the freestanding lipases.

It is advantageous to apply these peptide nanotubes as enzyme supports because the nanotubes can immobilize enzymes on the surfaces with a simple procedure and provide appropriate environment for the active conformation of lipases. The peptide nanotube can also be decorated by magnetic materials, which is beneficial to develop recyclable sensors and high-throughput catalysts.

Appendix

Synthesis of bis(N-α- amido-glycylglycine)-1,7-heptane dicarboxylate monomer(*58*)

First, 0.5g Azelaic acid ($HO_2C(CH_2)_7CO_2H$) and 0.65g 1-hydroxylbenzotriazole were dissolved in 250mL Dimethyl Formamide(DMF) solution and this solution was put on the bath of ice with stirrer. Then 10mL Chloroform (CH_3Cl) solution with 0.92g of 1-ethyl-3-(3-dimethylaminopropyl)-carbodiimide hydrochloride (EDAC) was added. After 1 hour stirring, a solution of 1.88g Gly-Gly benzyl ester p-toluenesulfonate salt in 10mL methanol and 0.67mL of triethylamine was added into reaction mixture. After this addition, the mixture was stirred for 24 hours at 0ºC and allowed to gradually warm to room temperature. Evaporation of solvent gave a white power, which was washed with 10% citric acid, distill water, then washed with 4% sodium hydrogencarbonate and distill water. This recrystallization process from DMF can gave about 1g benzyl ester white power. Then the intermediate power was dissolved in the 200ml DMF solution again and heated to about 85ºC. After stirring for 4 hours , the solution was allowed to cool to room temperature (about 10 min) and 5mL 1M HCl was added for the acidification. The solvent was evaporated again under reduced pressure to leave a white powder and after relatively dry, the product was thoroughly washed with acetone and distill water. The yield is about 60%. For the assembly of the peptide nanotubes, the bolaamphiphile monomers powder (10

mM) was dissolved in NaOH solution and then adjusted the pH to 4.5 by citric acid. After filtering of this monomer solution, the solvent was allowed to stand still for 2 weeks to self-assemble into nanotubes.

References:

(1) Contributors, W., Wikipedia, The Free Encyclopedia.

(2) Franke, M. E. (1959) There is lenty of Room at the Botton. *Engineering and Science*.

(3) Johnson, J. C., Choi, H. J., Knutsen, K. P., Schaller, R. D., Yang, P. D., and Saykally, R. J. (2002) Single gallium nitride nanowire lasers. *Nature Materials 1*, 106-110.

(4) Hamad-Schifferli, K., Schwartz, J. J., Santos, A. T., Zhang, S. G., and Jacobson, J. M. (2002) Remote electronic control of DNA hybridization through inductive coupling to an attached metal nanocrystal antenna. *Nature 415*, 152-155.

(5) Cui, Y., Wei, Q. Q., Park, H. K., and Lieber, C. M. (2001) Nanowire nanosensors for highly sensitive and selective detection of biological and chemical species. *Science 293*, 1289-1292.

(6) Collins, P. C., Arnold, M. S., and Avouris, P. (2001) Engineering carbon nanotubes and nanotube circuits using electrical breakdown. *Science 292*, 706-709.

(7) Murray, C. B., Kagan, C. R., and Bawendi, M. G. (2000) Synthesis and characterization of monodisperse nanocrystals and close-packed nanocrystal assemblies. *Annual Review Of Materials Science 30*, 545-610.

(8) Alivisatos, A. P. (1996) Semiconductor clusters, nanocrystals, and quantum dots. *Science 271*, 933-937.

(9) Brust, M., and Kiely, C. J. (2002) Some recent advances in nanostructure preparation from gold and silver particles: a short topical review. *Colloids And Surfaces A-Physicochemical And Engineering Aspects 202*, 175-186.

(10) Daniel, M. C., and Astruc, D. (2004) Gold Nanoparticles: Assembly, Supramolecular Chemistry, Quantum-Size-Related Properties, and Applications toward Biology, Catalysis, and Nanotechnology. *Chem. Rev. 104*, 293-346.

(11) Henglein, A. (1993) Physicochemical Properties Of Small Metal Particles In Solution - Microelectrode Reactions, Chemisorption, Composite Metal Particles, And The Atom-To-Metal Transition. *Journal Of Physical Chemistry 97*, 5457-5471.

(12) Fendler, J. H. (1996) Self-assembled nanostructured materials. *Chemistry Of Materials 8*, 1616-1624.

(13) Belloni, J. (1996) Metal nanocolloids. *Current Opinion In Colloid & Interface Science 1*, 184-196.

(14) Andres, R. P., Bein, T., Dorogi, M., Feng, S., Henderson, J. I., Kubiak, C. P., Mahoney, W., Osifchin, R. G., and Reifenberger, R. (1996) "Coulomb staircase" at room temperature in a self-assembled molecular nanostructure. *Science 272*, 1323-1325.

(15) Zhong, Z. H., Wang, D. L., Cui, Y., Bockrath, M. W., and Lieber, C. M. (2003) Nanowire crossbar arrays as address decoders for integrated nanosystems. *Science 302*, 1377-1379.

(16) Chen, R. J., Bangsaruntip, S., Drouvalakis, K. A., Kam, N. W. S., Shim, M., Li, Y. M., Kim, W., Utz, P. J., and Dai, H. J. (2003) Noncovalent functionalization of carbon nanotubes for highly specific electronic biosensors. *Proceedings Of The National Academy Of Sciences Of The United States Of America 100*, 4984-4989.

(17) Fennimore, A. M., Yuzvinsky, T. D., Han, W. Q., Fuhrer, M. S., Cumings, J., and Zettl, A. (2003) Rotational actuators based on carbon nanotubes. *Nature 424*, 408-410.

(18) Modi, A., Koratkar, N., Lass, E., Wei, B. Q., and Ajayan, P. M. (2003) Miniaturized gas ionization sensors using carbon nanotubes. *Nature 424*, 171-174.

(19) Badia, A., Singh, S., Demers, L., Cuccia, L., Brown, G. R., and Lennox, R. B. (1996) Self-assembled monolayers on gold nanoparticles. *Chemistry-A European Journal 2*, 359-363.

(20) Yao, H., Momozawa, O., Hamatani, T., and Kimura, K. (2001) Stepwise size-selective extraction of carboxylate-modified gold nanoparticles from an aqueous suspension into toluene with tetraoctylammonium cations. *Chemistry Of Materials 13*, 4692-4697.

(21) Miyazaki, A., and Nakano, Y. (2000) Morphology of platinum nanoparticles protected by poly(N-isopropylacrylamide). *Langmuir 16*, 7109-7111.

(22) Bonnemann, H., Brijoux, W., and Joussen, T. (1990) The Preparation Of Finely Divided Metal And Alloy Powders. *Angewandte Chemie-International Edition In English 29*, 273-275.

(23) Viau, G., Fievet-Vincent, F., and Fievet, F. (1996) Nucleation and growth of bimetallic CoNi and FeNi monodisperse particles prepared in polyols. *Solid State Ionics 84*, 259.

(24) Chen, S. H., and Kimura, K. (1999) Water soluble silver nanoparticles functionalized with thiolate. *Chemistry Letters*, 1169-1170.

(25) Han, M. Y., Quek, C. H., Huang, W., Chew, C. H., and Gan, L. M. (1999) A Simple and Effective Chemical Route for the Preparation of Uniform Nonaqueous Gold Colloids. *Chem. Mater. 11*, 1144-1147.

(26) Tan, Y. W., Dai, X. H., Li, Y. F., and Zhu, D. B. (2003) Preparation of gold, platinum, palladium and silver nanoparticles by the reduction of their salts with a weak reductant-potassium bitartrate. *Journal Of Materials Chemistry 13*, 1069-1075.

(27) Chen, D. H., and Hsieh, C. H. (2002) Synthesis of nickel nanoparticles in aqueous cationic surfactant solutions. *Journal Of Materials Chemistry 12*, 2412-2415.

(28) Gui, Z., Fan, R., Mo, W., Chen, X., Yang, L., and Hu, Y. (2003) Synthesis and characterization of reduced transition metal oxides and nanophase metals with hydrazine in aqueous solution. *Materials Research Bulletin 38*, 169.

(29) Shipway, A. N., Katz, E., and Willner, I. (2000) Nanoparticle arrays on surfaces for electronic, optical, and sensor applications. *Chemphyschem 1*, 18-52.

(30) Katz, E., and Willner, I. (2004) Integrated nanoparticle-biomolecule hybrid systems: Synthesis, properties, and applications. *Angewandte Chemie-International Edition 43*, 6042-6108.

(31) Mirkin, C. A., Letsinger, R. L., Mucic, R. C., and Storhoff, J. J. (1996) A DNA-based method for rationally assembling nanoparticles into macroscopic materials. *Nature 382*, 607-609.

(32) Greig, L. M., and Philp, D. (2001) Applying biological principles to the assembly and selection of synthetic superstructures. *Chemical Society Reviews 30*, 287-302.

(33) Niemeyer, C. M. (2001) Nanoparticles, proteins, and nucleic acids: Biotechnology meets materials science. *Angewandte Chemie-International Edition 40*, 4128-4158.

(34) Seidel, R., Mertig, M., and Pompe, W. (2002) Scanning force microscopy of DNA metallization. *Surface And Interface Analysis 33*, 151-154.

(35) Dujardin, E., Peet, C., Stubbs, G., Culver, J. N., and Mann, S. (2003) Organization of metallic nanoparticles using tobacco mosaic virus templates. *Nano Letters 3*, 413-417.

(36) Zhang, C. L., Vali, H., Romanek, C. S., Phelps, T. J., and Liu, S. V. (1998) Formation of single-domain magnetite by a thermophilic bacterium. *American Mineralogist 83*, 1409-1418.

(37) Zhang, C. L., Liu, S., Logan, J., Mazumder, R., and Phelps, T. J. (1996) Enhancement of Fe(III), Co(III), and Cr(VI) reduction at elevated temperatures and by a thermophilic bacterium. *Applied Biochemistry And Biotechnology 57-8*, 923-932.

(38) Zhang, C. L., Liu, S., Phelps, T. J., Cole, D. R., Horita, J., Fortier, S. M., Elless, M., and Valley, J. W. (1997) Physiochemical, mineralogical, and isotopic characterization of magnetite-rich iron oxides formed by thermophilic iron-reducing bacteria. *Geochimica Et Cosmochimica Acta 61*, 4621-4632.

(39) Roh, Y., Liu, S. V., Li, G. S., Huang, H. S., Phelps, T. J., and Zhou, J. Z. (2002) Isolation and characterization of metal-reducing Thermoanaerobacter strains from deep subsurface environments of the Piceance Basin, Colorado. *Applied And Environmental Microbiology 68*, 6013-6020.

(40) Roh, Y., Lauf, R. J., McMillan, A. D., Zhang, C., Rawn, C. J., Bai, J., and Phelps, T. J. (2001) Microbial synthesis and the characterization of metal-substituted magnetites. *Solid State Communications 118*, 529-534.

(41) Gardea-Torresdey, J. L., Parsons, J. G., Gomez, E., Peralta-Videa, J., Troiani, H. E., Santiago, P., and Yacaman, M. J. (2002) Formation and growth of Au nanoparticles inside live alfalfa plants. *Nano Letters 2*, 397-401.

(42) McInnes, B. I. A., Dunn, C. E., Cameron, E. M., and Kameko, L. (1996) Biogeochemical exploration for gold in tropical rain forest regions of Papua New Guinea. *Journal Of Geochemical Exploration 57*, 227-243.

(43) Banerjee, I. A., Yu, L. T., and Matsui, H. (2003) Application of host-guest chemistry in nanotube-based device fabrication: Photochemically controlled immobilization of azobenzene nanotubes on patterned alpha-CD monolayer/Au substrates via molecular recognition. *Journal Of The American Chemical Society 125*, 9542-9543.

(44) Matsui, H., and MacCuspie, R. (2001) Metalloporphyrin nanotube fabrication using peptide nanotubes as templates. *Nano Letters 1*, 671-675.

(45) Gyorvary, E., Schroedter, A., Talapin, D. V., Weller, H., Pum, D., and Sleytr, U. B. (2004) Formation of nanoparticle arrays on S-layer protein lattices. *Journal Of Nanoscience And Nanotechnology 4*, 115-120.

(46) Mbindyo, J. K. N., Reiss, B. D., Martin, B. R., Keating, C. D., Natan, M. J., and Mallouk, T. E. (2001) DNA-directed assembly of gold nanowires on complementary surfaces. *Advanced Materials 13*, 249-+.

(47) Braun, E., Eichen, Y., Sivan, U., and Ben-Yoseph, G. (1998) DNA-templated assembly and electrode attachment of a conducting silver wire. *Nature 391*, 775-778.

(48) Iijima, S. (1991) Helical Microtubules Of Graphitic Carbon. *Nature 354*, 56-58.

(49) Iijima, S., and Ichihashi, T. (1993) Single-Shell Carbon Nanotubes Of 1-Nm Diameter (Vol 363, Pg 603, 1993). *Nature 364*, 737-737.

(50) Amlani, I., Zhang, R., Tresek, J., and Tsui, R. K. (2003) Room-temperature single-electron charging effects in an ambipolar single-walled carbon nanotube grown by chemical vapor deposition. *Journal Of Vacuum Science & Technology B 21*, 2848-2851.

(51) Hartgerink, J. D., Granja, J. R., Milligan, R. A., and Ghadiri, M. R. (1996) Self-assembling peptide nanotubes. *Journal Of The American Chemical Society 118*, 43-50.

(52) Shenton, W., Douglas, T., Young, M., Stubbs, G., and Mann, S. (1999) Inorganic-organic nanotube composites from template mineralization of tobacco mosaic virus. *Advanced Materials 11*, 253-+.

(53) Ghadiri, M. R., Granja, J. R., Milligan, R. A., McRee, D. E., and Khazanovich, N. (1993) Self-Assembling Organic Nanotubes Based On A Cyclic Peptide Architecture. *Nature 366*, 324-327.

(54) Shimizu, T., Kogiso, M., and Masuda, M. (1997) Noncovalent formation of polyglycine II-type structure by hexagonal self-assembly of linear polymolecular chains. *Journal Of The American Chemical Society 119*, 6209-6210.

(55) Lu, K., Jacob, J., Thiyagarajan, P., Conticello, V. P., and Lynn, D. G. (2003) Exploiting amyloid fibril lamination for nanotube self-assembly. *Journal Of The American Chemical Society 125*, 6391-6393.

(56) Vauthey, S., Santoso, S., Gong, H. Y., Watson, N., and Zhang, S. G. (2002) Molecular self-assembly of surfactant-like peptides to form nanotubes and nanovesicles. *Proceedings Of The National Academy Of Sciences Of The United States Of America 99*, 5355-5360.

(57) Matsui, H., and Gologan, B. (2000) Crystalline Glycylglycine Bolaamphiphile Tubules and Their pH-Sensitive Structural Transformation. *J. Phys. Chem. B 104*, 3383-3386.

(58) Kogiso, M., Ohnishi, S., Yase, K., Masuda, M., and Shimizu, T. (1998) Dicarboxylic Oligopeptide Bolaamphiphiles: Proton-Triggered Self-Assembly of Microtubes with Loose Solid Surfaces. *Langmuir 14*, 4978-4986.

(59) Kogiso, M., Masuda, M., and Shimizu, T. (1998) Supramolecular polyglycine II-type structure of glycylglycine bolaamphiphile. *Supramolecular Chemistry 9*, 183-189.

(60) Douberly, G. E., Pan, S., Walters, D., and Matsui, H. (2001) Fabrication of protein tubules: Immobilization of proteins on peptide tubules. *Journal Of Physical Chemistry B 105*, 7612-7618.

(61) Djalali, R., Chen, Y., and Matsui, H. (2002) Au nanowire fabrication from sequenced histidine-rich peptide. *Journal Of The American Chemical Society 124*, 13660-13661.

(62) Nuraje, N., Banerjee, I. A., MacCuspie, R. I., Yu, L. T., and Matsui, H. (2004) Biological bottom-up assembly of antibody nanotubes on patterned antigen arrays. *Journal Of The American Chemical Society 126*, 8088-8089.

(63) Yu, L. T., Banerjee, I. A., and Matsui, H. (2003) Direct growth of shape-controlled nanocrystals on nanotubes via biological recognition. *Journal Of The American Chemical Society 125*, 14837-14840.

(64) Djalali, R., Chen, Y. F., and Matsui, H. (2003) Au nanocrystal growth on nanotubes controlled by conformations and charges of sequenced peptide templates. *Journal Of The American Chemical Society 125*, 5873-5879.

(65) Banerjee, I. A., Yu, L. T., and Matsui, H. (2003) Cu nanocrystal growth on peptide nanotubes by biomineralization: Size control of Cu nanocrystals by tuning peptide conformation. *Proceedings Of The National Academy Of Sciences Of The United States Of America 100*, 14678-14682.

(66) Yu, L. T., Banerjee, I. A., and Matsui, H. (2004) Incorporation of sequenced peptides on nanotubes for Pt coating: smart control of nucleation and morphology via activation of metal binding sites on amino acids. *Journal Of Materials Chemistry 14*, 739-743.

(67) Yu, L. T., Banerjee, I. A., Shima, M., Rajan, K., and Matsui, H. (2004) Size-controlled ni nanocrystal growth on peptide nanotubes and their magnetic properties. *Advanced Materials 16*, 709-+.

(68) Field, M., Smith, C. J., Awschalom, D. D., Mendelson, N. H., Mayes, E. L., Davis, S. A., and Mann, S. (1998) Ordering nanometer-scale magnets using bacterial thread templates. *Applied Physics Letters 73*, 1739-1741.

(69) Behrens, S., Rahn, K., Habicht, W., Bohm, K. J., Rosner, H., Dinjus, E., and Unger, E. (2002) Nanoscale particle arrays induced by highly ordered protein assemblies. *Advanced Materials 14*, 1621-1625.

(70) Seeman, N. C., and Belcher, A. M. (2002) Emulating biology: Building nanostructures from the bottom up. *Proceedings Of The National Academy Of Sciences Of The United States Of America 99*, 6451-6455.

(71) Douglas, T., and Young, M. (1999) Virus particles as templates for materials synthesis. *Advanced Materials 11*, 679-+.

(72) Demir, M., and Stowell, M. H. B. (2002) A chemoselective biomolecular template for assembling diverse nanotubular materials. *Nanotechnology 13*, 541-544.

(73) Gao, Y., and Koumoto, K. (2005) Bioinspired Ceramic Thin Film Processing: Present Status and Future Perspectives. *Crystal Growth & Design 5*, 1983-2017.

(74) Orme, C. A., Noy, A., Wierzbicki, A., McBride, M. T., Grantham, M., Teng, H. H., Dove, P. M., and DeYoreo, J. J. (2001) Formation of chiral morphologies through selective binding of amino acids to calcite surface steps. *Nature 411*, 775-779.

(75) Belcher, A. M., Wu, X. H., Christensen, R. J., Hansma, P. K., Stucky, G. D., and Morse, D. E. (1996) Control of crystal phase switching and orientation by soluble mollusc-shell proteins. *Nature 381*, 56-58.

(76) Smith, B. L., Schaffer, T. E., Viani, M., Thompson, J. B., Frederick, N. A., Kindt, J., Belcher, A., Stucky, G. D., Morse, D. E., and Hansma, P. K. (1999) Molecular mechanistic origin of the toughness of natural adhesives, fibres and composites. *Nature 399*, 761-763.

(77) Wang, R. Z., Suo, Z., Evans, A. G., Yao, N., and Aksay, I. A. (2001) Deformation mechanisms in nacre. *Journal Of Materials Research 16*, 2485-2493.

(78) Liang, H., Angelini, T. E., Ho, J., Braun, P. V., and Wong, G. C. L. (2003) Molecular Imprinting of Biomineralized CdS Nanostructures: Crystallographic Control Using Self-Assembled DNA-Membrane Templates. *J. Am. Chem. Soc. 125*, 11786-11787.

(79) Aizenberg, J., Black, A. J., and Whitesides, G. M. (1999) Control of crystal nucleation by patterned self-assembled monolayers. *Nature 398*, 495-498.

(80) Xu, G. F., Aksay, I. A., and Groves, J. T. (2001) Continuous crystalline carbonate apatite thin films. A biomimetic approach. *Journal Of The American Chemical Society 123*, 2196-2203.

(81) Naka, K., and Chujo, Y. (2001) Control of Crystal Nucleation and Growth of Calcium Carbonate by Synthetic Substrates. *Chem. Mater. 13*, 3245-3259.

(82) Fortin, D., and Beveridge, T. J. (1997) Microbial sulfate reduction within sulfidic mine tailings: Formation of diagenetic Fe sulfides. *Geomicrobiology Journal 14*, 1-21.

(83) Sano, K. I., Sasaki, H., and Shiba, K. (2005) Specificity and Biomineralization Activities of Ti-Binding Peptide-1 (TBP-1). *Langmuir 21*, 3090-3095.

(84) Dujardin, E., and Mann, S. (2002) Bio-inspired materials chemistry. *Advanced Materials 14*, 775-788.

(85) Jung, J. H., and Shinkai, S. (2004) Gels as templates for nanotubes, in *Templates In Chemistry I* pp 223-260.

(86) Jong Hwa Jung, S. S. T. S. (2003) Organic supramolecular architectures and their sol-gel transcription to Silica nanotubes. *The Chemical Record 3*, 212-224.

(87) Loweth, C. J., Caldwell, W. B., Peng, X. G., Alivisatos, A. P., and Schultz, P. G. (1999) DNA-based assembly of gold nanocrystals. *Angewandte Chemie-International Edition 38*, 1808-1812.

(88) Beveridge, T. J. (1989) *Metal Ions and Bacteria*, Wiley, New York.

(89) Lower, S. K., Hochella, M. F., and Beveridge, T. J. (2001) Bacterial recognition of mineral surfaces: Nanoscale interactions between Shewanella and alpha-FeOOH. *Science 292*, 1360-1363.

(90) Naik, R. R., Stringer, S. J., Agarwal, G., Jones, S. E., and Stone, M. O. (2002) Biomimetic synthesis and patterning of silver nanoparticles. *Nature Materials 1*, 169-172.

(91) Cha, J. N., Stucky, G. D., Morse, D. E., and Deming, T. J. (2000) Biomimetic synthesis of ordered silica structures mediated by block copolypeptides. *Nature 403*, 289-292.

(92) Whaley, S. R., English, D. S., Hu, E. L., Barbara, P. F., and Belcher, A. M. (2000) Selection of peptides with semiconductor binding specificity for directed nanocrystal assembly. *Nature 405*, 665-668.

(93) Lee, S. W., Mao, C. B., Flynn, C. E., and Belcher, A. M. (2002) Ordering of quantum dots using genetically engineered viruses. *Science 296*, 892-895.

(94) Mao, C. B., Solis, D. J., Reiss, B. D., Kottmann, S. T., Sweeney, R. Y., Hayhurst, A., Georgiou, G., Iverson, B., and Belcher, A. M. (2004) Virus-based toolkit for the directed synthesis of magnetic and semiconducting nanowires. *Science 303*, 213-217.

(95) Schembri, M. A., Kjaergaard, K., and Klemm, P. (1999) Bioaccumulation of heavy metals by fimbrial designer adhesins. *Fems Microbiology Letters 170*, 363-371.

(96) Mao, C. B., Flynn, C. E., Hayhurst, A., Sweeney, R., Qi, J. F., Georgiou, G., Iverson, B., and Belcher, A. M. (2003) Viral assembly of oriented quantum dot nanowires. *Proceedings Of The National Academy Of Sciences Of The United States Of America 100*, 6946-6951.

(97) Abdelouas, A., Gong, W. L., Lutze, W., Shelnutt, J. A., Franco, R., and Moura, I. (2000) Using cytochrome c(3) to make selenium nanowires. *Chemistry Of Materials 12*, 1510-+.

(98) Gates, B., Mayers, B., Cattle, B., and Xia, Y. N. (2002) Synthesis and characterization of uniform nanowires of trigonal selenium. *Advanced Functional Materials 12*, 219-227.

(99) Sumerel, J. L., Yang, W. J., Kisailus, D., Weaver, J. C., Choi, J. H., and Morse, D. E. (2003) Biocatalytically templated synthesis of titanium dioxide. *Chemistry Of Materials 15*, 4804-4809.

(100) Reches, M., and Gazit, E. (2003) Casting metal nanowires within discrete self-assembled peptide nanotubes. *Science 300*, 625-627.

(101) Alivisatos, P. (2004) The use of nanocrystals in biological detection. *Nature Biotechnology 22*, 47-52.
(102) West, J. L., and Halas, N. J. (2003) Engineered nanomaterials for biophotonics applications: Improving sensing, imaging, and therapeutics. *Annual Review Of Biomedical Engineering 5*, 285-292.
(103) Yu, L., Banerjee, I. A., Gao, X., Nuraje, N., and Matsui, H. (2005) Fabrication and Application of Enzyme-Incorporated Peptide Nanotubes. *Bioconjugate Chem.*
(104) Gou, L., and Murphy, C. J. (2003) Solution-Phase Synthesis of Cu₂O Nanocubes. *Nano Lett. 3*, 231-234.
(105) Puntes, V. F., Krishnan, K. M., and Alivisatos, A. P. (2001) Colloidal nanocrystal shape and size control: The case of cobalt. *Science 291*, 2115-2117.
(106) Chen, S., Fan, Z., and Carroll, D. L. (2002) Silver Nanodisks: Synthesis, Characterization, and Self-Assembly. *J. Phys. Chem. B 106*, 10777-10781.
(107) Taton, T. A. (2003) Bio-nanotechnology: Two-way traffic. *Nature Materials 2*, 73-74.
(108) Matsui, H., Porrata, P., and Douberly, G. E. (2001) Protein tubule immobilization on self-assembled monolayers on Au substrates. *Nano Letters 1*, 461-464.
(109) Banerjee, I. A., Yu, L. T., and Matsui, H. (2003) Location-specific biological functionalization on nanotubes: Attachment of proteins at the ends of nanotubes using Au nanocrystal masks. *Nano Letters 3*, 283-287.
(110) Mertig, M., Colombi Ciacchi, L., Seidel, R., Pompe, W., and De Vita, A. (2002) DNA as a Selective Metallization Template. *Nano Lett. 2*, 841-844.
(111) Warner, M. G., and Hutchison, J. E. (2003) Linear assemblies of nanoparticles electrostatically organized on DNA scaffolds. *Nature Materials 2*, 272-277.
(112) Remacle, F., Beverly, K. C., Heath, J. R., and Levine, R. D. (2002) Conductivity of 2-D Ag Quantum Dot Arrays: Computational Study of the Role of Size and Packing Disorder at Low Temperatures. *J. Phys. Chem. B 106*, 4116-4126.
(113) Aizenberg, J., Lambert, G., Weiner, S., and Addadi, L. (2002) Factors Involved in the Formation of Amorphous and Crystalline Calcium Carbonate: A Study of an Ascidian Skeleton. *J. Am. Chem. Soc. 124*, 32-39.
(114) Shi, D. H., Hambley, T. W., and Freeman, H. C. (1999) Three new platinum(II)-dipeptide complexes. *Journal Of Inorganic Biochemistry 73*, 173-186.
(115) Pappalardo, G., Impellizzeri, G., Bonomo, R. P., Campagna, T., Grasso, G., and Saita, M. G. (2002) Copper(II) and nickel(II) binding modes in a histidine-containing model dodecapeptide. *New Journal Of Chemistry 26*, 593-600.
(116) Tsiveriotis, P., and Hadjiliadis, N. (1999) Studies on the interaction of histidyl containing peptides with palladium(II) and platinum(II) complex ions. *Coordination Chemistry Reviews 192*, 171-184.

(117) Blundell, T. L., and Jenkins, J. A. (1977) Binding Of Heavy-Metals To Proteins. *Chemical Society Reviews 6*, 139-171.

(118) Casolaro, M., Chelli, M., Ginanneschi, M., Laschi, F., Muniz-Miranda, M., Papini, A. M., and Sbrana, G. (1999) Spectroscopic and potentiometric study of copper(II) complexes with L-histidyl-glycyl-L-histidyl-glycine in aqueous solution. *Spectrochimica Acta Part A-Molecular And Biomolecular Spectroscopy 55*, 1675-1689.

(119) Torreggiani, A., Taddei, P., and Fini, G. (2002) Characterization of dioxygenated cobalt(II)-carnosine complexes by Raman and IR spectroscopy. *Biopolymers 67*, 70-81.

(120) Miura, T., Hori-i, A., Mototani, H., and Takeuchi, H. (1999) Raman spectroscopic study on the copper(II) binding mode of prion octapeptide and its pH dependence. *Biochemistry 38*, 11560-11569.

(121) Miura, T., Suzuki, K., Kohata, N., and Takeuchi, H. (2000) Metal binding modes of Alzheimer's amyloid beta-peptide in insoluble aggregates and soluble complexes. *Biochemistry 39*, 7024-7031.

(122) Puntes, V. F., Zanchet, D., Erdonmez, C. K., and Alivisato, A. D. (2002) Synthesis of hcp-Co Nanodisks. *J. Am. Chem. Soc. 124*, 12874-12880.

(123) Wang, Z. L., Dai, Z. R., and Sun, S. H. (2000) Polyhedral shapes of cobalt nanocrystals and their effect on ordered nanocrystal assembly. *Advanced Materials 12*, 1944-+.

(124) Hansen, P. L., Wagner, J. B., Helveg, S., Rostrup-Nielsen, J. R., Clausen, B. S., and Topsoe, H. (2002) Atom-resolved imaging of dynamic shape changes in supported copper nanocrystals. *Science 295*, 2053-2055.

(125) Filankembo, A., and Pileni, M. P. (2000) Shape control of copper nanocrystals. *Applied Surface Science 164*, 260-267.

(126) Markovich, G., Collier, C. P., Henrichs, S. E., Remacle, F., Levine, R. D., and Heath, J. R. (1999) Architectonic quantum dot solids. *Accounts Of Chemical Research 32*, 415-423.

(127) Dujardin, E., Peet, C., Stubbs, G., Culver, J. N., and Mann, S. (2003) Organization of Metallic Nanoparticles Using Tobacco Mosaic Virus Templates. *Nano Lett. 3*, 413-417.

(128) Banerjee, S., and Wong, S. S. (2002) Synthesis and Characterization of Carbon Nanotube-Nanocrystal Heterostructures. *Nano Lett. 2*, 195-200.

(129) Remacle, F., and Levine, R. D. (2000) Electronic Response of Assemblies of Designer Atoms: The Metal-Insulator Transition and the Role of Disorder. *J. Am. Chem. Soc. 122*, 4084-4091.

(130) Gardea-Torresdey, J. L., Parsons, J. G., Gomez, E., Peralta-Videa, J., Troiani, H. E., Santiago, P., and Yacaman, M. J. (2002) Formation and Growth of Au Nanoparticles inside Live Alfalfa Plants. *Nano Lett. 2*, 397-401.

(131) Ziegler, J., Chang, R. T., and Wright, D. W. (1999) Multiple-Antigenic Peptides of Histidine-Rich Protein II of Plasmodium falciparum: Dendrimeric Biomineralization Templates. *J. Am. Chem. Soc. 121*, 2395-2400.

(132) Beverly, K. C., Sample, J. L., Sampaio, J. F., Remacle, F., Heath, J. R., and Levine, R. D. (2002) Quantum dot artificial solids: Understanding the static and dynamic role of size and packing disorder. *Proceedings Of The National Academy Of Sciences Of The United States Of America 99*, 6456-6459.
(133) Pileni, M. P. (2001) Mesostructured Fluids in Oil-Rich Regions: Structural and Templating Approaches. *Langmuir 17*, 7476-7486.
(134) Shimizu, T., Kogiso, M., and Masuda, M. (1996) Vesicle assembly in microtubes. *Nature 383*, 487-488.
(135) Halverson, K. J., Sucholeiki, I., Ashburn, T. T., and Lansbury, P. T. (1991) Location Of Beta-Sheet-Forming Sequences In Amyloid Proteins By Ftir. *Journal Of The American Chemical Society 113*, 6701-6703.
(136) Djalali, R., Chen, Y.-f., and Matsui, H. (2003) Au Nanocrystal Growth on Nanotubes Controlled by Conformations and Charges of Sequenced Peptide Templates. *J. Am. Chem. Soc. 125*, 5873.
(137) Yu, L., Banerjee, I. A., and Matsui, H. (2003) Direct Growth of Shape-Controlled Nanocrystals on Nanotubes via Biological Recognition. *J. Am. Chem. Soc. 125*, 14837.
(138) Baeuerlein, E. (2000) *Biomineralization*, Wiley-VCH, Cambridge.
(139) Mann, S. (2001) *Biomineralization*, Oxford University Press, New York.
(140) Casolaro, M., Chelli, M., Ginanneschi, M., Laschi, F., Muniz-Miranda, M., Papini, A. M., and Sbrana, G. (1999) Spectroscopic and potentiometric study of copper(II) complexes with L-hisdidyl-glycyl-L-glycine in aqueous solution. *Spectrochim. Acta A. 55*, 1675-1689.
(141) Pappalardo, G., Impellizzeri, G., Bonomo, R. P., Campagna, T., Grasso, G., and Saita, M. G. (2002) Copper(II) and nickel(II) binding modes in a histidine-containing model dodecapeptide. *New J. Chem. 26*, 593-600.
(142) Banerjee, I. A., Yu, L., and Matsui, H. (2003) Cu Nanocrystal Growth on Peptide Nanotubes via Biomineralization: Size Control of Cu Nanocrystals by Tuning Peptide Conformation. *Proc. Natl. Acad. Sci. USA 100*, 14678.
(143) Russier, V., Petit, C., and Pileni, M. P. (2003) Hysteresis curve of magnetic nanocrystals monolayers: Influence of the structure. *J. Appl. Phys. 93*, 10001.
(144) Perez, J. M., Josephson, L., O'Loughlin, T., Hogemann, D., and Weissleder, R. (2002) Magnetic relaxation switches capable of sensing molecular interactions. *Nature Biotechnol. 20*, 816.
(145) Perez, J. M., Simeone, F. J., Saeki, Y., Josephson, L., and Weissleder, R. (2003) Viral-induced self-assembly of magnetic nanoparticles allows the detection of viral particles in biological media. *J. Am. Chem. Soc. 125*, 10192.
(146) Baselt, D. R., Lee, G. U., Natesan, M., Metzger, S. W., Sheehan, P. E., and Colton, R. J. (1998) A biosensor based on magnetoresistance technology. *Biosens. Bioelectron 13*, 731.
(147) Chemla, Y. R., Crossman, H. L., Poon, Y., McDermott, R., Stevens, R., Alper, M. D., and Clarke, J. (2000) Ultrasensitive magnetic biosensor for homogeneous immunoassay. *Proc. Natl. Acad. Sci. USA 97*, 14268.

(148) Flynn, C. E., Mao, C. B., Hayhurst, A., Williams, J. L., Georgiou, G., Iverson, B., and Belcher, A. M. (2003) Synthesis and organization of nanoscale II-VI semiconductor materials using evolved peptide specificity and viral capsid assembly. *Journal Of Materials Chemistry 13*, 2414-2421.

(149) Zhang, H. Z., Gilbert, B., Huang, F., and Banfield, J. F. (2003) Water-driven structure transformation in nanoparticles at room temperature. *Nature 424*, 1025-1029.

(150) Ding, Y., Wang, X. D., and Wang, Z. L. (2004) Phase controlled synthesis of ZnS nanobelts: zinc blende vs wurtzite. *Chemical Physics Letters 398*, 32-36.

(151) Zhao, Y. W., Zhang, Y., Zhu, H., Hadjipianayis, G. C., and Xiao, J. Q. (2004) Low-temperature synthesis of hexagonal (wurtzite) ZnS nanocrystals. *Journal Of The American Chemical Society 126*, 6874-6875.

(152) Naik, R. R., Stringer, S. J., Agarwal, G., Jones, S. E., and Stone, M. O. (2002) Biomimetic synthesis and patterning of silver nanoparticles. *Nature Mater. 1*, 169-172.

(153) Cha, N. J., Stucky, G. D., Morse, D. E., and Deming, T. J. (2000) Biomimetic syntheses of ordered silica structures mediated by block copolypeptides. *Nature 403*, 289-292.

(154) Sarikaya, M., Tamerler, C., Jen, A. K. Y., and Schulten, K. (2003) Molecular biomimetics: nanotechnology through biology. *Nature Mater. 2*, 577-585.

(155) Reches, M., and Gazit, E. (2003) Casting metal nanowires within discrete self-assembled peptide nanotubes. *Science 300*, 625.

(156) Sano, K. I., Sasaki, H., and Shiba, K. (2005) Specificity and biomineralization activities of Ti-binding peptide-1 (TBP-1). *Langmuir 21*, 3090.

(157) Kho, R., Nguyen, L., Torres-Martinez, C. L., and Mehra, R. K. (2000) Zinc-histidine as nucleation centers for growth of ZnS nanocrystals. *Biochemical And Biophysical Research Communications 272*, 29-35.

(158) Zoueva, O. P., Bailly, J. E., Nicholls, R., and Brown, E. G. (2002) Aggregation of influenza virus ribonucleocapsids at low pH. *Virus Research 85*, 141-149.

(159) Okada, A., Miura, T., and Takeuchi, H. (2003) Zinc- and pH-Dependent Conformational Transition in a Putative Interdomain Linker Region of the Influenza Virus Matrix Protein M1. *Biochemistry 42*, 1978-1984.

(160) Miura, T., Satoh, T., and Takeuchi, H. (1998) Role of metal-ligand coordination in the folding pathway of zinc finger peptides. *Biochimica Et Biophysica Acta-Protein Structure And Molecular Enzymology 1384*, 171-179.

(161) Hsu, A. F., Foglia, T. A., and Shen, S. (2000) Immobilization of Pseudomonas cepacia lipase in a phyllosilicate sol-gel matrix: effectiveness as a biocatalyst. *Biotechnol. Appl. Biochem. 31*, 179-183.

(162) Junjie Liu, C.-H. W. (2002) Aldolase-Catalyzed Asymmetric Synthesis of Novel Pyranose Synthons as a New Entry to Heterocycles and Epothilones. *Angewandte Chemie International Edition 41*, 1404-1407.

(163) Cao, L. Q., Bornscheuer, U. T., and Schmid, R. D. (1999) Lipase-catalyzed solid-phase synthesis of sugar esters. Influence of immobilization on productivity and stability of the enzyme. *J. Mol. Catal. B: Enzy. 6*, 279-285.
(164) Letant, S. E., Hart, B. R., Kane, S. R., Hadi, M. Z., Shields, S. J., and Reynolds, J. G. (2004) Enzyme immobilization on porous silicon surfaces. *Adv. Mater. 16*, 689-692.
(165) Reetz, M. T., Zonta, A., Vijayakrishnan, V., and Schimossek, K. (1998) Entrapment of lipases in hydrophobic magnetite-containing sol-gel materials: magnetic separation of heterogeneous biocatalysts. *Journal of Molecular Catalysis A: Chemical 134*, 251.
(166) de Oliveira, P. C., Alves, G. M., and de Castro, H. F. (2000) Immobilisation studies and catalytic properties of microbial lipase onto styrene-divinylbenzene copolymer. *Biochemical Engineering Journal 5*, 63.
(167) Cao, L., Bornscheuer, U. T., and Schmid, R. D. (1999) Lipase-catalyzed solid-phase synthesis of sugar esters. Influence of immobilization on productivity and stability of the enzyme. *Journal of Molecular Catalysis B: Enzymatic 6*, 279.
(168) Letant, S. E., Hart, B. R., Kane, S. R., Hadi, M. Z., Shields, S. J., and Reynolds, J. G. (2004) Enzyme immobilization on porous silicon surfaces. *Advanced Materials 16*, 689-+.
(169) Dumitriu, E., Secundo, F., Patarin, J., and Fechete, L. (2003) Preparation and properties of lipase immobilized on MCM-36 support. *Journal Of Molecular Catalysis B-Enzymatic 22*, 119-133.
(170) Seetharam, G., and Saville, B. A. (2002) L-DOPA production from tyrosinase immobilized on zeolite. *Enzyme And Microbial Technology 31*, 747-753.
(171) Huang, S. H., Liao, M. H., and Chen, D. H. (2003) Direct binding and characterization of lipase onto magnetic nanoparticles. *Biotechnology Progress 19*, 1095-1100.
(172) Dyal, A., Loos, K., Noto, M., Chang, S. W., Spagnoli, C., Shafi, K., Ulman, A., Cowman, M., and Gross, R. A. (2003) Activity of Candida rugosa lipase immobilized on gamma-Fe2O3 magnetic nanoparticles. *Journal Of The American Chemical Society 125*, 1684-1685.
(173) Schmid, R. D., and Verger, R. (1998) Lipases: Interfacial enzymes with attractive applications. *Angew. Chem. Int. Ed. Engl. 37*, 1609-1633.
(174) Phadtare, S., Kumar, A., Vinod, V. P., Dash, C., Palaskar, D. V., Rao, M., Shukla, P. G., Sivaram, S., and Sastry, M. (2003) Direct assembly of gold nanoparticle "shells" on polyurethane microsphere "cores" and their application as enzyme immobilization templates. *Chemistry Of Materials 15*, 1944-1949.
(175) Caruso, F., Trau, D., Mohwald, H., and Renneberg, R. (2000) Enzyme encapsulation in layer-by-layer engineered polymer multilayer capsules. *Langmuir 16*, 1485-1488.

(176) Fojan, P., Jonson, P. H., Petersen, M. T. N., and Petersen, S. B. (2000) What distinguishes an esterase from a lipase: A novel structural approach. *Biochimie 82*, 1033-1041.

(177) Dumitriu, E., Secundo, F., Patarin, J., and Fechete, L. (2003) Preparation and properties of lipase immobilized on MCM-36 support. *J. Mol. Catal. B: Enzy. 22*, 119-133.

(178) Fernandez-Lafuente, R., Armisen, P., Sabuquillo, P., Fernandez-Lorente, G., and Guisan, J. M. (1998) Immobilization of lipases by selective adsorption on hydrophobic supports. *Chemistry And Physics Of Lipids 93*, 185-197.

(179) Sugiura, M., and Isobe, M. (1975) STUDIES ON ENZYME.109. STUDIES ON MECHANISM OF LIPASE REACTION.2. COMPARATIVE STUDIES ON ADSORPTION OF LIPASES AND VARIOUS PROTEINS AT AIR-WATER-INTERFACE. *Biochim. Biophys. A. 397*, 412-417.

(180) Sugiura, M., and Isobe, M. (1975) STUDIES ON ENZYME.101. STUDIES ON MECHANISM OF LIPASE REACTION.1. INHIBITION OF LIPASE ACTIVITY BY EMULSION OF ORGANIC-SOLVENTS. *Chem. Pharm. Bull. 23*, 1221-1225.

(181) Tinoco, I. J., Sauer, K., and Wang, J. C. (1995) *Physical Chemistry – Principles and Applications in Biological Sciences*, 3rd ed., Simon & Schuster Co. Publishers.

(182) Lopez-Amaya, C. I., and Marangoni, A. G. (2003) Binding parameters for the interaction between Candida rugosa lipase and DPPC liposomes. *Colloids and Surfaces B: Biointerfaces 32*, 263.

(183) Acharya, P., and Rao, N. M. (2003) Stability studies on a lipase from Bacillus subtilis in guanidinium chloride. *J. Protein Chem. 22*, 51-60.

(184) Jutila, A., Zhu, K., Patkar, S. A., Vind, J., Svendsen, A., and Kinnunen, P. K. J. (2000) Detergent-induced conformational changes of Humicola lanuginosa lipase studied by fluorescence spectroscopy. *Biophysical Journal 78*, 1634-1642.